ESL-TR-83-34

Development of a Preliminary ALRS Stabilized Material Pavement Analysis System (SPAS)

B.J. DEMPSEY, D. JANSSEN, J. THOMAS,
P. FREY, A. IOANNIDES, and R. ELLIOTT

DEPARTMENT OF CIVIL ENGINEERING
UNIVERSITY OF ILLINOIS
URBANA, ILLINOIS 61801

AUGUST 1984

FINAL REPORT
APRIL 1982 - MAY 1983

AFESC

ENGINEERING AND SERVICES LABORATORY
AIR FORCE ENGINEERING AND SERVICES CENTER
TYNDALL AIR FORCE BASE, FLORIDA 32403

NOTICE

PLEASE DO NOT REQUEST COPIES OF THIS REPORT FROM HQ AFESC/RD (ENGINEERING AND SERVICES LABORATORY). ADDITIONAL COPIES MAY BE PURCHASED FROM:

NATIONAL TECHNICAL INFORMATION SERVICE
5285 PORT ROYAL ROAD
SPRINGFIELD, VIRGINIA 22161

FEDERAL GOVERNMENT AGENCIES AND THEIR CONTRACTORS REGISTERED WITH DEFENSE TECHNICAL INFORMATION CENTER SHOULD DIRECT REQUESTS FOR COPIES OF THIS REPORT TO:

DEFENSE TECHNICAL INFORMATION CENTER
CAMERON STATION
ALEXANDRIA, VIRGINIA 22314

REPORT DOCUMENTATION PAGE

1a. REPORT SECURITY CLASSIFICATION UNCLASSIFIED	1b. RESTRICTIVE MARKINGS
2a. SECURITY CLASSIFICATION AUTHORITY	3. DISTRIBUTION/AVAILABILITY OF REPORT Approved for public release; distribution unlimited.
2b. DECLASSIFICATION/DOWNGRADING SCHEDULE	
4. PERFORMING ORGANIZATION REPORT NUMBER(S)	5. MONITORING ORGANIZATION REPORT NUMBER(S) ESL-TR-83-34
6a. NAME OF PERFORMING ORGANIZATION Department of Civil Engineering University of Illinois 6b. OFFICE SYMBOL (If applicable)	7a. NAME OF MONITORING ORGANIZATION Air Force Engineering and Services Center (RDCR)
6c. ADDRESS (City, State and ZIP Code) Urbana, Illinois 61801	7b. ADDRESS (City, State and ZIP Code) Tyndall AFB FL 32403
8a. NAME OF FUNDING/SPONSORING ORGANIZATION 8b. OFFICE SYMBOL (If applicable)	9. PROCUREMENT INSTRUMENT IDENTIFICATION NUMBER ~~PR~~ FY8952-82-60024
8c. ADDRESS (City, State and ZIP Code)	10. SOURCE OF FUNDING NOS PROGRAM ELEMENT NO. 64708F; PROJECT NO. 2621; TASK NO. 40; WORK UNIT NO. 05
11. TITLE (Include Security Classification) Dev. of a Prelim. ALRS Stabilized Mater. Pavement Anal. Sys. (SPAS)	
12. PERSONAL AUTHOR(S) Thompson, Marshall R.; Dempsey, B.J.; Janssen, D.; Thomas, J.; Frey, P.; Ioannides, A.; Elliott, R.	
13a. TYPE OF REPORT FINAL	13b. TIME COVERED FROM Apr 82 TO May 83
14. DATE OF REPORT (Yr., Mo., Day) 1984 March	15. PAGE COUNT 169
16. SUPPLEMENTARY NOTATION	

17. COSATI CODES			18. SUBJECT TERMS (Continue on reverse if necessary and identify by block number)
FIELD	GROUP	SUB. GR.	
13	02		Airfields — Soil Mechanics
08	13		ALRS — Soil Stabilization
			Stabilized Pavements — Alternate Launch and Recovery Surfaces

19. ABSTRACT (Continue on reverse if necessary and identify by block number)

This report is an analytical study of soil stabilization as used in Alternate Launch and Recovery Surface (ALRS) design. The study proposes that ALRS pavements can be designed using a mechanistic design approach and a stabilized pavement analysis system (SPAS) is proposed. Stabilized material properties (strength, modulus, fatigue), structural modeling and behavior concepts, and environmental factors (freeze-thaw, frost depth) are utilized in the SPAS development. Inputs required to establish a stabilized base thickness for an ALRS pavement (F-4 loading) are the field strength of the stabilized material and the E_{Ri} (measure of resilient modulus) of the fine-grained subgrade.

A properly designed ALRS pavement for F-4 loading can accommodate a limited number of C-130 and F-15 load applications. The SPAS thickness design concepts (based on an intact slab approach) are applicable to a broad range of cementitious-stabilized materials (soil-cement, lime-fly ash-aggregate, soil-lime mixtures, similar high strength and modulus (con't)

20. DISTRIBUTION/AVAILABILITY OF ABSTRACT UNCLASSIFIED/UNLIMITED ☒ SAME AS RPT. ☐ DTIC USERS ☐	21. ABSTRACT SECURITY CLASSIFICATION UNCLASSIFIED
22a. NAME OF RESPONSIBLE INDIVIDUAL DAVID F. RUSCHMANN, Capt, USAF	22b. TELEPHONE NUMBER (Include Area Code) (904) 283-6329 22c. OFFICE SYMBOL HQ AFESC/RDCR

materials.

>SPAS F-4 thickness requirements appear reasonable. Further research and development activities are required to validate SPAS. Technical report ESL-TR-84-25, Response and Performance of Alternate Launch and Recovery Surfaces Containing Stabilized Material Layers, shall report on predicting structural responses for ALRS pavements using stabilized material. Validation of the research shall use information from Test Report ESL-TR-83-46, Performance Data for F-4 Load Cart Operations on Alternate Launch and Recovery Surfaces.

PREFACE

This report was prepared by the Department of Civil Engineering, University of Illinois @ Urbana-Champaign, Illinois under contract FY8952-82-60024, for the Air Force Engineering and Services Center, Engineering and Services Laboratory, Tyndall Air Force Base, Florida.

The current USAF Project Officer is Captain D. F. Ruschmann; Captains J. D. Wilson and H. Kelly also served as Project Officers.

The contents of this report reflect the views of the authors who are responsible for the facts and the accuracy of the data presented herein. The contents do not necessarily reflect the official views or policies of the U.S. Air Force. This report does not consititute a standard, specification, or regulation.

This report has been reviewed by the Public Affairs Office (PA) and is releasable to the National Technical Information Service (NTIS). At NTIS it will be available to the general public including foreign nationals.

This technical report has been reviewed and is approved for publication.

David F. Ruschmann

DAVID F. RUSCHMANN, Capt, USAF
ALRS Project Officer

LOREN M. WOMACK
Chief, Engineering Research Division

James R. VanOrman

JAMES R. VAN ORMAN
Chief, Rapid Runway Repair Branch

ROBERT E. BOYER, Col, USAF
Director, Engineering and Services Laboratory

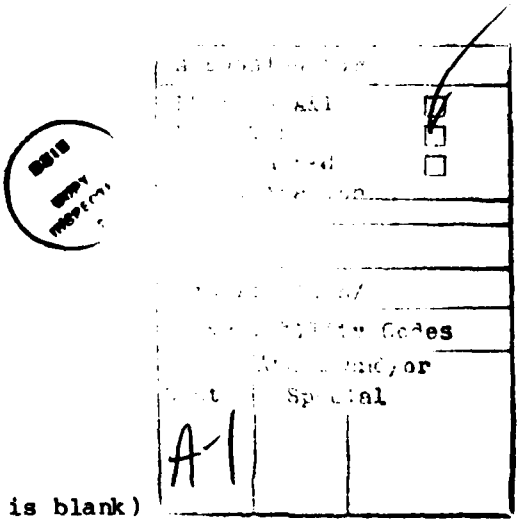

(The reverse of this page is blank)

TABLE OF CONTENTS

TABLE OF CONTENTS
(CONTINUED)

LIST OF FIGURES

LIST OF FIGURES
(CONTINUED)

LIST OF FIGURES
(CONTINUED)

LIST OF TABLES

SECTION I

INTRODUCTION

The USAF's Rapid Runway Repair (RRR) Research and Development Program contains a program component called Alternate Launch and Recovery Surfaces (ALRS). General requirements for ALRS are (1) a 20-year design life, (2) capability of accommodating 150 passes of an F-4 and 25 C-130 passes at any time, and (3) low cost. The research program incorporated passes of the F-15 at increased wheel loads and tire pressures.

The F-4 design wheel load is 27 kips with an average contact pressure of 265 psi (Reference 1). The radius of an equivalent circular tire contact area is approximately 6 inches, which is similar to normal highway (9-kip) loading. That is fortunate since many analytical and experimental studies have been conducted with loading areas of approximately 6-inch radii.

C-130 maximum single-wheel loading is 42 kips with a tire contact pressure of 95 psi (Reference 1). The radius of an equivalent circular contact area is approximately 12 inches. Center-to-center tandem spacing is 60 inches. The equivalent single-wheel load is approximately 42 kips.

Possible F-15 wheel-loading conditions are 30 kips with a 355 psi contact pressure and 36 kips with a 400 psi contact pressure. The radii of the equivalent circular contact areas are 5.18 inches (30-kip loading) and 5.35 inches (36-kip loading).

Pavements containing stabilized soil layers demonstrate significant potential for ALRS applications. Many studies and field experiences have demonstrated that stabilized material (soil-lime, soil-cement, lime-fly ash-aggregate) pavement sections can support ALRS type traffic requirements. Stabilized layers can be used as:

1. A base course for a conventional pavement (AC surface + stabilized base);

2. A subbase for an inverted pavement (AC surface + granular base + stabilized subbase); or

3. Modified subgrade (working platform) to facilitate the construction of a conventional flexible pavement (AC surface + granular base over modified subgrade layer) in which no structural credit is given to the stabilized layer.

The low-cost requirement places a premium on the use of the best technology in developing material requirements and pavement thickness design concepts for ALRS. The 100-percent availability requirement for accommodating the aircraft passes means that under the worst circumstances (freeze-thaw (F-T) softened subgrades; high water tables; maximum possible F-T-stabilized material strength reductions, etc.), a satisfactory pavement structural capacity and acceptable levels of pavement surface geometry (ruts, roughness, etc.) must be provided to meet ALRS requirements.

Thus it is essential to develop sound concepts for:

1. Determining structural thickness requirements for a broad range of stabilized material qualities (high to low strength, etc.) and subgrade support conditions (very soft to stiff; CBR 2-20); and

2. Quantifying site "environmental factors" and developing concepts for relating environmental factors (F-T action, frost penetration, moisture increases, etc.) to the engineering properties of the subgrade soil and stabilized material pavement layers.

Combining the structural design and environmental factor technologies will facilitate the development of a comprehensive system for considering ALRS-stabilized material applications.

SECTION II

STRUCTURAL DESIGN CONSIDERATIONS

A. STABILIZED MATERIALS

The use of cementitious stabilizers is likely for ALRS stabilized material pavement construction. Cement, lime, and lime-fly ash are cementitious stabilization procedures.

Cementitious stabilizers typically increase compressive strength, shear strength (large increase in cohesion), tensile strength (flexural and split tensile), and modulus of elasticity. Freeze-thaw and moisture resistance are significantly enhanced by stabilization. If the stabilized materials are of structural layer quality, the controlling thickness design criterion for the stabilized material is generally the flexural stress at the bottom of the layer. A brief summary of the strength, modulus, and fatigue properties for cementitiously stabilized materials is presented in Appendix A.

The structural response and performance of the stabilized layer (for a given wheel loading) are influenced by the flexural strength, modulus, and thickness of the stabilized layer and subgrade modulus and strength. Stabilized materials of the same quality (strength, modulus) should display similar structural responses. Thus, thickness design concepts are relatively independent of material type.

B. STABILIZED-LAYER ANALYSIS

A mechanistic design concept uses a structural model to calculate pavement responses (stresses, deflections, strains). Transfer functions are required to relate pavement performance to pavement response. Typical transfer function response parameters are surface deflection, radial tensile strain in the asphalt concrete layer(s), subgrade stress and/or strain, and radial tensile stress in the stabilized base.

For high strength and modulus stabilized materials, a "fatigue approach" is frequently used to relate stress ratio (S = radial tensile stress/flexural strength) to number of load applications to failure (initial cracking). A conservative S-log N plot is shown in Figure 1. Similar relations have been developed based on stabilized material radial tensile strain. A more comprehensive fatigue discussion is presented in Appendix A.

It is generally accepted that the fatigue concept relates to crack initiation in the stabilized material and that additional load repetitions are required to propagate the crack to the surface of the layer. A recent study (Reference 2) of 10 heavily loaded (axle loads from 40 to 200 kips) cement-stabilized base projects indicated that present PCA design procedures (Reference 3) based on fatigue concepts (crack initiation) were conservative. Shift factors (the ratio of number of load repetitions for "crack propagation"to number of load repetitions for "crack initiation") are frequently used in practical pavement design situations.

Raad's investigation (Reference 4) indicated that the shift factor is variable. His suggested shift factors ranged from 1.07 to 4.6. For typical ALRS applications, Raad's higher values (3.8, 4.6) appear to be more appropriate. South African mechanistic pavement design concepts for highway pavements (Reference 5) indicate the shift factor varies and is related to traffic and layer thickness. For less than 3 million 18-kip single axles, the shift factor is 3 for layers less than 8 inches and 7.5 for layers greater than 8 inches. It is apparent that there is no concurrence on shift factor values. However a factor of about 2 or 3 seems conservative.

1. Layered System Theory

Extensive structural modeling and pavement nondestructive testing activities (References 6,7) have demonstrated that the ILLI-PAVE stress-dependent finite element program is adequate for characterizing the structural response of flexible pavement systems containing

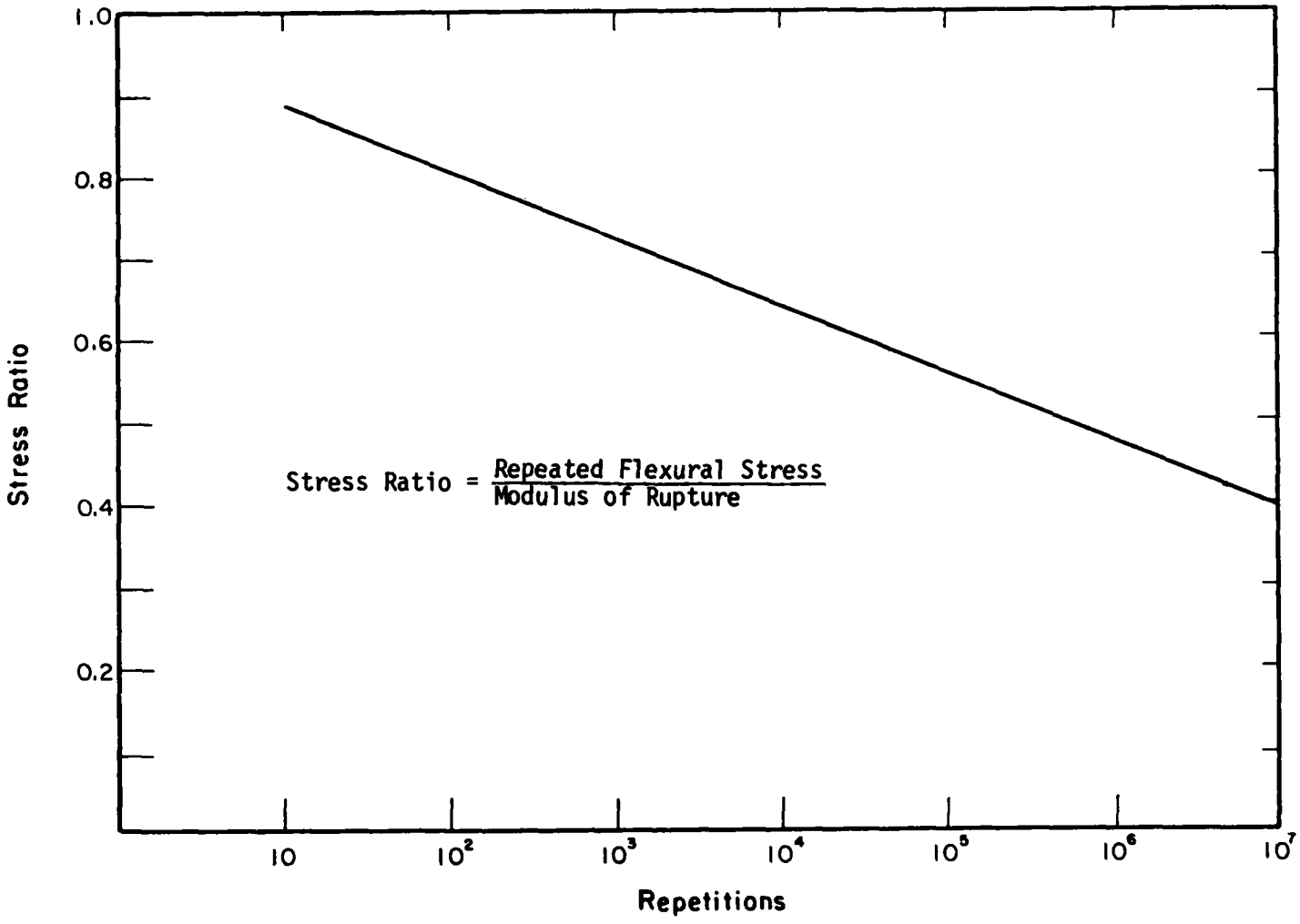

Figure 1. Recommended Stress Ratio-Fatigue Relation for Cementitiously Stabilized Materials.

stabilized layers. Traditional linear elastic theory models tend to predict unrealistically large bending stresses and strains for the stabilized layer and are not recommended (Reference 6).

A comprehensive ILLI-PAVE study was conducted for F-4 interior loading conditions. The system analyzed is shown in Figure 2.

The parameters considered were:

Stabilized layer thickness: 9, 12, 15, 18 inches
Stabilized material modulus: 100,200,500,1000,2000, and 300 ksi
Subgrade strength: *very soft, soft, medium, stiff

(*Resilient modulus-deviator stress relations are shown in Figure 3).

Pertinent subgrade property data are summarized in Table 1.

Pavement response data for the 96 ILLI-PAVE runs are presented in Appendix B. A typical run requires 20-30 cpu seconds on a CDC Cyber 175 system. Various graphical data presentations are included in Figures 4 through 13.

Design algorithms were developed based on statistical analyses of the ILLI-PAVE data. The major pavement response for thickness design purposes is the flexural tensile stress in the stabilized layer. The algorithms for flexural stress (interior loading) are:

For E < 500 ksi:

$$\sigma = 405 - 18.68T - 3.49\ E_{Ri} \qquad (1)$$

$R^2 = 0.868$ SEE = 26.0

$$\text{Log}\,\sigma = 2.987 - 0.0634T - 0.0116\,E_{Ri} \quad (2)$$
$$R^2 = 0.937 \quad SEE = 0.058$$

For E > 500 ksi:

$$\sigma = 510 - 24.77T - 1.48\,E_{Ri} \quad (3)$$
$$R^2 = 0.914 \quad SEE = 26.2$$

$$\text{Log}\,\sigma = 3.086 - 0.0668T - 0.00351\,E_{Ri} \quad (4)$$
$$R^2 = 0.982 \quad SEE = 0.031$$

where:

E_{Ri} = Resilient modulus of cohesive subgrade soil (repeated deviator stress = 6 psi)
T = Stabilized layer thickness, inches
E = Modulus of stabilized layer, ksi
σ = Flexural stress (interior loading) at bottom of stabilized layer, psi
R^2 = Coefficient of determination
SEE = Standard error of estimate

The major factor controlling flexural stress is stabilized layer thickness. Subgrade E_{Ri} has a very limited influence.

F-15 loading effects were considered by comparing F-15 wheel-load induced flexural and subgrade deviator stresses for typical ALRS stabilized base pavements. Base thicknesses were 9, 12, 15 and 18 inches and the stabilized material modulus was 2,000 ksi. Subgrade E_{Ri} values were primarily for soft conditions. Subgrade E_{Ri} values for a medium subgrade were considered for stabilized base thicknesses of 12 and 18 inches. ILLI-PAVE pavement responses are summarized in Table 2. The F-15 30-kip-load stabilized base course flexural stresses are approximately 19 percent greater than the F-4 stresses and the F-15 36-kip load increases (relative to the F-4) are approximately 41 percent. Note that the load ratio for the F-15 at 30 kips is 1.11 (30/27) and 1.33 (36/27) for 36-kip loading.

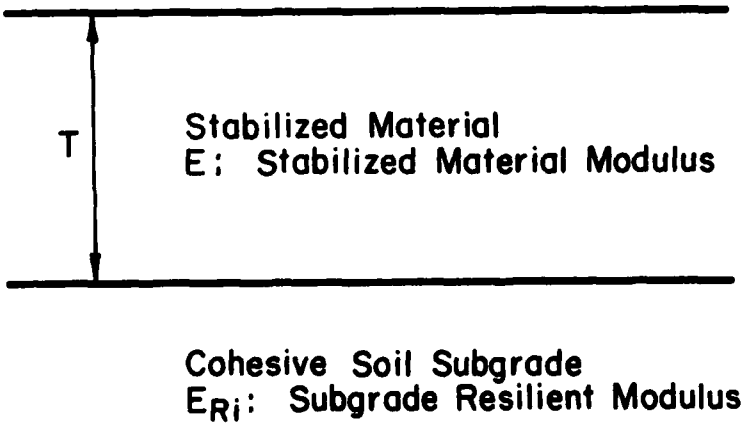

Figure 2. Typical ALRS Stabilized Base Section Pavement.

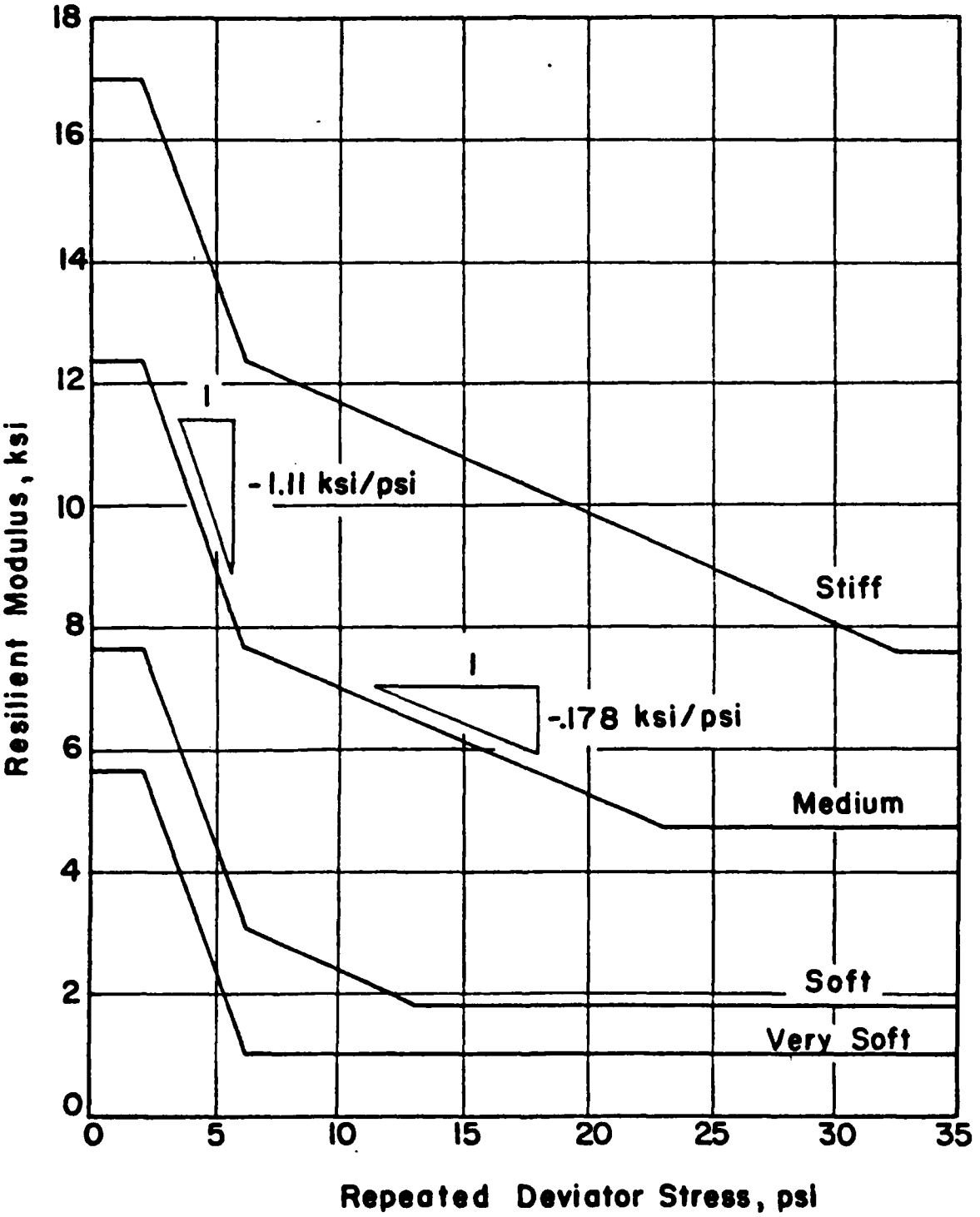

Figure 3. Subgrade Soil Material Models for ILLI-PAVE Analyses.

TABLE 1. SUBGRADE SOIL PROPERTIES

	SUBGRADE CLASS			
	Stiff	Medium	Soft	Very Soft
Unit Weight, pcf	125.0	120.0	115.0	110.0
Poisson's Ratio	0.45	0.45	0.45	0.45
Unconfined Compressive Strength, psi	32.8	22.9	12.9	6.2
E_{ri}, ksi*	12.34	7.68	3.02	1.0
Friction Angle (Ø), degrees	0	0	0	0
Cohesion (c), psi	16.4	11.45	6.45	3.1

*E_{ri} is the resilient modulus at a repeated deviator stress of approximately 6 psi (see Figure 3)

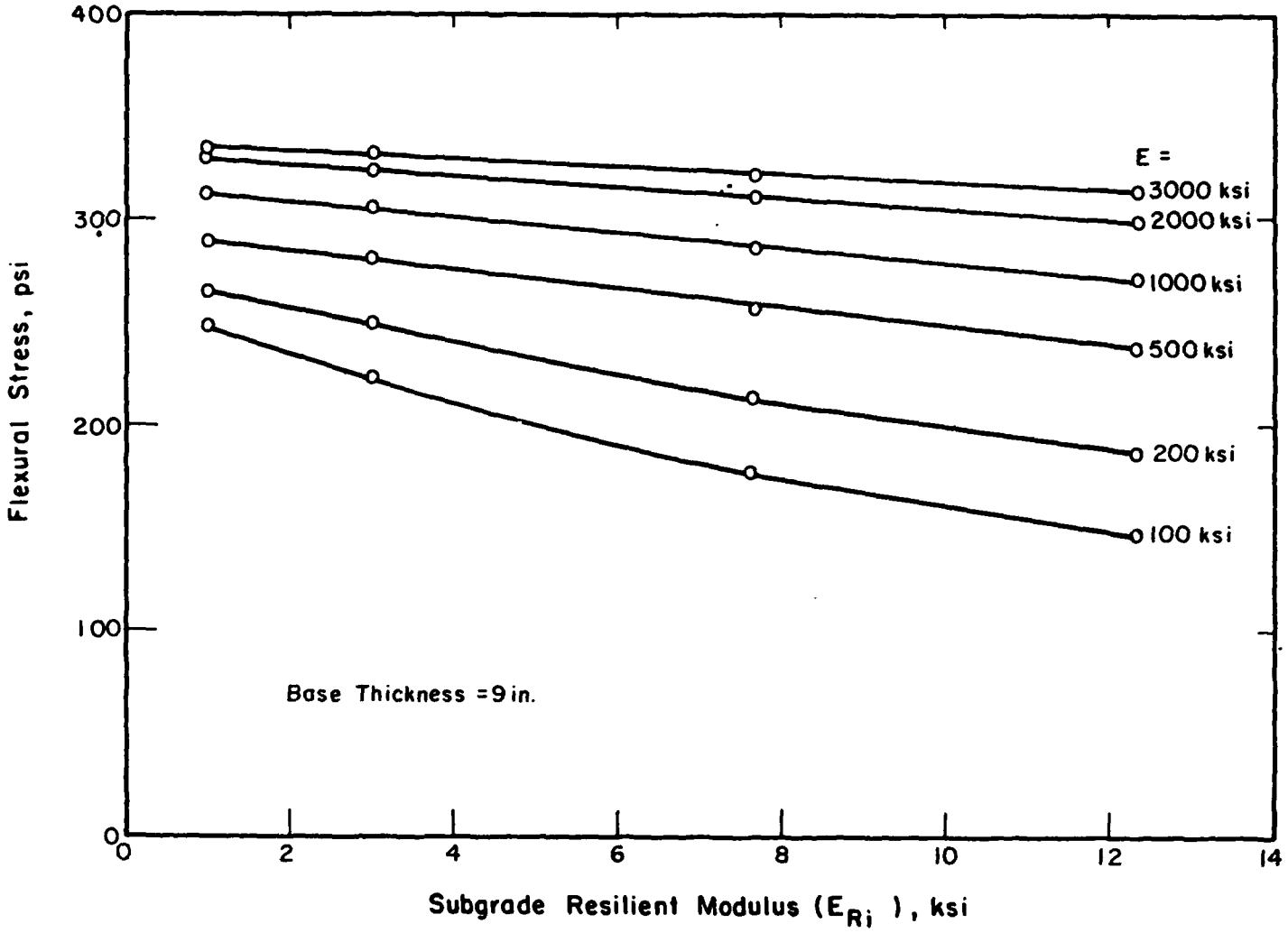

Figure 4. Flexural Stress-Subgrade Modulus-Base Modulus Relations (9-inch base).

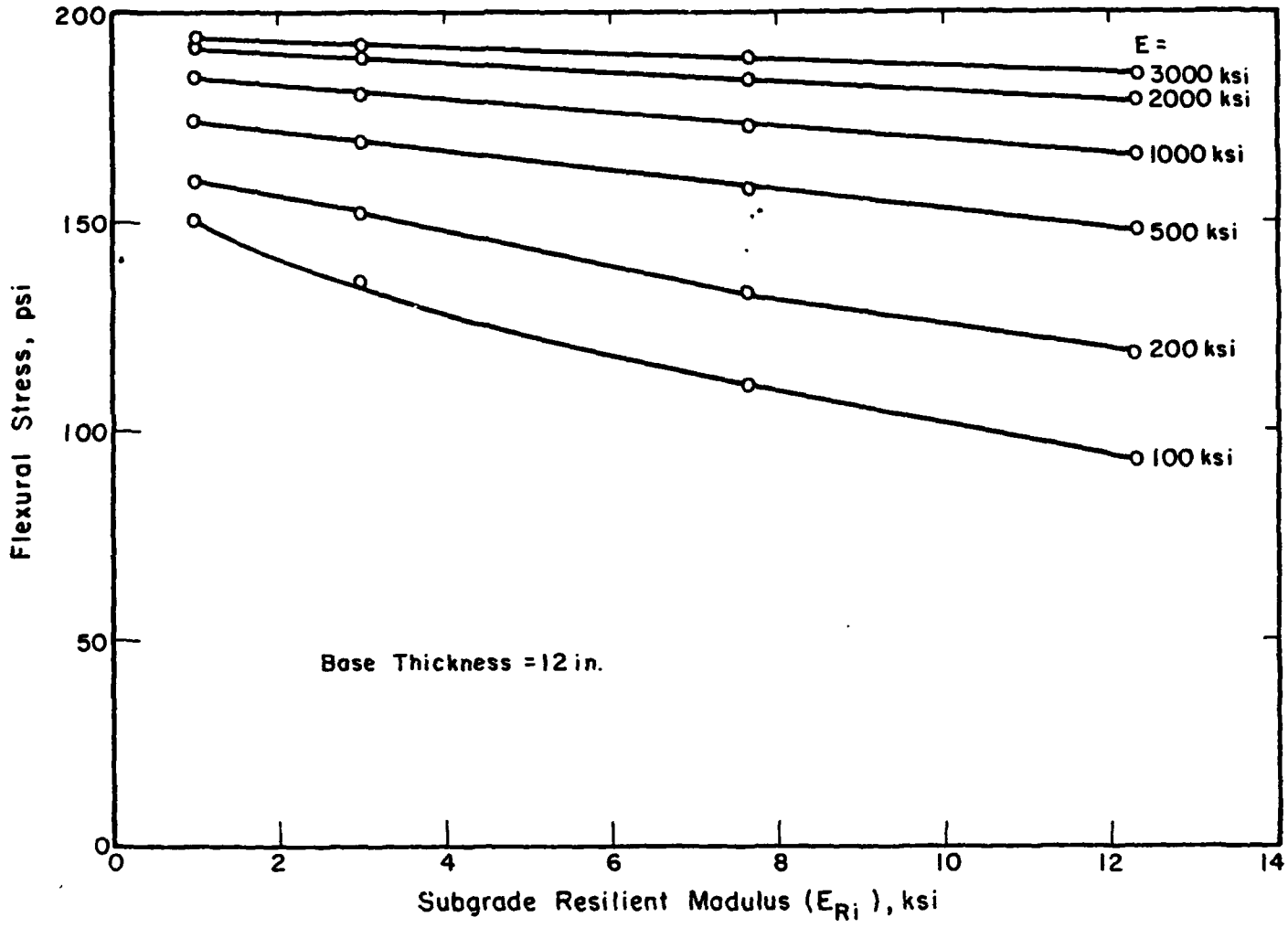

Figure 5. Flexural Stress-Subgrade Modulus-Base Modulus Relations (12-inch base).

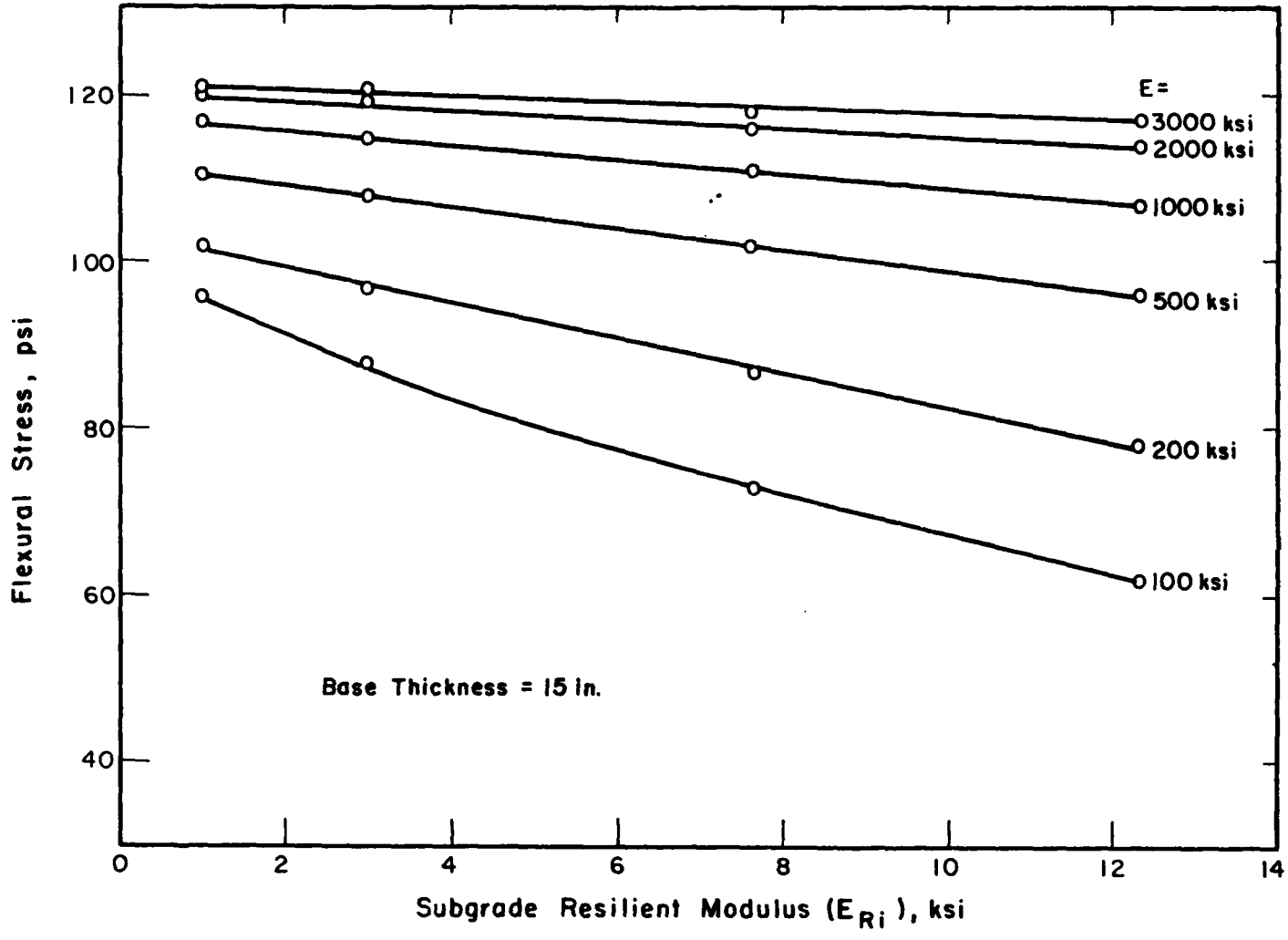

Figure 6. Flexural Stress-Subgrade Modulus-Base Modulus Relations (15-inch base).

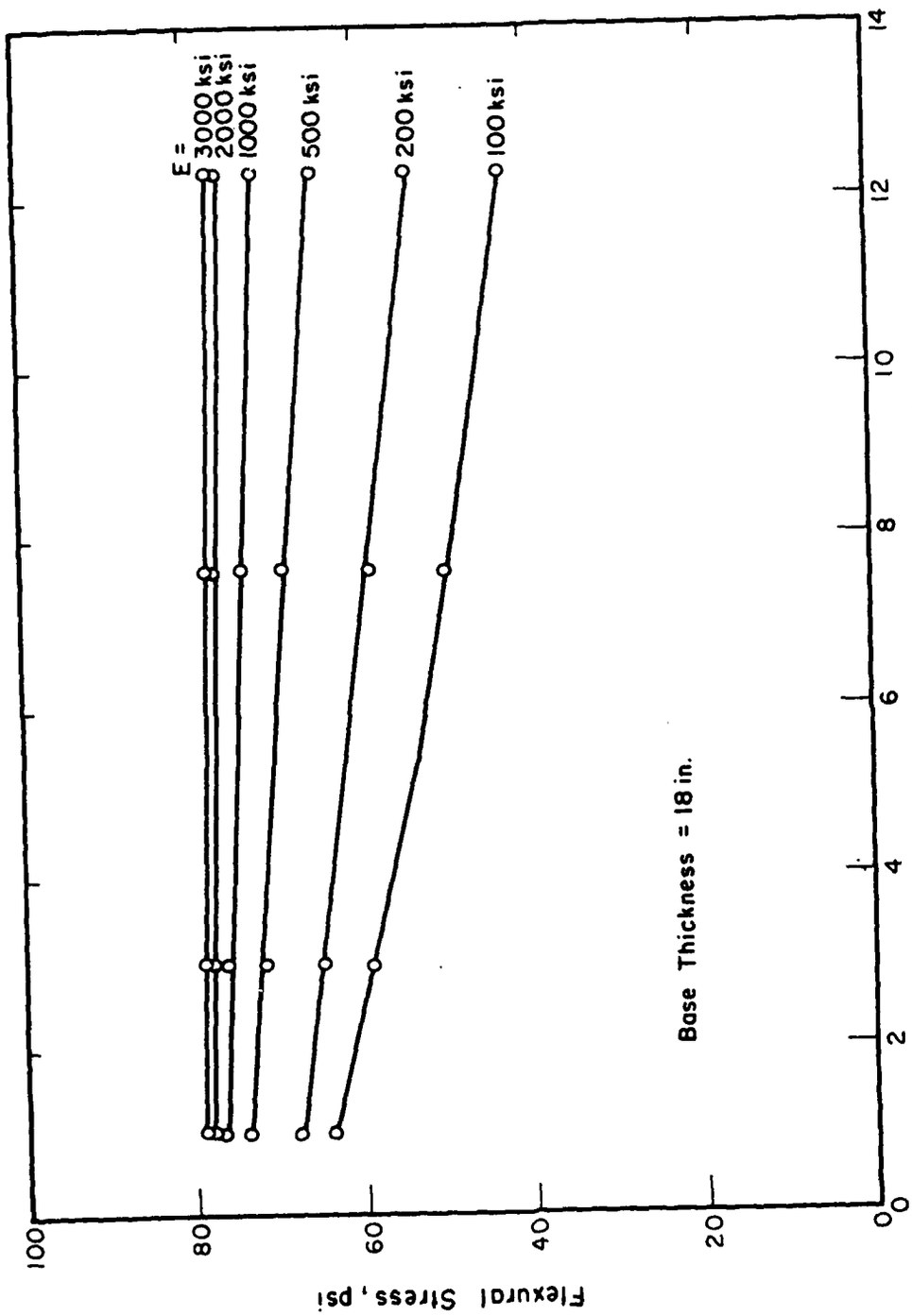

Figure 7. Flexural Stress-Subgrade Modulus-Base Modulus Relations (18-inch base).

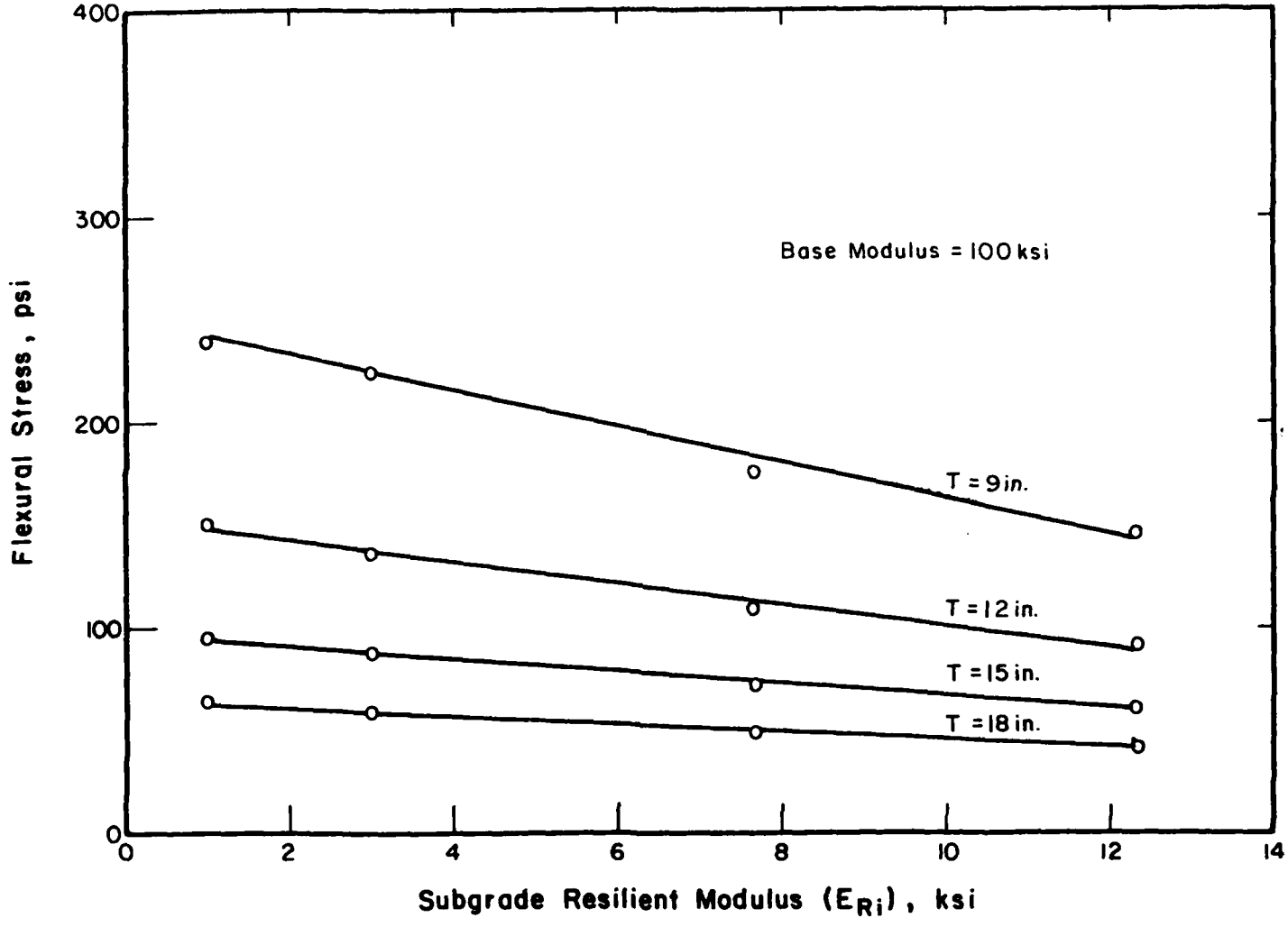

Figure 8. Flexural Stress-Subgrade Modulus-Thickness Relations (base modulus = 100 ksi).

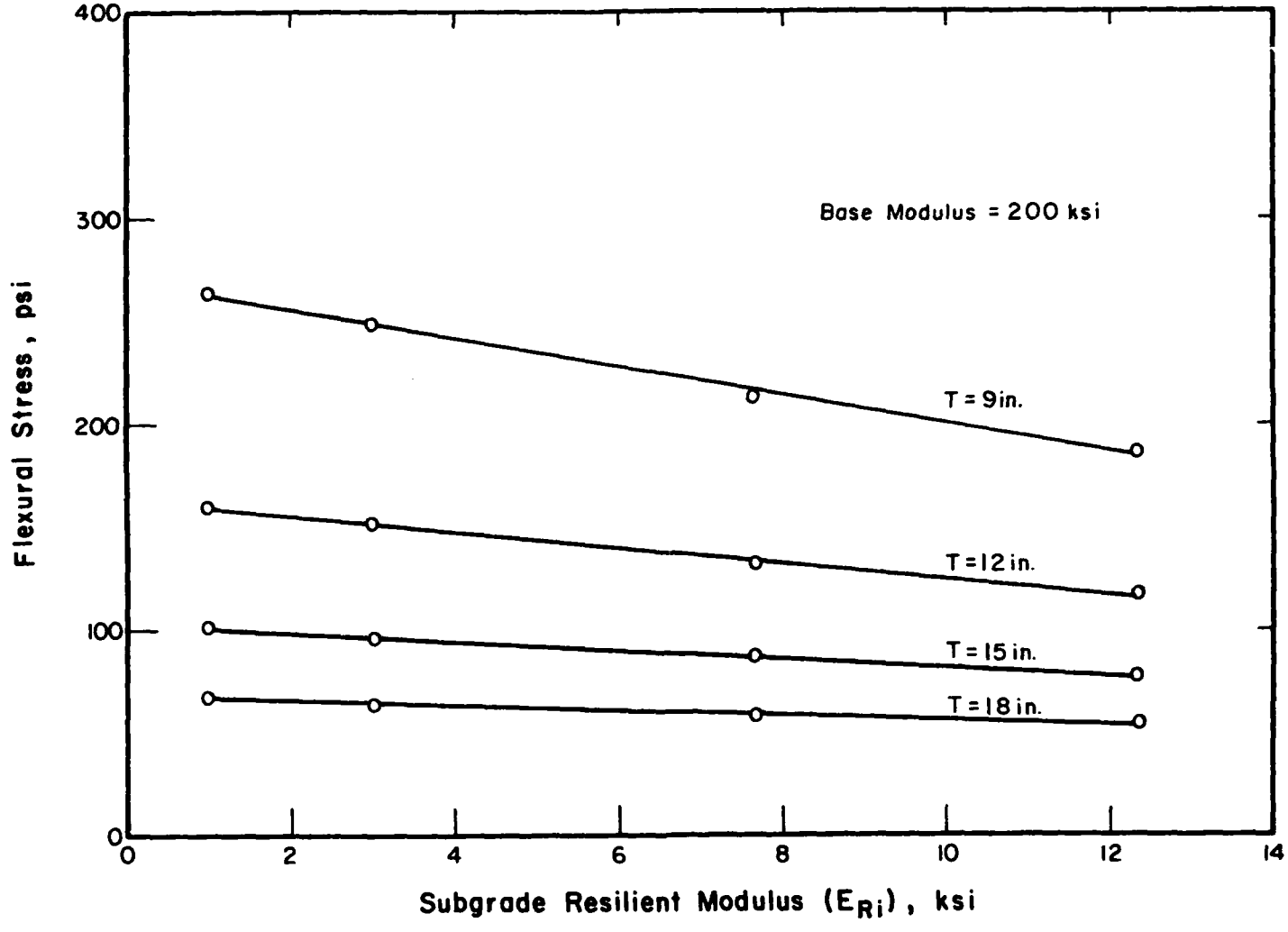

Figure 9. Flexural Stress-Subgrade Modulus-Thickness Relations (base modulus = 200 ksi).

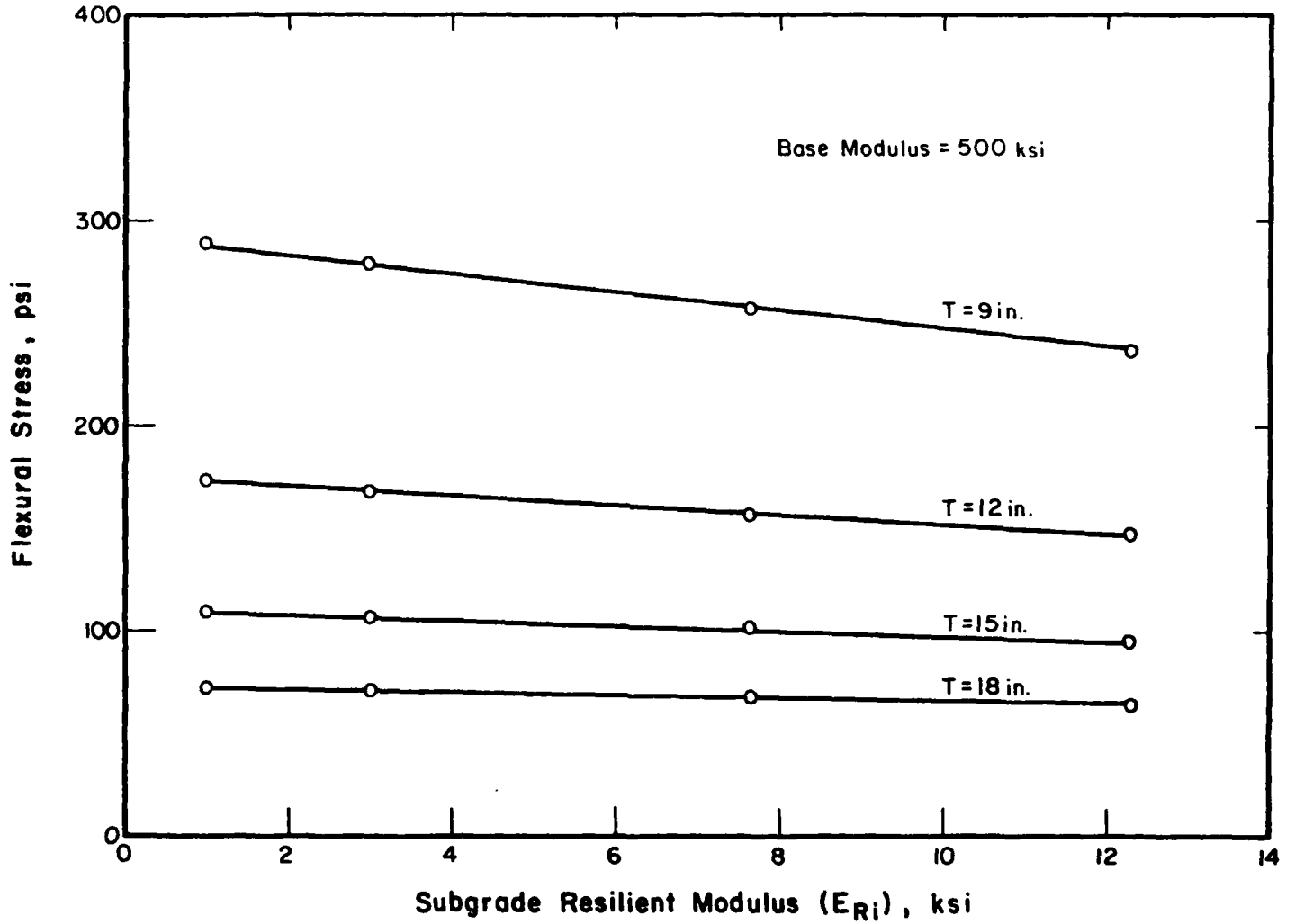

Figure 10. Flexural Stress-Subgrade Modulus-Thickness Relations (base modulus = 500 ksi).

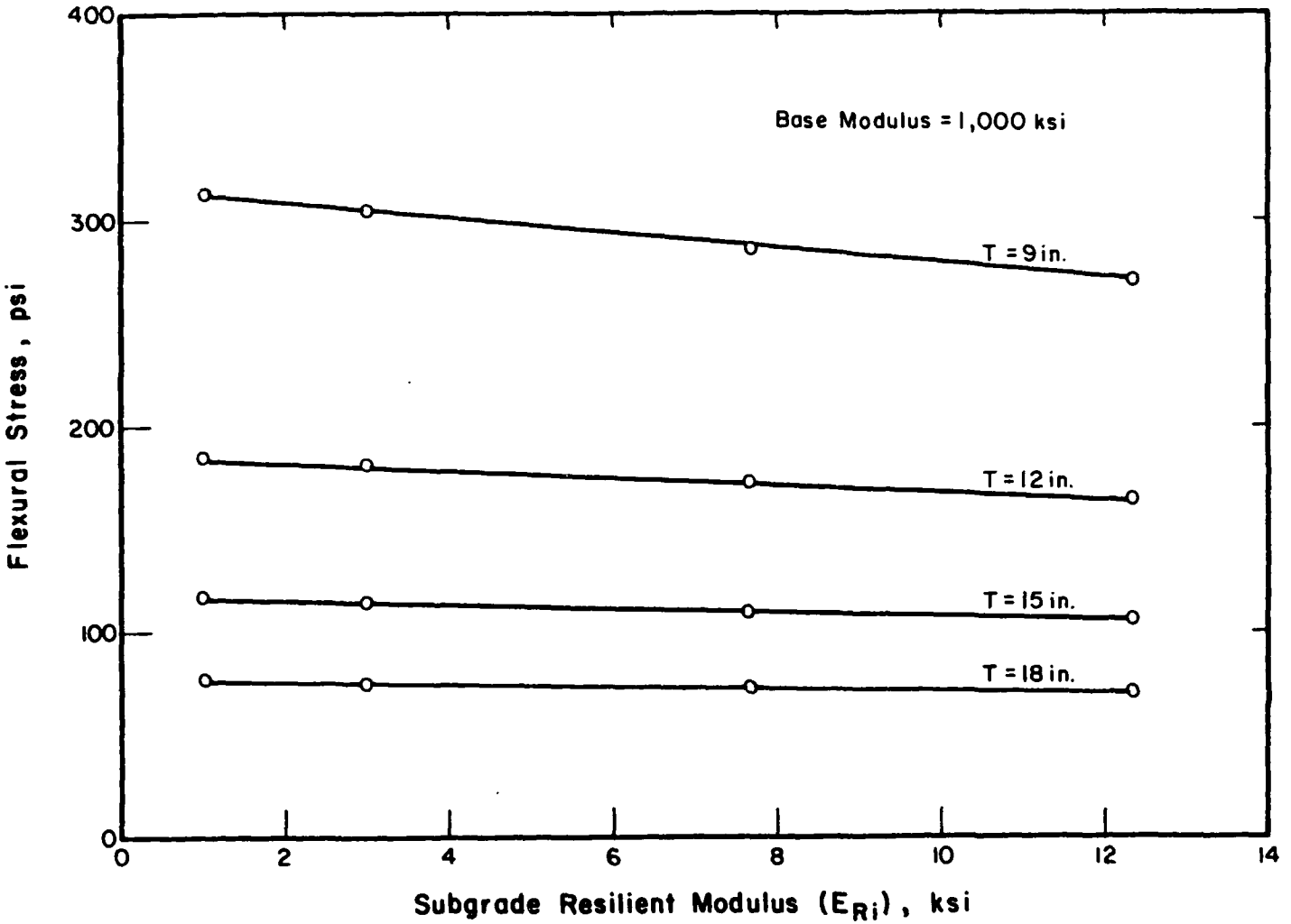

Figure 11. Flexural Stress-Subgrade Modulus-Thickness Relations (base modulus = 1000 ksi).

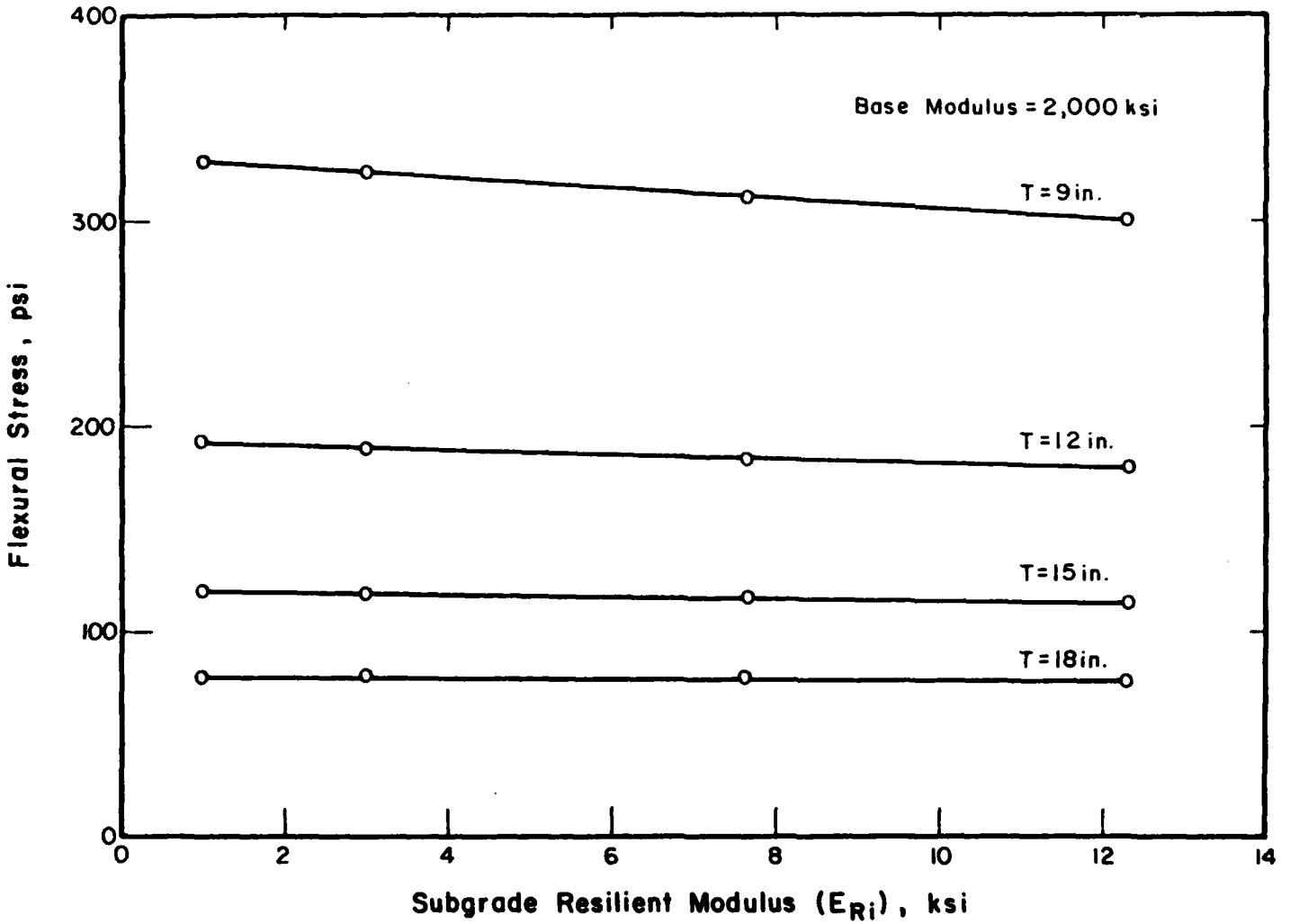

Figure 12. Flexural Stress-Subgrade Modulus-Thickness Relations (base modulus = 2000 ksi).

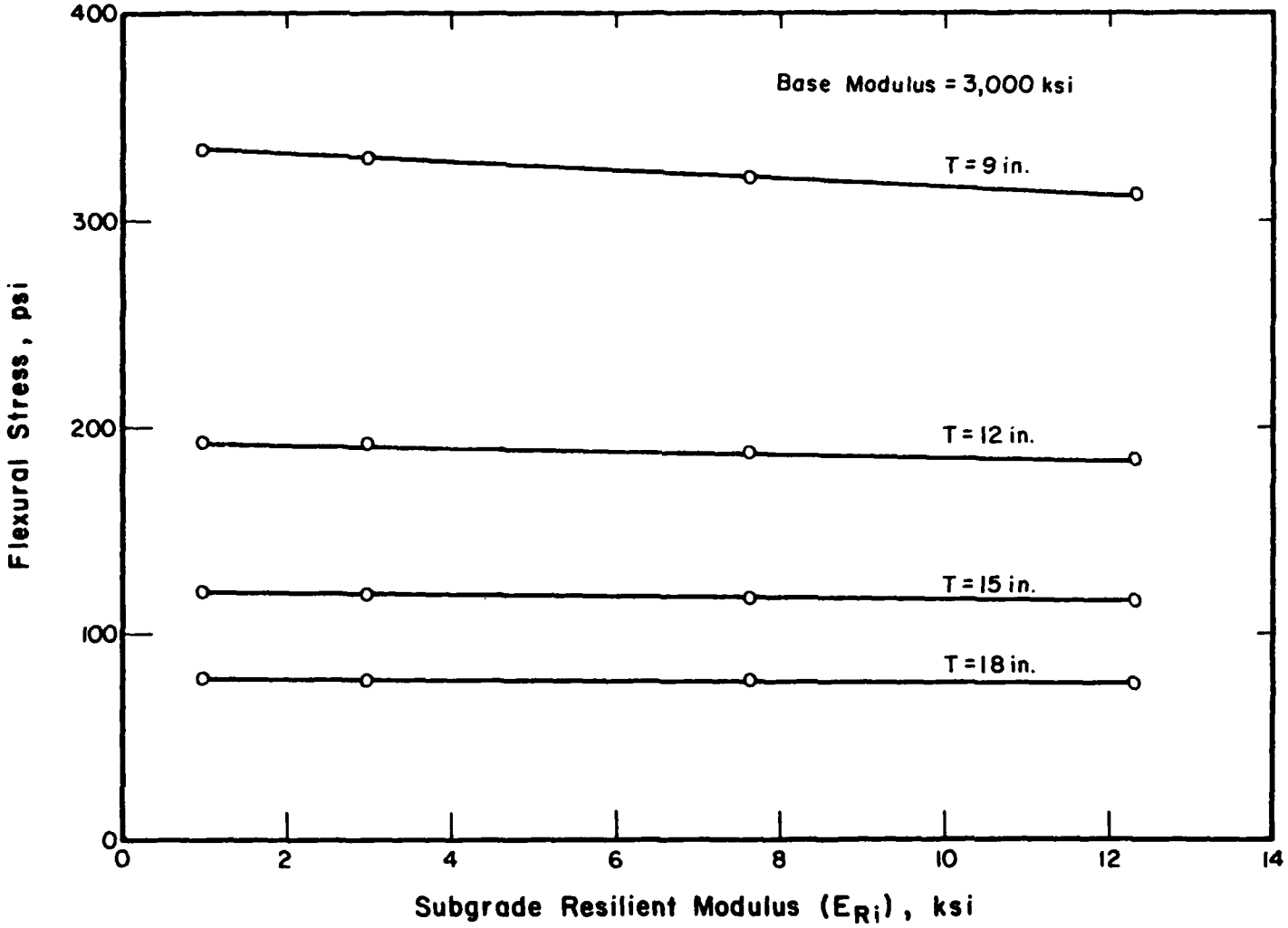

Figure 13. Flexural Stress-Subgrade Modulus-Thickness Relations (base modulus = 3000 ksi).

TABLE 2. F-15 LOADING EFFECTS

Stabilized-Base Thickness, inches*	Subgrade E_{Ri}, ksi	F-15 Wheel Load, kips	Stabilized-Base Flexural Stress, psi	Subgrade Deviator Stress, psi	Surface Deflection, mils
9	3.02	30	400	3.1	30.7
12	3.02	30	225	2.1	26.1
12	7.68	30	220	2.9	18.0
15	3.02	30	140	1.6	23.9
18	3.02	30	90	1.2	22.7
18	7.68	30	90	1.5	14.9
9	3.02	36	470	3.6	36.8
12	3.02	36	270	2.5	31.2
12	7.68	36	260	3.3	21.4
15	3.02	36	165	1.8	28.6
18	3.02	36	110	1.4	27.2
18	7.68	36	105	1.9	17.7

* Stabilized base modulus = 2000 ksi

C-130 loading effects (42-kip wheel load, 95 psi contact pressure) were considered by comparing F-4 and C-130 wheel load-induced flexural stresses for typical ALRS-stabilized base pavements. The stabilized base thickness was 12 inches and the material modulus was 1,000 ksi. E_{Ri} values were for very soft, soft, and medium subgrade conditions (see Table 1). ILLI-PAVE pavement responses are summarized in Table 3. The C-130 base course flexural stresses and subgrade deviator stresses are approximately 10 percent greater than the F-4 stresses.

2. Slab Theories

A high strength and modulus stabilized pavement layer displays a "slab-type" behavior. Westergaard theory has traditionally been used to analyze such a structural system. The pavement is characterized by the thickness, modulus, and Poisson's ratio of the pavement layer and k (the modulus ot subgrade reaction). The Westergaard approach is limited to interior, edge, and corner loading conditions.

ILLI-SLAB, a versatile finite element slab model (varied load locations, nonuniform slab thickness and k, joint modelling, etc.), has been developed at the University of Illinois (Reference 8). In a recent AFOSR study (Reference 9) at the University of Illinois, ILLI-SLAB was modified to permit the consideration of a stress-dependent subgrade. The concept of a resilient modulus of subgrade reaction (K_R) was developed. Comparisons with theoretical solutions show that ILLI-SLAB agrees with Westergaard's "ordinary thoeory" for the interior condition (Reference 10) and Westergaard`s "new formula" (Reference 11) for the edge condition, provided appropriate slab size, mesh fineness and loaded-area size conditions are satisfied (Reference 9). For the corner condition, ILLI-SLAB principal stresses fell in the narrow band between values predicted by Westergaard's empirical equation (Reference 10) and the slightly higher ones calculated with Bradbury's formula (Reference 12).

ILLI-SLAB analyses (interior loading conditions,F-15 loading) were conducted for a wide range of conditions (E, base modulus; T, base

TABLE 3. C-130 LOADING EFFECTS

Subgrade E_{Ri}, ksi	Aircraft Loading	Stabilized Base Flexural Stress, psi	Subgrade Deviator Stress, psi	Surface, Deflection, mils
1.0	F-4	185	2.4	35.0
1.0	C-130	205	2.8	52.5
3.02	F-4	181	3.0	27.9
3.02	C-130	199	3.3	40.9
7.68	F-4	173	4.0	20.2
7.68	C-130	188	4.5	28.8

thickness; k, modulus of subgrade reaction). The ranges of the parameters considered were:

E (base modulus): 1000,2000 ksi
T (base thickness): 9,12,15,18,21 inches
k (modulus of subgrade reaction): 100,150, psi/in.
K_R (resilient modulus of subgrade reaction): soft, medium subgrades

The slab size was 12 feet wide by 15 feet long. Zero load transfer between slabs was assumed.

A summary of the maximum flexural stresses (the major design consideration for ALRS stabilized layer applications) is presented in Tables 4 and 5.

Algorithms were developed for predicting the maximum F-15 36 kip interior loading condition flexural stress.

$$\text{Log}\sigma = 4.281 - 1.683 \log T + 0.105 \text{ Log } (E/k) \quad (5)$$
$$R^2 = 0.99 \quad \text{SEE} = 1 \text{ psi}$$

$$\text{Log}\sigma = 4.371 - 1.687 \text{ Log } T \quad (6)$$
$$R^2 = 0.97 \quad \text{SEE} = 1.1 \text{ psi}$$

where:

σ = Maximum flexural stress, psi
T = Stabilized layer thickness, inches
E = Stabilized material modulus, ksi
k = Modulus of subgrade reaction psi/in.

Flexural stresses for the F-4 (27k, 265 psi) and F-15 (30k, 365 psi) can be accurately estimated by multiplying the F-15 (36k, 400 psi) stress by 27/36 and 30/36, respectively. For practical purposes, the loading effects for the F-4 (27 kips), F-15 (30 kips), and F-15 (36 kips)

TABLE 4. ILLI-SLAB RESULTS: F-15 LOADING/INTERIOR

Base Thickness, in.	Stabilized Base Modulus, ksi*	Modulus of Subgrade Reaction, psi/in	Maximum Flexural Stress, psi
9	1000	100	600
9	1000	150	573
9	2000	100	653
9	2000	150	621
12	1000	100	375
12	1000	150	357
12	2000	100	406
12	2000	150	388
15	1000	100	259
15	2000	150	248
15	2000	100	276
15	2000	150	266
18	1000	100	189
18	1000	150	182
18	2000	100	198
18	2000	150	193
21	1000	100	144
21	1000	150	140
21	2000	100	149
21	2000	150	146

TABLE 5. ILLI-SLAB RESULTS: F-15 LOADING/INTERIOR
(RESILIENT MODULUS OF SUBGRADE REACTION)

Base Thickness, in.	Stabilized-Base Modulus, ksi	Subgrade*	Maximum Flexural Stress, psi
9	1000	S	511
9	2000	S	553
12	1000	S	317
12	1000	M	298
12	2000	S	341
12	2000	M	322
15	1000	S	218
15	2000	S	237
18	1000	S	162
18	1000	M	152
18	2000	S	176
18	2000	M	165
21	1000	S	126
21	2000	S	135

* S - Soft Subgrade (see Figure 3 ; K_R = 430 psi/in. @ low deflections)

M - Medium Subgrade (see Figure 3 ; K_R = 725 psi/in. @ low deflections)

are linear. Note that the radii of the contact areas only range from 5.2 to 6 inches.

3. Ultimate Load Theory

Ultimate load carrying capacity tests of stabilized layers over cohesive subgrades (References 6,13,14) have demonstrated the effectiveness of stabilized layers. Meyerhof's (Reference 15) ultimate load-carrying capacity analysis procedures can be used to predict the behavior of typical stabilized-layer pavements. An important feature of the ultimate load-carrying capacity approach is the ability to accommodate load position effects (interior, edge, corner). Appendix C summarizes the Meyerhof equations and a graphical solution is presented in Figure 14.

Ahlberg and Barenberg (Reference 13), Barenberg (Reference 14) and Suddath and Thompson (Reference 6) indicated the Meyerhof predictions for interior loading of stabilized layers were conservative by a factor of at least 2. For edge loading, Ahlberg and Barenberg (Reference 13) and Barenberg (Reference 14) found the measured and Meyerhof theory predictions of load-carrying capacities compared favorably.

Meyerhof theory was used to predict the ultimate load-carrying capacity of typical stabilized-layer pavements for F-4 and F-15 loading. The range of parameters and calculated load-carrying capacities are shown in Tables 6 and 7. Various graphical data presentations for the F-4 are included in Figures 15 to 19.

The C-130 gear is a single-tandem configuration (Reference 1) with a total gear load of approximately 84 kips. Meyerhof interior load comparisons (F-4 vs C-130) for a range of stabilized material properties layer thicknesses, and subgrade strengths are shown in Table 8. Meyerhof (Reference 15) suggests that the edge-load ultimate-load carrying capacity is approximately 60 percent of the interior value.

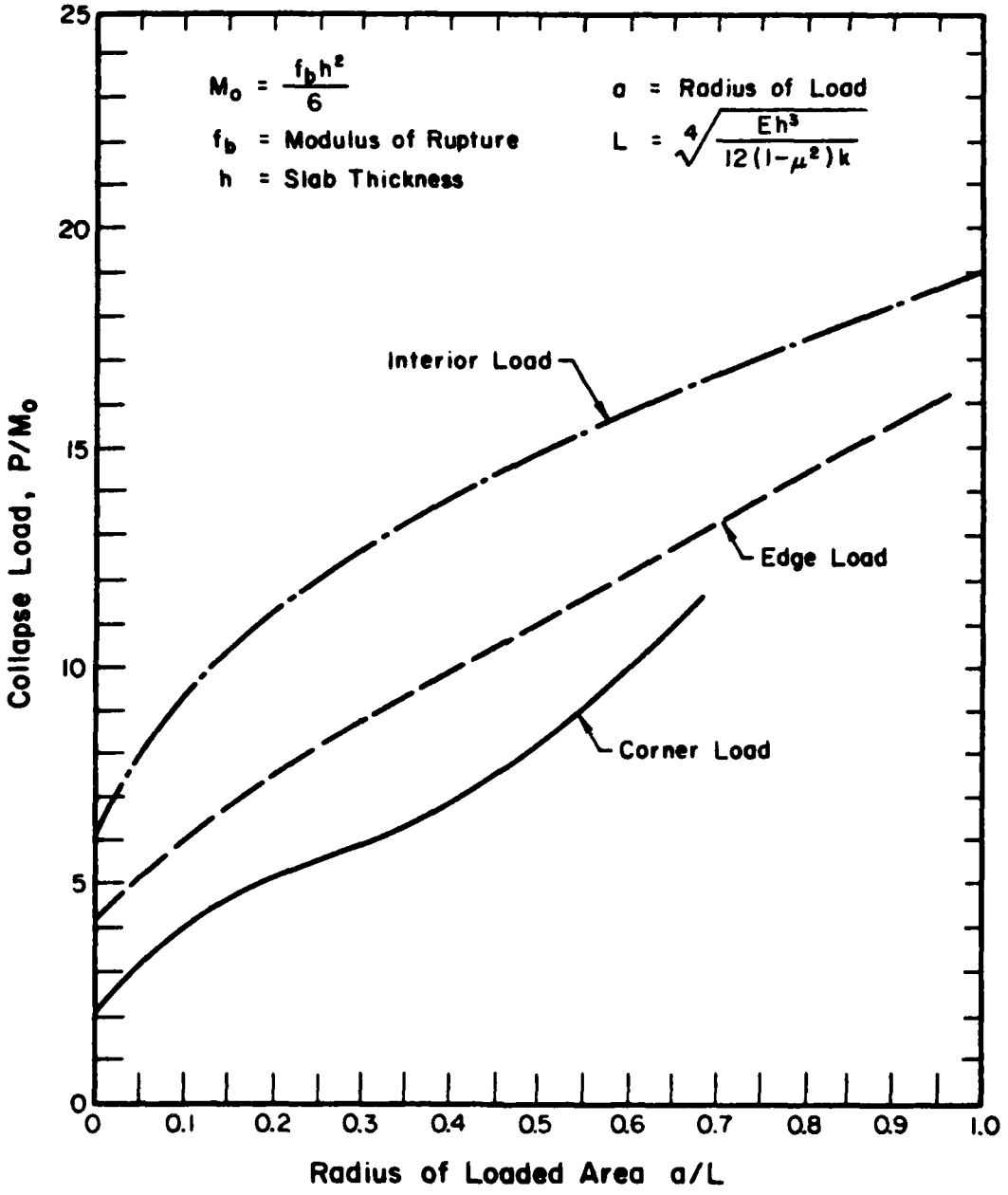

Figure 14. Graphical Solution for Meyerhof Ultimate Load Equations.

TABLE 6. ULTIMATE LOAD DATA: F-4 LOADING

Material Properties			Ultimate Load Carrying Capacity, Kips								
			Interior			Edge			Corner		
Flexural Strength, psi	Modulus, psi	Thickness, inches	k=50*	k=150*	k=250*	k=50*	k=150*	k=250*	k=50*	k=150*	k=250*
50	$1x10^5$	6	4.4	4.6	4.7	2.9	3.3	3.6	2.0	2.6	3.1
		9	9.4	9.8	10.0	6.0	6.6	6.9	3.9	4.5	4.9
		12	16.4	16.9	17.2	10.2	10.9	11.3	6.3	7.1	7.6
		15	25.3	25.9	26.3	15.5	16.4	16.9	9.5	10.3	10.9
		18	29.7	36.8	37.3	19.4	22.9	23.5	13.5	14.2	14.8
100	$5x10^5$	6	8.3	8.6	8.7	[illegible]	5.6	5.9	3.3	3.8	4.1
		9	18.2	18.6	18.9	[illegible]	11.7	12.1	6.8	7.4	7.8
		12	25.0	32.5	32.8	[illegible].4	20.0	20.5	11.5	12.2	12.7
		15	38.8	40.9	50.6	25.9	26.6	31.1	17.7	18.2	18.9
		18	52.5	57.2	59.5	34.6	37.3	39.0	22.7	25.7	27.1
200	$1.4x10^6$	6	16.2	16.6	16.9	10.0	10.5	10.9	6.1	6.7	7.0
		9	28.1	36.4	36.8	18.4	22.4	22.9	13.0	13.6	14.1
		12	48.0	51.4	53.3	32.1	33.6	35.0	21.6	23.0	24.5
		15	71.2	76.5	78.0	46.4	50.3	51.0	30.0	34.5	36.0
		18	100.3	104.8	111.2	63.7	68.0	74.5	42.1	46.4	50.8
300	$2x10^6$	6	19.8	24.7	25.0	13.0	15.5	15.9	8.8	9.7	10.2
		9	41.3	44.6	54.8	27.1	29.2	33.7	18.6	19.8	20.6
		12	69.8	74.9	72.0	45.4	49.0	50.4	31.0	33.8	34.6
		15	104.5	112.5	77.0	67.5	73.1	76.5	45.0	49.5	52.9
		18	149.0	154.0	162.0	95.6	100.4	105.3	63.2	67.2	71.3

* k (Modulus of subgrade reaction) psi/in

NOTE: Contact area diameter= 12 inches

TABLE 7. ULTIMATE LOAD DATA: F-15 LOADING

Material Properties			Ultimate Load Carrying Capacity, Kips								
			Interior			Edge			Corner		
Flexural Strength, psi	Modulus, psi	Thickness, inches	k=50*	k=150*	k=250*	k=50*	k=150*	k=250*	k=50*	k=150*	k=250*
100	5×10^5	9	14.8	18.5	18.7	9.7	11.5	11.8	6.6	7.2	7.5
		12	25.0	26.9	32.6	16.3	17.5	20.2	11.3	12.0	12.4
		15	36.8	39.8	41.2	24.0	26.2	27.2	16.5	18.0	18.4
		18	50.2	55.6	57.8	33.5	36.7	37.8	22.4	25.4	25.9
		21	68.4	73.5	76.4	44.1	47.8	50.0	29.4	32.3	34.5
200	1.4×10^6	9	27.8	29.7	36.6	18.1	19.4	22.5	12.4	13.2	13.8
		12	46.6	49.9	51.4	30.2	32.6	33.6	20.6	22.6	23.0
		15	69.8	75.0	77.2	45.0	48.8	51.0	30.0	33.0	35.2
		18	97.2	103.7	108.0	62.6	67.0	70.2	41.6	44.8	47.5
		21	129.4	136.7	141.1	82.3	88.2	91.1	54.4	58.8	61.0
300	2×10^6	9	40.5	43.7	45.4	26.3	28.4	29.6	17.8	19.4	20.2
		12	67.7	73.4	76.3	43.9	48.2	49.7	30.2	33.1	34.2
		15	102.4	109.1	113.6	65.2	70.9	74.2	43.3	48.4	50.6
		18	144.2	150.7	157.1	90.7	97.2	102.1	55.9	64.8	69.7
		21	187.4	200.6	207.3	119.1	127.9	132.3	78.3	84.9	88.2

*K (Modulus of Subgrade Reaction) psi/in.

Note: Contact area diameter = 10.5 inches

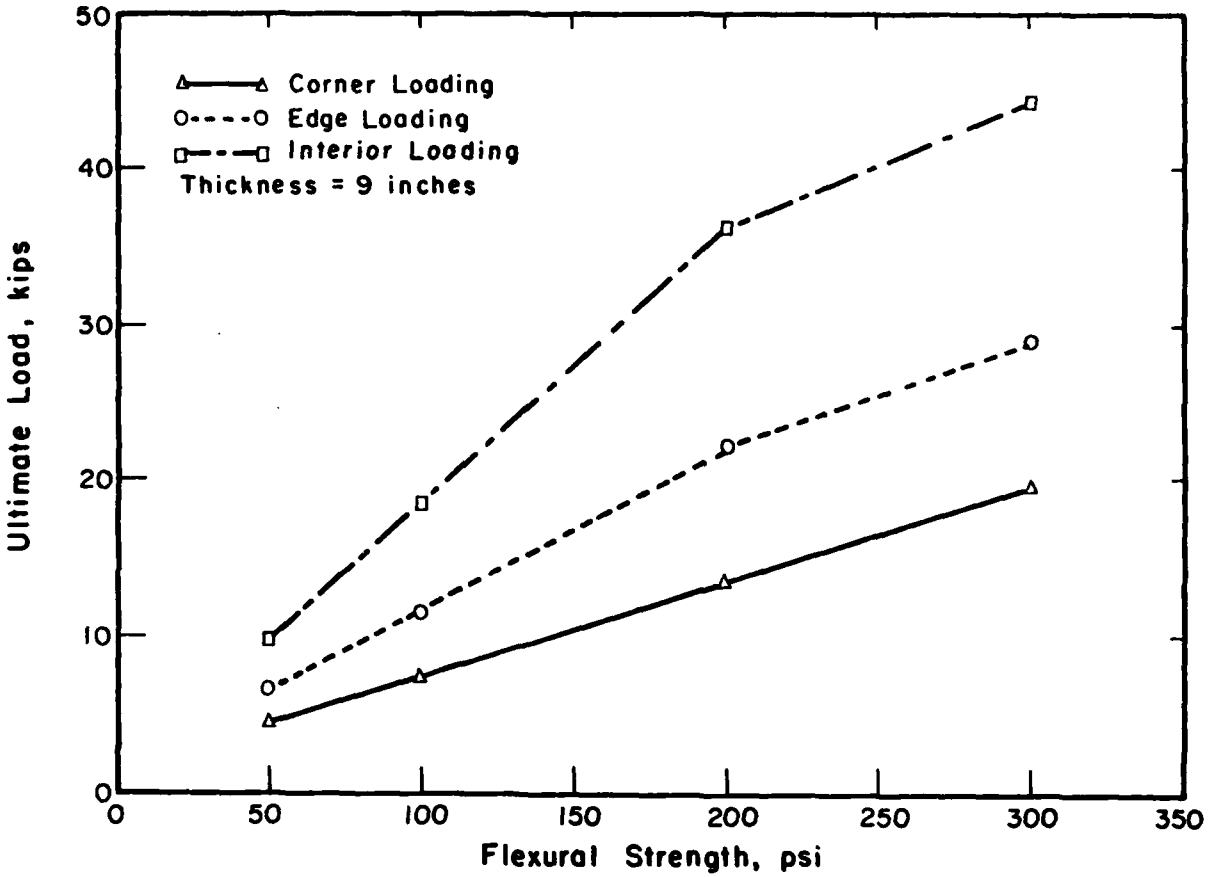

Figure 15. Ultimate Load vs Flexural Strength Relation (9-inch Thickness).

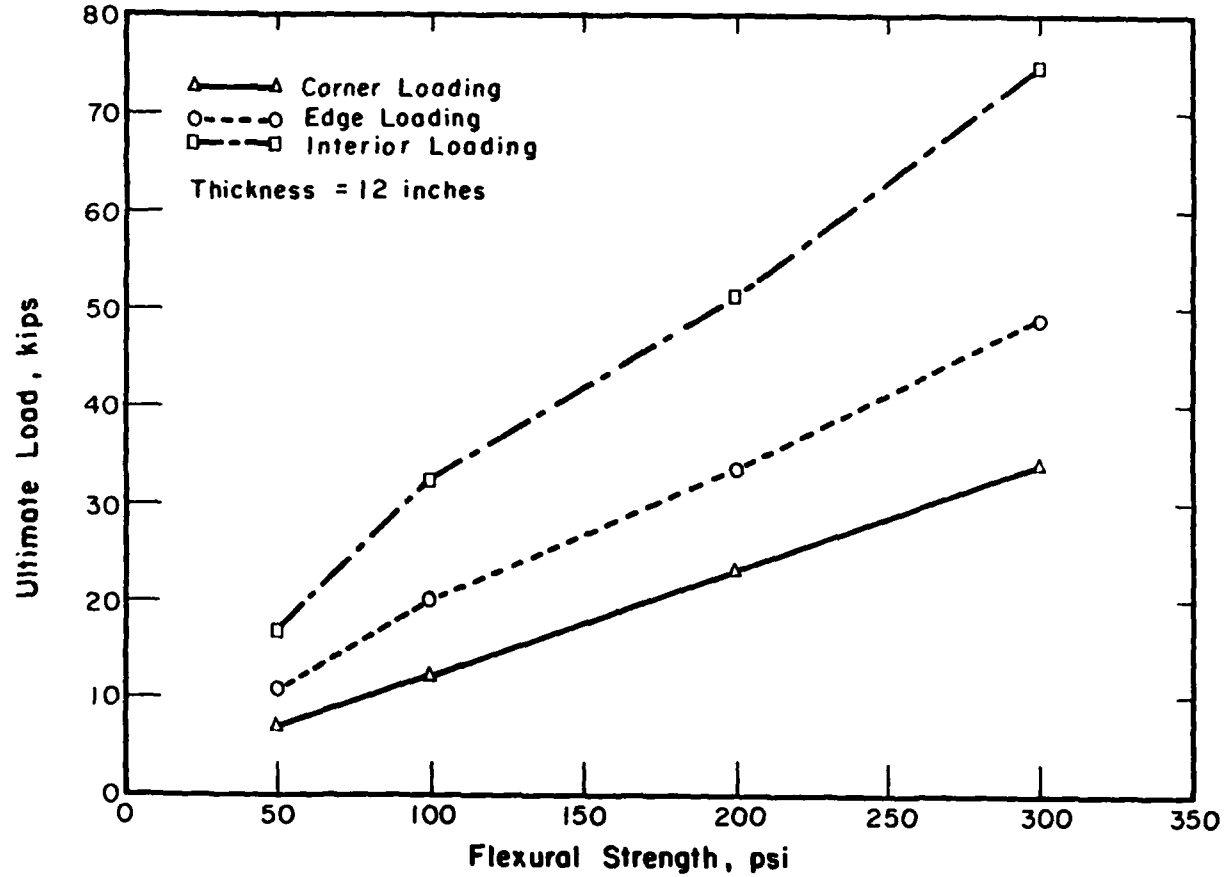

Figure 16. Ultimate Load vs Flexural Strength Relations (12-inch Thickness).

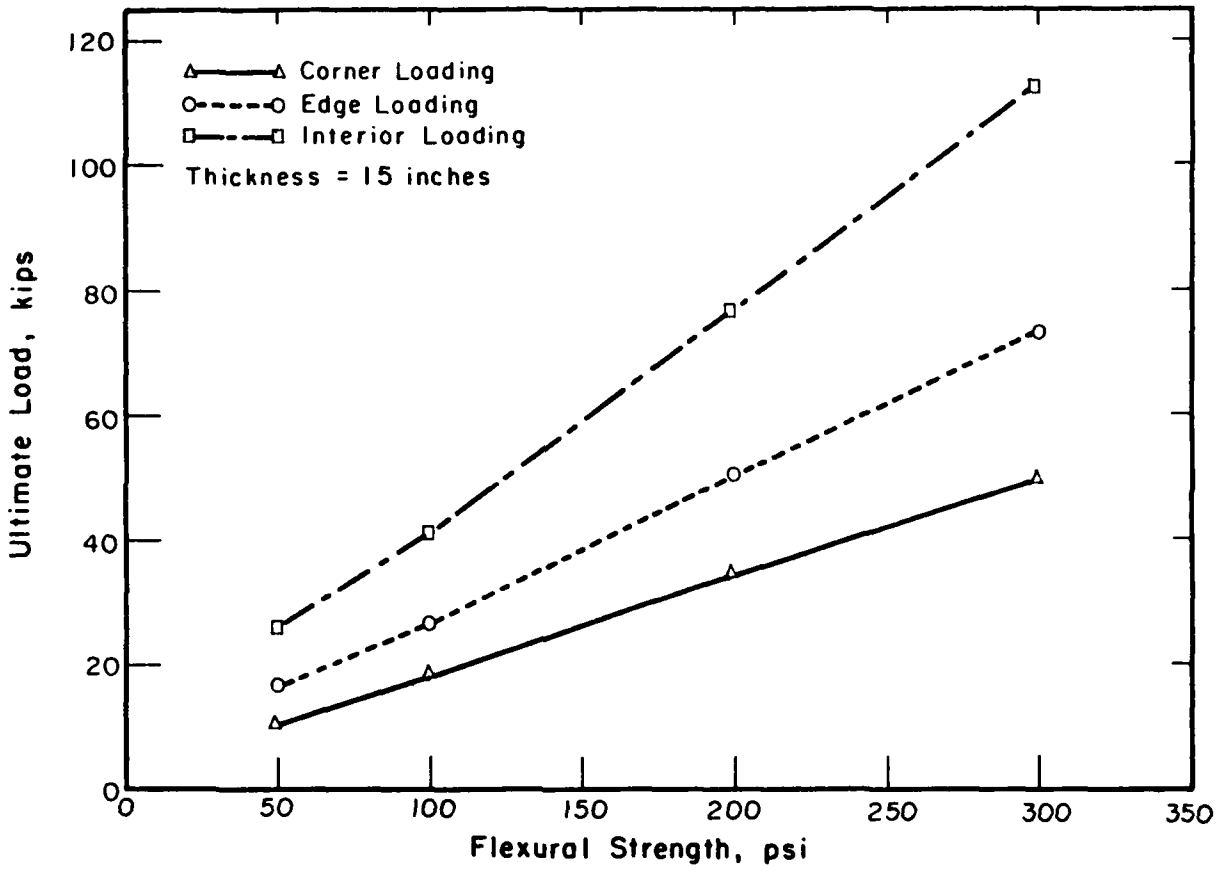

Figure 17. Ultimate Load vs Flexural Strength Relations (15-inch Thickness).

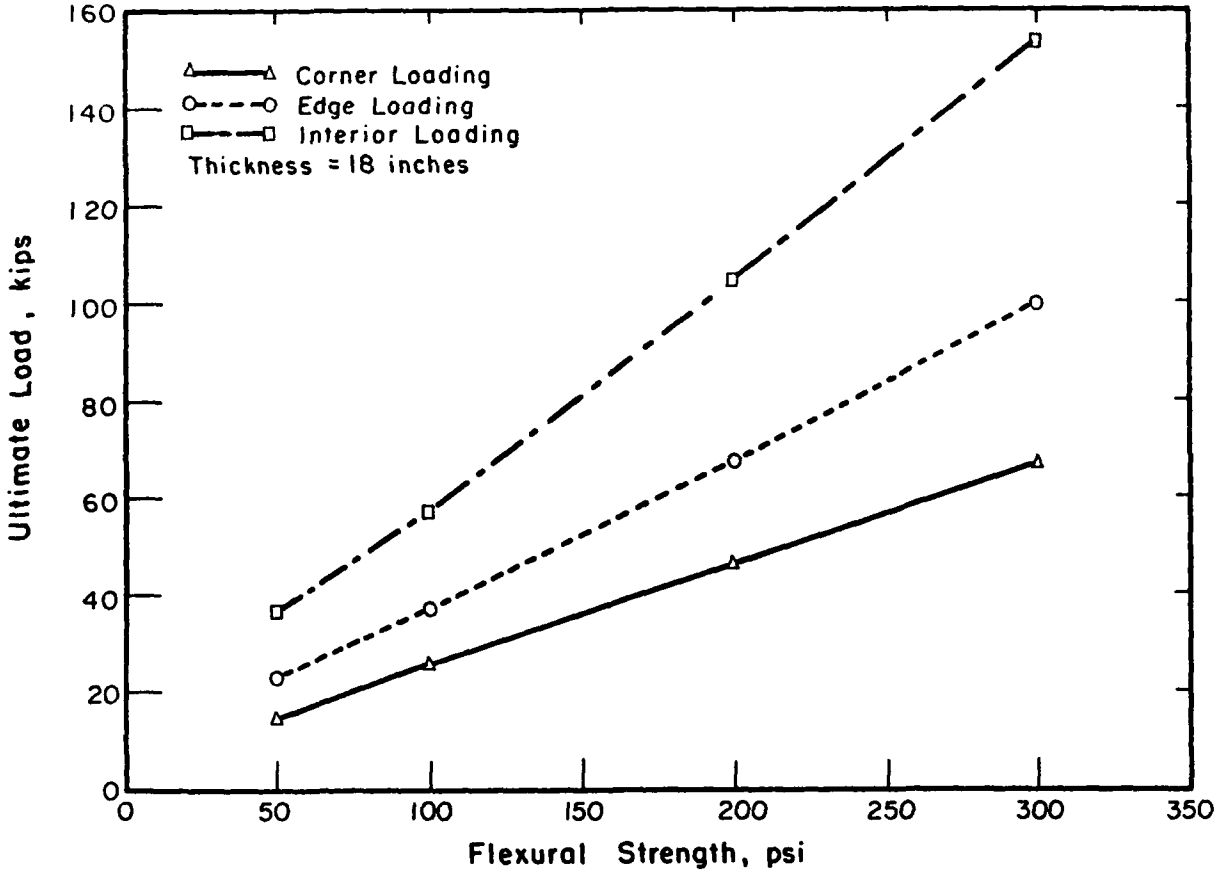

Figure 18. Ultimate Load vs Flexural Strength Relations (18-inch Thickness).

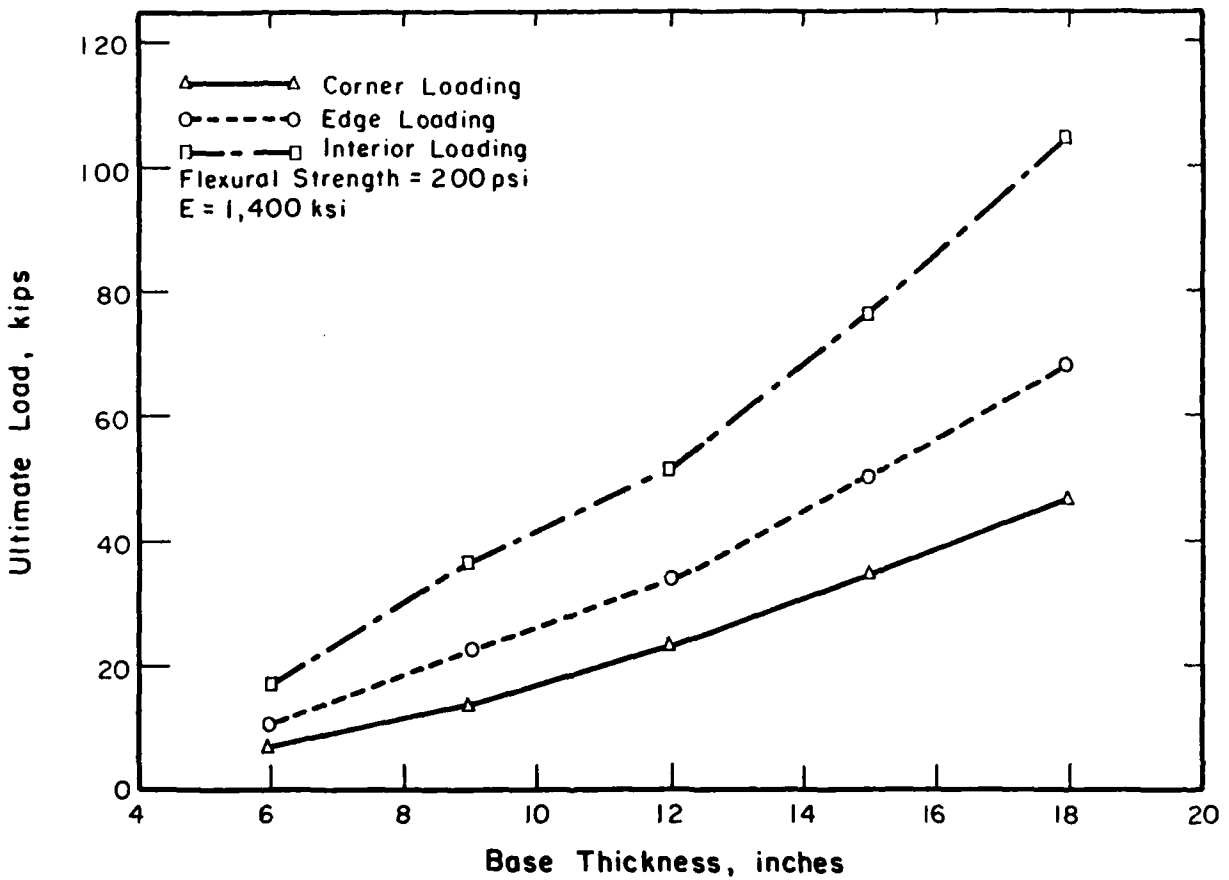

Figure 19. Ultimate Load vs Base Thickness Relations (Flexural Strength-200 psi).

TABLE 8. ULTIMATE LOAD DATA: C-130 AND F-4

Material Properties			Interior Ultimate Load Carrying Capacity, Kips					
			F-4			C-130		
Flexural Strength, psi	Modulus psi	Thickness, inches	k=50*	k=150*	k=250*	k=50*	k=150*	k=250*
50	$1x10^5$	6	4.4	4.6	4.7	9.4	13.2	16.6
		9	9.4	9.8	10.0	16.5	20.6	23.6
		12	16.4	16.9	17.2	25.7	30.6	33.8
		15	25.3	25.9	26.3	37.0	42.7	46.4
		18	29.7	36.8	37.3	50.3	56.9	61.1
100	$5x10^5$	6	8.3	8.6	8.7	23.1	26.9	29.5
		9	18.2	18.6	18.9	46.2	51.3	54.5
		12	25.0	32.5	32.8	77.1	83.7	87.8
		15	38.8	40.9	50.6	115.9	124.0	129.1
		18	52.5	57.2	59.5	162.4	172.3	178.2
200	$1.4x10^6$	6	16.2	16.6	16.9	24.0	27.8	30.3
		9	28.1	36.4	36.8	47.7	53.2	56.6
		12	48.0	51.4	53.3	79.4	86.7	91.0
		15	71.2	76.5	78.0	119.0	128.1	133.5
		18	100.3	104.8	111.2	(a)	177.4	183.9
300	$2x10^6$	6	19.8	24.7	25.0	34.5	39.5	42.7
		9	41.3	44.6	54.8	69.6	76.7	81.2
		12	69.8	74.9	72.0	116.4	126.0	131.8
		15	104.5	112.5	77.0	175.1	187.2	194.4
		18	149.0	154.0	162.0	(a)	260.1	268.9

* k (Modulus of subgrade reaction) psi/in

(a) a/L < 0.2, Meyerhof not applicable

The tread distances for the C-130 and F-4 are 172 inches and 215 inches, respectively. If paving lane widths are properly selected, true C-130 edge-loading conditions (single-tandem gear) will not be experienced. Thus, load-carrying capacities in excess of the Meyerhof C-130 single-tandem edge-loading (60 percent of the C-130 interior values shown in Table 8) can be achieved. If the C-130 single-tandem gear is tracking near the center of the paving lane, the most critical loading conditions will be when one wheel is at a transverse crack location and the other wheel is tracking 60 inches back. As soon as the leading wheel clears the transverse crack, only one wheel remains on the slab (assume zero load transfer). Meyerhof solutions (Reference 15) are not available for the condition where one wheel is at the transverse crack and tracking wheel is on the same slab at a location away from the crack. Meyerhof edge-ultimate load-carrying capacities for a C-130 wheel (contact radius of 12 inches) and typical ALRS pavement conditions are summarized in Table 9.

In general, an ALRS pavement with adequate ultimate load-carrying capacity for F-4 traffic can accommodate a limited number of C-130 load repetitions.

C. INVERTED PAVEMENT SECTIONS

An inverted pavement section includes a surface course (either an AC layer or a nonstructural type surface treatment), a high-stability granular layer, and a stabilized material base layer. The design variables are AC thickness, granular material layer thickness, strength and thickness of stabilized base, and subgrade modulus (E_{Ri}).

The ILLI-PAVE analyses of ALRS stabilized base sections (II.B.1) indicated that for good quality stabilized material the flexural stress in the stabilized base is primarily controlled by base course thickness. The surface course and granular layer of an inverted pavement section (1) alleviate reflection cracking from the stabilized base course, (2) reduce freeze-thaw cycles in stabilized base, and (3) reduce base course flexural stress.

TABLE 9. EDGE-ULTIMATE LOAD: C-130 SINGLE WHEEL

Material Properties			Edge Ultimate Load, kips		
Flexural Strength, psi	Modulus, psi	Thickness inches	k = 50*	k = 150**	k = 250*
50	$1x10^5$	6	5.1	8.9	15.7
		9	8.4	11.0	13.3
		12	13.1	15.6	17.6
		15	18.9	21.7	23.7
		18	25.8	28.9	31.0
100	$5x10^5$	6	7.0	8.7	10.1
		9	13.5	15.4	16.8
		12	22.2	24.6	26.1
		15	33.2	36.0	37.7
		18	46.4	49.6	51.6
200	$1.4x10^6$	6	12.2	14.1	15.5
		9	24.7	27.2	28.8
		12	41.7	44.7	46.7
		15	63.0	66.8	69.1
		18	78.5	93.2	45.9
300	$2x10^6$	6	17.7	20.1	21.7
		9	36.2	39.4	41.4
		12	61.4	65.4	67.9
		15	93.1	98.1	101.1
		18	115.0	137.3	140.9

* k (Modulus of subgrade reaction) psi/in.

Several ILLI-PAVE analyses were made for typical ALRS inverted pavement sections. Pavement response data for F-4 and F-15 loading are summarized in Table 10. Flexural base stresses for the inverted pavements were compared to the predicted flexural stresses (Equation (3)) for the base course thickness only. The comparisons indicate that the combined effect of the AC and granular layer is to reduce the stabilized base flexural stress to approximately 65 to 70 percent of the value for the "stabilized base course only," condition. Practical construction considerations limit the minimum thickness of AC plus granular layers to about 6 inches (2 inches AC + 4 inches of granular material).

D. LOAD PLACEMENT EFFECTS

Load placement influences pavement structural response. Flexural stress in the stabilized base course is the controlling design criterion. For given conditions (material strength and modulus, subgrade support, base thickness, loading) flexural stresses are lowest for interior loading and are greater for corner and edge locations.

Stabilized base courses are not continuous slabs. Transverse shrinkage cracks and longitudinal construction joints break the continuity of the stabilized layer. Other than interior loading will thus frequently occur, resulting in increased stabilized base course tensile stresses.

Cementitious base materials typically develop a transverse shrinkage cracking pattern following construction. The intervals between the cracks and the crack width are related to stabilized base strength. Higher strength materials display long intervals between cracks and the crack widths are wider. Lower-strength materials have shorter intervals between cracks and the crack widths are less. Mitchell et al. (Reference 16) have suggested typical values of 10-foot crack spacing for cement-treated fine-grained soils and 20 feet for cement-treated granular materials.

TABLE 10. ILLI-PAVE DATA FOR INVERTED PAVEMENTS

Loading		Thickness, in.		Stabilized Base		Surface Deflection, mils	Stabilized Layer Flexural σ, psi	Maximum Subgrade Deviator σ, psi
A/C	Wheel Load, Kips	AC*	Crushed Stone	Thickness, inches	Modulus, ksi			
F-4	27	2	6	10	1,400	29	159	3.2
F-4	27	2	6	10	2,000	27	169	2.6
F-4	27	-	6	8	700	38.4	213	5.9
F-4	27	-	6	10	700	34.1	160	4.9
F-4	27	-	6	12	700	31.3	117	4.1
F-4	27	-	6	14	700	29.7	91	3.5
F-4	27	-	8	12	1,400	32	118	2.6
F-4	27	-	8	12	2,000	31	123	2.2
F-15	30	2	6	9	2,000	41.5	260	2.5
F-15	30	2	6	12	2,000	38.0	160	1.8
F-15	30	2	6	15	2,000	36.2	100	1.4
F-15	30	2	9	12	2,000	43.1	140	1.7
F-15	36	2	6	9	2,000	48.1	310	2.8
F-15	36	2	6	12	2,000	43.9	185	2.1
F-15	36	2	6	15	2,000	41.8	120	1.6
F-15	36	2	9	12	2,000	49.5	165	2.0

Notes

* Asphalt Concrete Modulus = 500 ksi
Medium Subgrade for all F-4 Sections and Soft Subgrade for all F-15 Sections (Figure 3).

Longitudinal construction joints are also present in a stabilized base course. Typical base paving widths are 10-15 feet. A minimum of 4 longitudinal joints would be present in a nominal 60-foot wide ALRS runway.

Corner loading conditions develop at locations where longitudinal and transverse cracks intersect. For joint locations removed from the intersection points, edge-loading conditions prevail. Construction width layout can be arranged to develop an F-4 trafficking pattern, resulting primarily in interior and edge loading conditions.

It is necessary to consider load placement effects in thickness design. Based on the assumption that longitudinal construction joints will be properly located, it is proposed that interior and edge loading be considered for ALRS stabilized pavement thickness design. Linear elastic layer and the ILLI-PAVE stress-dependent finite element programs are only for interior loading conditions. Westergaard slab and Meyerhof ultimate load theories consider interior, corner, and edge loading. ILLI-SLAB (a finite element model) has no restrictions on load placement and can also accommodate varying degrees of load transfer between adjacent slab segments.

E. INTENSITY FACTORS

For routine thickness design, it is proposed that a stress intensity factor be applied to the calculated interior flexural stress to estimate the increased edge loadings. It is recommended that the ILLI-PAVE structural model be used for calculating the interior flexural stress.

Several approaches can be used to consider the intensity factors:

Westergaard edge stress is approximately 50 percent greater than the interior stress.

Pretorius (Reference 17) and Otte (Reference 18) utilized prismatic-solid finite element analysis techniques to consider

the behavior of "cracked " pavement sections containing high strength/modulus-stabilized materials. The studies indicated that the maximum edge-loading tensile stresses are generally not more than 1.4 to 1.45 times the interior-loading condition tensile stress.

Meyerhof's ultimate load theory relations are shown in Figure 14. For a/L values of approximately 0.2 (typical of ALRS stabilized base pavements), the interior collapse load is 50 percent greater than the edge collapse load.

Intensity factors suggested for design purposes generally are about 1.4 to 1.5. Brown (Reference 19) recommended 1.25 for lean-concrete base thickness design. Otte (Reference 18) suggests a range of values varying from 1.1 for moderate cracking with crack widths less than 2 mm to 1.4 for sections that are extensively cracked. Mitchell et al. (Reference 14) suggested a factor of 1.5.

An intensity factor of 1.5 is recommended for ALRS design purposes.

F. SLAB SIZE-JOINT EFFICIENCY EFFECTS

The ILLI-PAVE model can be programmed to simulate a circular slab of finite size. A ring of low modulus elements is used to simulate the "crack" in the slab. The modulus of the ring of low modulus elements also represents (to a limited extent) the effect of "crack transfer efficiency." A circular loaded area (center of slab loading) is applied. Thus, the effect of "slab size" can be considered for interior loading conditions.

A limited study was conducted for F-4 loading conditions and three circular slab sizes. The ranges of parameters considered and pertinent structural response data are summarized in Table 11.

Note that the effects of decreased slab size (for interior loading conditions) are:

TABLE 11. CIRCULAR SLAB SIZE EFFECTS

Base Material		Crack Material Modulus, psi	Crack Radius, inches	Pavement Responses			Subgrade Responses	
Thickness, in.	Modulus, psi			Maximum Flexural σ, psi	Maximum Deflection mils	Crack Efficiency, %	Maximum Vertical σ, psi	Maximum Strain, με
12	$1x10^6$	$1x10^6$	No Crack	175	20		7	400
12	$1x10^6$	1000	18	159	30	55	35	3800
12	$1x10^6$	1000	36	190	23	75	11	600
18	$1x10^6$	1000	18	64	24	55	31	3500
12	$1x10^6$	100	18	146	40	36	55	8000

Notes: 1) Medium subgrade conditions for all analyses

2) Loading: 265 psi; radius of loaded area = 6 inches

1. Increased maximum base course flexural stress;
2. Increased pavement deflection; and
3. Increased subgrade stress and strain.

For the F-4 loading condition, a minimum slab diameter of 36 inches (6 radii) closely approximates large slab responses.

A limited amount of load transfer between adjacent slab segments significantly decreases the edge stress. Load transfer efficiency is defined as:

$$\text{Efficiency (\%)} = \frac{\text{Adjacent Slab Deflection}}{\text{Loaded Slab Deflection}} \quad (100) \qquad (7)$$

Typical "load transfer" effects developed with the ILLI-SLAB model are shown in Table 12 for F-4 loading and typical ALRS type pavement sections. Maximum flexural stress and subgrade stress increase as joint efficiency decreases. Note that the flexural stress-joint efficiency relation is nonlinear. A small loss of joint efficiency significantly increases the flexural stress.

This review of cracked pavement behavior and load placement effects indicates that (compared to the interior loading condition):

1. Flexural stress will signficantly increase;
2. A small decrease in joint efficiency effects a large increase in flexural stress; and
3. Near boundary load placement or reduced effective slab size results in a large increase in subgrade stress.

Once the stabilized layer is extensively cracked (small slabs, etc.), excessive permanent subgrade deformations may occur. Performance will then be controlled primarily by subgrade strength. Subgrade strength and permanent deformation behavior are very sensitive to seasonal effects and are difficult to predict.

TABLE 12. JOINT EFFECTS FOR ALRS PAVEMENTS

Stabilized Base		Joint Efficiency,	Maximum Flexural Stress, psi	Subgrade Stress, psi
Thickness, in.	E, psi			
12	$1x10^6$	100	241	4.8
		91	351	5.0
		68	417	5.7
		40	458	6.9
		0	494	9.6
12	$2x10^6$	100	255	3.7
		87	400	4.0
		52	475	4.9
		0	520	7.4
16	$2x10^5$	100	125	6.4
		92	174	6.7
		57	222	8.2
		0	257	12.9

Notes: F-4 loading conditions

Subgrade k = 100 psi/inch

G. SUMMARY

It is proposed that ALRS stabilized pavements be designed using an "intact slab" approach. Although the pavements will initially develop longitudinal and transverse cracks, the slab thickness should be adequate to prevent significant additional cracking under aircraft loading. Thickness design should be based on edge loading conditions.

It is recommended that an intensity factor of 1.5 be used for initial ALRS design. If ILLI-PAVE interior radial tensile stresses are increased by 50 percent, the predicted stresses will probably be conservative (predicted stress < actual stress). This area needs further analytical and experimental study.

SECTION III

CLIMATIC MODEL FOR EVALUATING TEMPERATURE AND FROST ACTION IN ALTERNATE LAUNCH AND RECOVERY SURFACES (ALRS)

A. BACKGROUND AND DEVELOPMENT OF CLIMATIC MODELS

1. Heat Transfer and Moisture Transfer Models

A comprehensive literature review will indicate that numerical methods provide the most promising procedures for studying temperature and moisture in pavement systems with transient climatic conditions at the surface. The mathematics in the numerical method are simple, flexible, and well-suited for computer solution. The method can be adapted to the complex heat and moisture transfer conditions in multilayered pavement systems that occur as a result of changing thermal properties and changing climatic conditions.

The numerical methods generally utilize the Fourier diffusion equation for determining conductive heat transfer in building materials. The Fourier equation in the general one-dimensional form for heat transfer is as follows:

$$\frac{\partial^2 T}{\partial z^2} = \frac{1}{\alpha} \frac{\partial T}{\partial t} \tag{8}$$

In Equation (8), T is the temperature at some specific depth, z, in a material at time t. The thermal diffusivity, α, is related to the thermal conductivity, heat capacity, and unit weight of the material.

A review of the literature indicates that considerable effort has been made to solve heat transfer problems in soils and pavement systems. Table 13 shows that explicit and implicit finite difference programs as well as finite element programs which have been used to solve

TABLE 13. NUMERICAL METHODS APPLIED TO HEAT TRANSFER IN SOIL-WATER SYSTEMS

Name	Date	Type			Dimension				Soil				Boundary Conditions							Init. Conditions		Thermal Properties						Heat Transfer Mechanism				Type of Solution			
		Finite Diff.							Isotropic				Upper					Lower										Mass Flux							
		Explicit	Implicit	Finite Element	One-Dimensional	Radial	Two-Dimensional	Three-Dimensional	Homogeneous	Layered	Non-Homogeneous	Anisotropic	Air Temperature	Programmed Temp.	Surface Heat Flux	Constant Temp.	Periodic Temp.	Variable Temp.	Heat Flux.	Constant Temp.	Specified Temp.	Latent Heat	Unfrozen Moisture	k Constant w/Temp.	k Varies w/Temp.	c Constant w/Temp.	c Varies w/Temp.	Vapor	Vertical Liquid	Hor. Liquid	Conduction	Radiation	Temp. Profile	θ-F Isotherm	Tabular	Graphical
Hashari & Sliepcevich	1965		X		X	X	X		X	X			X		X			X	X		X	X	X		X			X	X		X	X		X
Carroll, Schenck, & Williams	1966	X			X				X	X			X		X	X					X	X			X		X			X		X		X	
Chwang	1967	X					X		X	X	X		X	X		X					X	X			X		X			X				X	
Dempsey & Thompson	1969	X			X				X	X			X		X	X					X	X			X		X			X		X	X	X	
Ho	1969		X		X		X		X	X			X	X		X					X	X	X		X		X			X		X	X	X	
Doherty	1970	X					X		X					X		X					X	X			X					X		X		X	
McDonnell-Douglas	1971	X			X	X	X		X	X	X		X	X	X	X					X	X	X		X		X			X		X	X	X	X
Makano & Brown	1971		X		X				X	X			X	X		X					X	X	X		X		X			X		X	X	X	
Pal'Kin	1971	X			X	X	X		X	1			X	X		X					1	X			X		X			X		X	X	X	
Perz & McDougall	1971	X			X				X	X			X	X		X					X	X		X		X				X		X	X	X	X
Esso Production	1970		X			X	X		X	X	X		X	X	X	X			X		X	X	X		X		X			X		X	X	X	X
Christison & Anderson	1972	X			X				X	X					X	X					X	X	X		X		X			X		1		1	
Dow Chemical Company	1972	X		X	X	X	X		X	X	X	X	X	X	X	X	X	X	X	X	X	X			X		X			X		X	X	X	
Goodrich	1972	X			X				X	X			X	X				X	X		X	X	X		X		X			X		X	X	X	X
Harlan	1972		X		X				X					X		X				X		X	X		X		1		X		X		1		1	
Huang, Murray, & Brooker	1972			X	X	X	X		X	X	X		X		X	X			X		X	X	X		X		X			X		X	X	X	
Meyer, Keller, & Couch	1972		X		X				X	X				X		X					X	X			X		X			X			X		X
Mohan	1972			X	X	X	X		X	X	X		X			X					X	X			X		X			X		X	X	X	
Williamson	1972	X			X				X	X			X		X	X					X				X		X			X		1		1	

Note: Dow Chemical Company has two programs.

heat transfer problems (Reference 20). Table 13 also shows that numerical methods can be programmed to consider many different soil conditions, boundary conditions, and soil thermal properties. Both one-dimensional and two-dimensional heat transfer can be determined by use of the numerical methods available.

Dusinberre (Reference 20) has contrasted the explicit and implicit finite difference methods for solving heat transfer problems. The explicit solution requires only one basic algebraic equation for each node which is used over and over again, and the future temperature of each node after a finite time step is computed from the present temperature. In the implicit solution, the future temperature of each node is determined after a finite time increment has passed. This method of solution requires a system of simultaneous algebraic equations and a large computer memory. An advantage of the implicit method is that it permits the use of large time steps while the explicit method requires a limit on the time step size in order to insure mathematical stability. In the explicit method the stability criteria require the use of small nodal depths also. The implicit method may become cumbersome when two-dimensional or complicated one-dimensional problems are solved, whereas the explicit procedure generally remains rather simple.

Berg (Reference 22) has indicated that the finite element techniques are very effective when solving heat transfer problems with complex geometries. He states that, for multidimensional heat flow problems, the finite element procedures frequently require less computer time than the finite difference procedures.

Carroll, Schenck, and Williams (Reference 23) were among the first to accurately predict the depth of frost penetration in a test pavement during a single winter period by using a finite difference, heat transfer model of the pavement and undertaking a stepwise digital computation in which actual weather data were used as the upper boundary condition of the model. This approach provided not only frost

penetration depth, which was taken as the 32°F isotherm, but, also, rather detailed predictions of temperatures throughout the pavement depth.

The computer program used by Carroll, Schenck, and Williams (Reference 23) to simulate the pavement temperatures was developed from a one-dimensional, explicit, heat transfer program developed by Schenck (Reference 24) for determining the frost penetration in moist homogeneous soil which had a surface boundary condition that varied in a sinusoidal manner over several years.

Straub, Schenck, and Przybycien (Reference 25) used a finite difference, heat transfer method for determining temperatures in an asphaltic concrete pavement system with much success. Since they were interested in extreme temperatures which occurred over short periods of time, they modified the finite difference computer program developed by Schenck (Reference 24) for exclusive daily use. This was accomplished by using smaller conduction nodes and time steps so as to obtain a more detailed picture of the subsurface temperature patterns than required when a complete year was involved. The finite difference heat transfer program was terminated at a depth below that which the daily temperature wave would penetrate. The basic principle of the finite difference method consisted of computing new sets of temperature in the pavement profile in response to changing air temperature and solar radiation conditions which were continually applied to the surface node during a daily time period. Straub, Schenck, and Przybycien (Reference 25) found that the pavement temperatures predicted by use of the finite difference method compared favorably with those actually measured in the pavement.

Numerous other investigators (References 26,27,28,29) have successfully used numerical finite difference methods to predict temperatures in pavement systems.

Corlew and Dickson (Reference 26) used a finite difference heat transfer method for studying the influence of temperature on field

compaction of hot-mix asphaltic concrete. They found that the finite difference method was well-suited to handling the complex boundary conditions peculiar to their study.

Christison and Anderson (Reference 27) adapted a finite difference heat transfer model to the study of thermal stresses in asphaltic concrete pavements in Western Canada. They concluded, that, in the absence of recorded pavement temperatures, a realistic assessment of the response of asphaltic concrete pavements to low-temperature climatic environments depends on a method whereby the pavement temperatures can be reliably predicted. Christison and Anderson were able to obtain reliable predictions of thermal regimes in asphaltic concrete surfaces subjected to actual climatic conditions by using numerical heat transfer methods.

Dempsey (Reference 28) and Dempsey and Thompson (Reference 29) developed a numerical heat transfer model for predicting the thermal regimes in multilayered pavement systems which considers many extrinsic climatic conditions and intrinsic pavement conditions. Many of these extrinsic and intrinsic conditions have been described by Johnson and Lovell (Reference 30). Dempsey (Reference 28) considered radiation, convection, and conduction in the development of his heat transfer model. The radiation heat transfer and convective heat transfer were related to the pavement surface by use of a micrometeorological energy balance technique. Dempsey (Reference 28) described the conductive heat transfer in the pavement system as a function of the unfrozen, freezing, and frozen states of the pavement materials.

Since temperatures and frost action in pavement systems are influenced by both moisture movement and material thermal properties, it is evident that complex analytical models are needed which account for moisture transfer as well as heat transfer.

The fact that temperature gradients can induce water movement in materials has been known for at least 50 years (Reference 31). Studies on the relative importance and interaction of thermal and suction

gradients in transporting moisture have been carried out by Hutchinson, Dixon, and Denbigh (Reference 32), Philip and de Vries (Reference 33), Taylor and Cary (Reference 34,35), Cassel (Reference 36), Cary (Reference 37), Hoekstra (Reference 38), Jumikis (Reference 39), and Dempsey (Reference 40). Jumikis (Reference 41), Harlan (Reference 42), Hoekstra (Reference 43), Berg, Guymon, and Johnson (Reference 44) and Dempsey and Thompson (Reference 45) are among those who have investigated moisture movement during the freezing process.

From a mechanistic approach, Phillip and de Vries (Reference 33) developed the following equation for water movement under a combined moisture and temperature gradient:

$$Q = D_\theta \nabla\theta + D_T \nabla T + K(\theta) \tag{9}$$

In Equation (9), Q is the net water flux, D_θ is the isothermal moisture diffusivity, $\nabla\theta$ is the moisture content gradient, D_T is the thermal moisture diffusivity, and ∇T is the temperature gradient. The terms D_θ and D_T are made up of two components each, one for vapor flow and one for liquid flow. The term $K(\theta)$ is the gravity term.

Dirksen (Reference 46) used the Philip and de Vries model to predict moisture movements in frozen soils. In his study, Dirksen (Reference 46) assumed that the soil-water diffusivity values could be expressed as exponential functions.

Dempsey (Reference 40) and Dempsey and Elzeftawy (Reference 47) have made reasonable predictions of transient moisture transfer in soils by using a finite element model based on the following form of the Philip and de Vries equation:

$$\frac{\partial\theta}{\partial T} = \nabla \cdot (D_T \nabla T) + \nabla \cdot (D_\theta \nabla\theta) + \frac{\partial K(\theta)}{\partial z} \tag{10}$$

Dempsey (Reference 40) has described the temperature gradient in Equation (10) as follows:

$$C \frac{\partial T}{\partial t} = \nabla \lambda \nabla T - L \nabla \cdot D_{\theta vap} \nabla \theta \qquad (11)$$

In Equation (11), C is the heat capacity, T is temperature, t is time, is λ thermal conductivity, L is heat of vaporization, $D_{\theta vap}$ is vapor diffusivity, and θ is water content.

In general, the temperature of a material influences water transport through its effect on the forces that cause the water to move, and through its effect on the conductivities and diffusivities in the various flux equations. In any given application of flow theory, the significance of the water transport due to nonisothermal conditions should be assessed. Water flow, in response to a temperature gradient, is usually in the direction of decreasing temperature. In porous media with a gas phase, a temperature gradient produces an associated vapor pressure gradient and a surface tension gradient. There is then a component of the vapor flux that can be related to the applied temperaure gradient, and a component of the liquid flux which is associated with the temperature gradient. Equations (10) and (11) can be used to model the moisture and temperature conditions in pavement systems as a function of time.

2. Extrinsic Factors in Climatic Modeling

Figure 20 shows many of the extrinsic factors which are important to a climatic model.

The extrinsic factors shown in Figure 20 indicate that a broad interpretation of climate is necessary when considering its influence on temperature and temperature effects in pavement systems. The climatic factors influencing pavement temperatures can be categorized as follows:

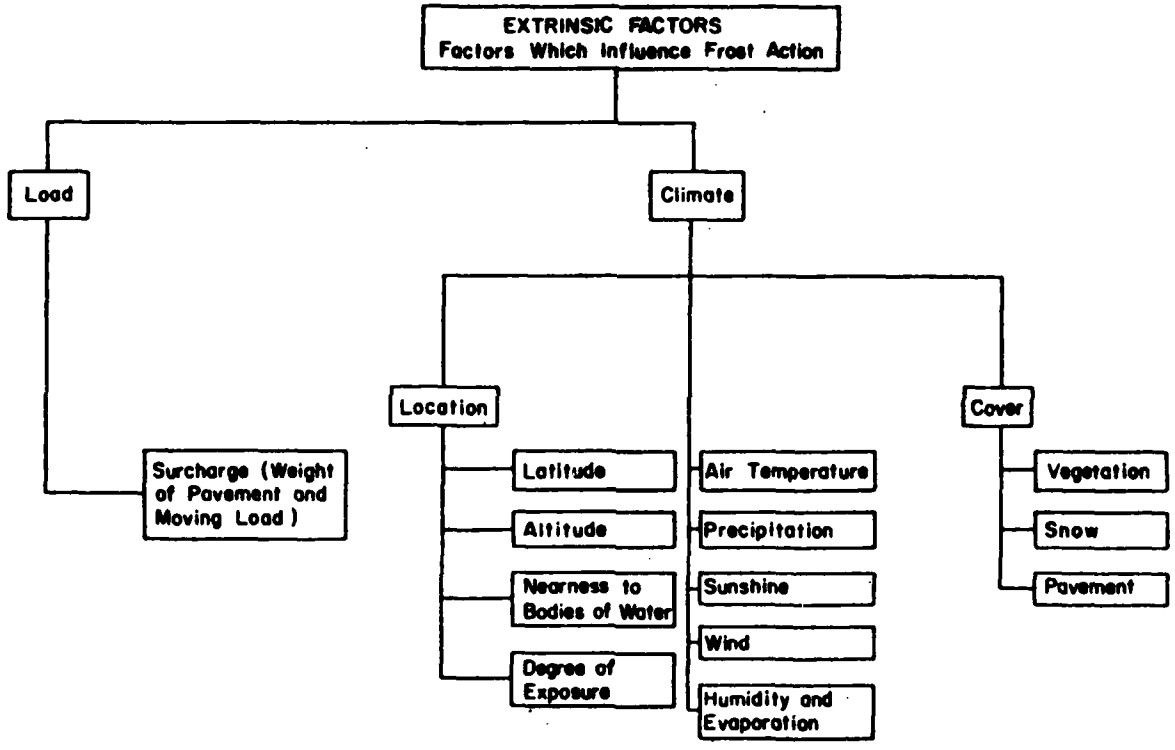

Figure 20. Extrinsic Factors Influencing Frost Action.

a. Temperature factors, which directly affect the transfer of heat to or from the pavement surface, such as air temperature, shortwave solar radiation, long-wave radiation, and wind.

b. Hydrologic factors, which exert an indirect influence on the temperature of the pavement system, such as precipitation, evaporation, and condensation.

c. Geographical factors, which exert a direct influence on weather and its outcome, such as elevation, latitude, degree of exposure, and nearness to bodies of water.

The temperature factors related to the pavement surface are among the most important input parameters in a climatic model. These factors are concerned with the net radiation heat transfer and the convective heat transfer into or out of the pavement system.

Although it is generally known that surface temperature and air temperature are related, the extent of the relationship is one of the most complex and fundamentally important problems to be solved when studying temperatures in pavement systems. The transfer of heat between the pavement surface and air is affected by evaporation and condensation of moisture, snow and ice melt, and most of all, by direct and diffuse solar radiation, net long-wave radiation between the surface and the sky, and convection. The radiation and convection heat transfer terms shown in Figure 21 are for a typical sunny day. The principal variables affecting the magnitude of thse factors are summarized as follows:

a. Solar and long-wave radiation:
   (1) Latitude and elevation of pavement system
   (2) Atmospheric vapor pressure
   (3) Type and amount of cloud cover
   (4) Atmospheric conditions (whether clear or hazy)
   (5) Type of pavement surface (color and texture influence the absorptivity and emissivity of radiant energy)

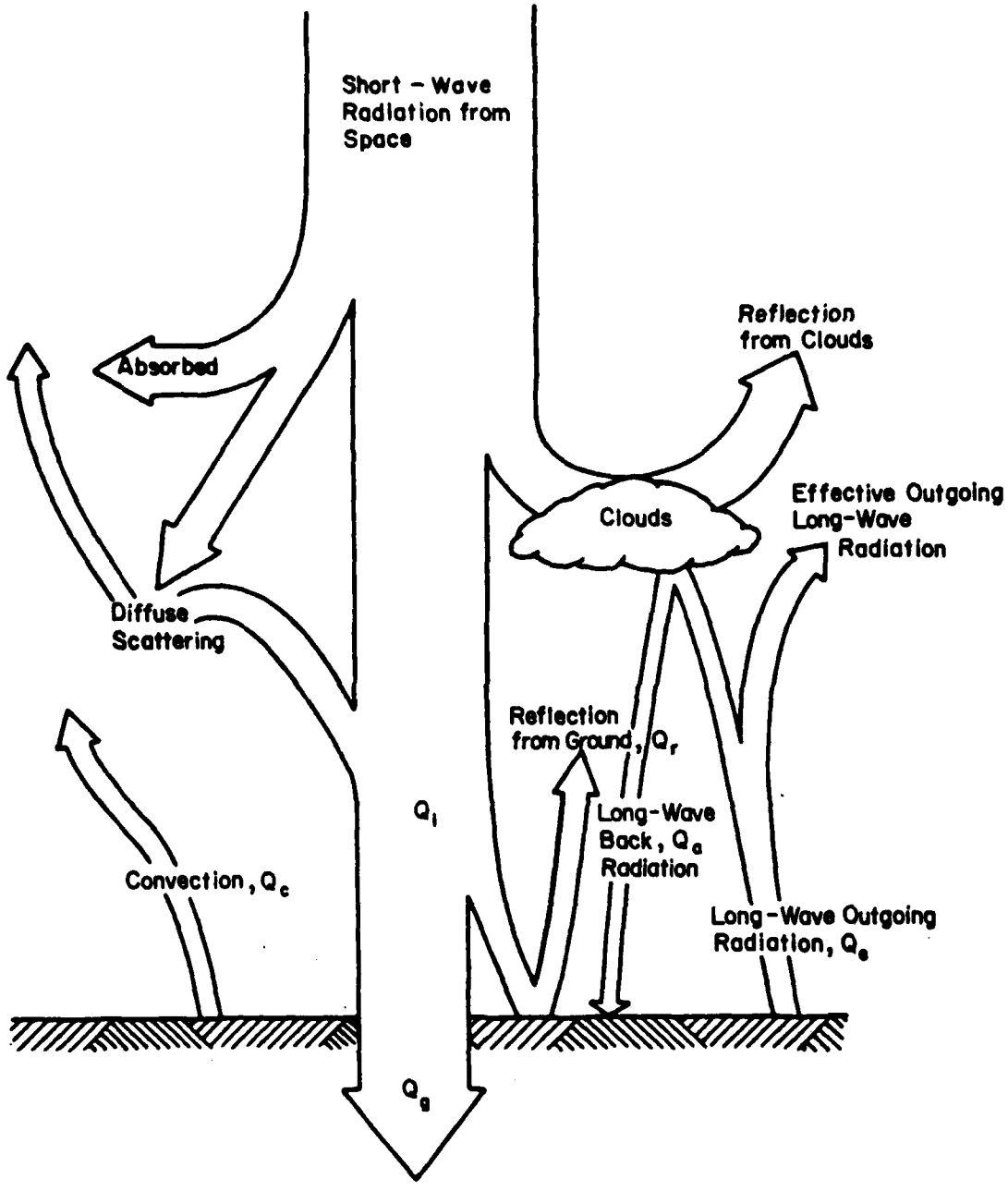

Figure 21. Heat Transfer between Pavement Surface and Air on a Sunny Day.

b. Convection:

(1) Wind velocity

(2) Type of pavement surface (surface roughnss)

(3) Type of topography and vegetation near the pavement

It is apparent that the magnitude of radiation and convection heat transfer depends on the unknown surface temperature itself; therefore, a detailed solution to the problem would have to involve a successive approximation procedure.

The simplest approach for developing a relationship between air temperature and pavement surface temperature is by use of a correction factor or n-factor to relate the temperature of the air to an equivalent temperature for the surface. However, the relatively wide range of values for the n-factor found for pavements (0.6-1.0) indicates the difficulty of using this procedure in analysis. It is evident that a more realistic approach for determining the relationship between air and pavement surface temperatures could be obtained by careful theoretical and experimental consideration of the controlling extrinsic variables.

By using meteorological parameters, Scott (Reference 48) found that the interaction between the air temperature and the pavement surface temperature could be analyzed more fully in terms of the climatic factors involved. Scott (Reference 48) and, more recently, Berg (Reference 49) performed elaborate analytical and experimental studies in order to establish a relationship between air temperature and pavement surface temperature based on a surface energy balance technique. In the energy balance approach, the algebraic sum of all heat flows at the surface must be zero. Both Scott (Reference 48) and Berg (Reference 49) considered heat flows toward the pavement surface as positive, heat flows away from the surface as negative, and heat flows in either direction as both positive and negative. A list of the various heat fluxes is shown in Table 14.

TABLE 14. HEAT FLUXES AT THE SURFACE OF A PAVEMENT

Flux	Symbol	Sign
Incident short wave radiation (solar radiation)	Q_i	+
Reflected short wave radiation	Q_r	-
Long wave radiation emitted by the atmosphere	Q_a	+
Long wave radiation emitted by the pavement surface	Q_e	-
Convection	Q_c	±
Transpiration, condensation, evaporation, and sublimation	Q_h	±
Conduction into air	Q_u	±
Mass flow to surface (precipitation)	Q_p	±
Conduction into the pavement	Q_g	±
Infiltration of moisture into pavement	Q_m	±

Based on the heat fluxes, shown in Table 14 Berg (Reference 49) derived the following energy balance equation:

$$Q_i - Q_r + Q_a - Q_e \pm Q_c \pm Q_h \pm Q_u \pm Q_p \pm Q_g \pm Q_m = D \quad (12)$$

A detailed discussion of the major climatic factors involved in Equation (12) has been given by Scott (Reference 48); however, the heat quantities will be briefly defined to provide a better understanding of the energy balance technique.

a. Shortwave Radiation

Shortwave radiation, which includes the complete spectrum of solar radiation and has wavelengths between 0.15μ and 3.5μ, is the principal source of heat energy during the day. The amount of energy received at a site depends upon the location, the time of day, time of year, and the weather. On its way through the atmosphere the solar radiation is reduced by air, dust, and clouds, and, at the surface, some energy is reflected back, leaving a net amount of shortwave radiation at the surface.

b. Longwave Radiation

Longwave radiation which has wavelengths between 3.5μ and 150 μ exists as an exchange of heat energy between the pavement surface and the sky or cloud cover. Longwave radiation arises from the fact that all bodies emit radiation according to their surface temperatures and properties. Since the intensity of radiation depends on the absolute temperature of the emitting body, it follows that the earth and clouds are comparatively long wave radiation emitters while the sun at its much hotter temperature would be a shortwave emitter. Longwave radiation is very evident on cold, cloudless nights in winter when large quantities of heat are radiated from the earth's surface.

c. Convective Heat Transfer at the Pavement Surface

Convective heat transfer is a process of energy transport by the combined action of heat conduction, energy storage, and mixing motion between a pavement surface and a surrounding fluid such as air. Heat transfer by convection is a complicated process and many attempts have been made to derive a sound theory for the transfer processes in air. Differences in the convection heat transfer coefficient depend upon the orientation of the surface, the surface roughness, and the type of cover. If a wind is blowing over the surface, the heat transfer process is accelerated by the air turbulence. Most of the convection data come from experiments in the field since most laboratory approaches to the problem have been unsuccessful. Data from wind tunnel and pipe flow measurements do not appear to be adaptable to the needs of the meteorological problem.

d. Transpiration, Condensation, Evaporation, and Sublimation

These heat quantities are involved in the phase changes of water substances and in part may be ignored in pavement computations where water and snow removal are fairly rapid.

e. Conduction into the Pavement System

The net amount of heat energy left for conduction into the pavement system depends upon the energy balance of the other quantities.

Useful correlations between cloud cover and the amount of total shortwave radiation received at the earth's surface have been made by Hamon, Weiss, and Wilson (Reference 50). They developed empirical relationships between the incident shortwave radiation received at the earth's surface and the percentage of possible sunshine, latitude, and time of year.

Similarly, Baker and Hanes (Reference 51) and Pochop, Shanklin, and Horner (Reference 52) have developed regression equations for correlating incident shortwave radiation, Q_s received at the earth's surface with the percentage of possible sunshine, S. The general form of the regression equation resulting from the work by Baker and Hanes (Reference 51) is as follows:

$$Q_s = R^* \left(A + B \frac{S}{100}\right) \tag{13}$$

The extraterrestrial radiation, R*, can be theoretically calculated for a given location from the solar declination, latitude, and solar constant which is about 442 Btu/ft^2-hr (Reference 52). The terms, A and B are constants for a given geographical area.

From Figure 22, it is observed that the intensity of solar radiation varies parabolically from sunrise to the time of sunset. Based on this observation, the amount of shortwave radiation received at a pavement surface during a finite time increment, t, can be calculated by assuming that the total daily extraterrestrial radiation varies in a parabolic manner from the time of sunrise to the time of sunset. The values for the total daily extraterrestrial radiation and the times of sunrise and sunset are easily used in the numerical model since they essentially do not change from year to year at any given site. Furthermore, the parabolic radiation distribution is readily programmed for a digital computer. The value of R* can be obtained from the parabolic radiation distribution at any specified time during the day. The value of R* is taken as zero during nighttime.

3. Intrinsic Factors in Climatic Modeling

Figure 23 shows the intrinsic factors influencing temperature and moisture in pavement systems. Dempsey (References 28,40) has discussed in detail most of the intrinsic factors which influence moisture and temperature pavement systems. It is generally agreed that

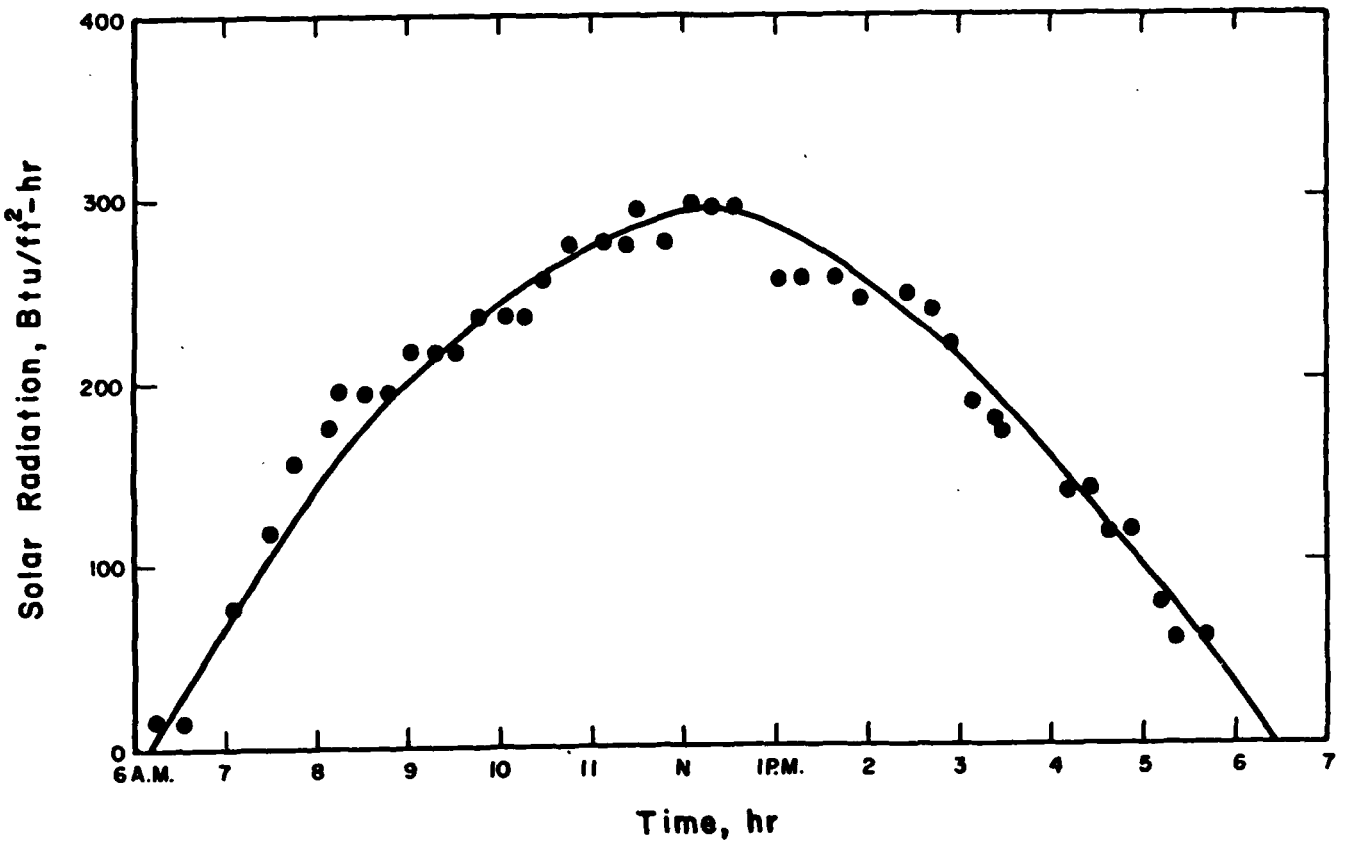

Figure 22. Variations in Solar Radiation Intensity.

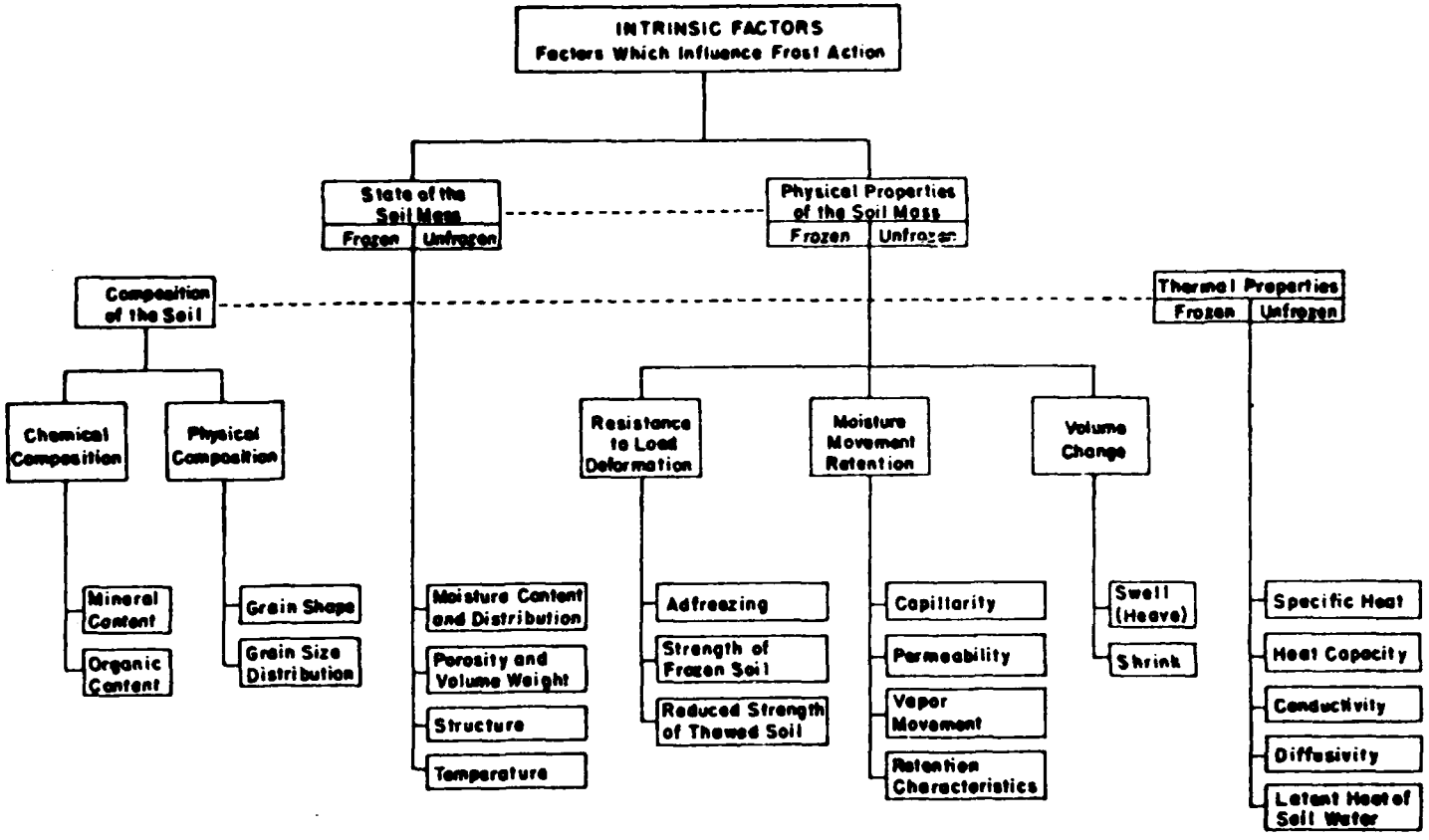

Figure 23. Intrinsic Factors Influencing Frost Action.

the most important intrinsic factors required in a climatic model are the material properties such as thermal conductivity, heat capacity, latent heat of fusion, and hydraulic conductivity.

The thermal conductivity, k, is the quantity of heat which flows normally across a surface of unit area per unit time under a unit thermal gradient. The most common units of thermal conductivity are Btu/hr-ft- °F, Btu/hr-ft^2 - °F/in., or Cal/sec-cm- °C. Experimental measurements of thermal conductivity can be accomplished by several methods, all of which are based on the observation of the temperature gradient across a given area of the material conducting heat at a known rate.

The heat capacity, c, is the amount of thermal energy necessary to cause a 1-degree temperature change in a unit mass or unit volume of substance. The units of heat capacity depend on whether mass heat capacity or volumetric heat capacity is used. Mass heat capacity has the units of Cal/g-°C or Btu/lb-°F. The units of volumetric heat capacity are Btu/ft^3- °F or Cal/cm^3- °C. Generally the heat capacity is computed from a heat balance between the heat gained by water in a calorimeter and the heat gained by the specimen.

The latent heat of fusion, L, is the change in thermal energy in a unit volume of material when the moisture in that material freezes or thaws at a constant temperature. The common units for the latent heat of fusion of soil moisture are Btu/ft^3, or Cal/cm^3. The latent heat depends upon the percentage of water which can be frozen in a given volume of material at any given temperature.

The hydraulic conductivity, $K(\theta)$, has the units of ft/sec or cm/sec and it provides a measure of the ability for a material to conduct moisture. The hydraulic conductivity is maximum for saturated conditions and decreases as a material becomes drier.

Most of the literature concerned with the thermal properties of pavement materials are found in general tables or are shown in scientific research. The values for hydraulic conductivity are shown in the literature or they can be determined experimentally in the laboratory.

B. CLIMATIC MODEL FOR ALRS

1. Heat Transfer Model

The model used to determine temperature and frost action in alternate launch and recovery surfaces as a function of time was based mainly on a previous heat transfer model developed by Dempsey (Reference 28) and Dempsey and Thompson (Reference 29). This model was developed from a temperature equation similar to Equation (11) by using five different mathematical procedures. Although transient moisture conditions could be predicted using a model based on Equation (10), only equilibrium moisture conditions were considered in predicting temperatures and frost action in ALRS. The moisture content of the pavement materials and subgrade is considered in the determination of the thermal properties of the various layers. This method of including moisture has been found to give predicted pavement temperatures which compare favorably with measured values in the field (Reference 3).

a. Pavement System Model

Figure 24 shows a typical finite difference pavement system used in the climatic model for computing pavement temperatures. The pavement system consists of a column of nodes that have a cross-sectional area of 1 square foot.

Nodes 2 through 37 are termed normal nodes. The nodal depth, X, and the number of nodes are chosen so as to ensure mathematical stability and so that the interface between pavement layers will be located at a nodal center. Nodes 2 and 6 are also mixed nodes because

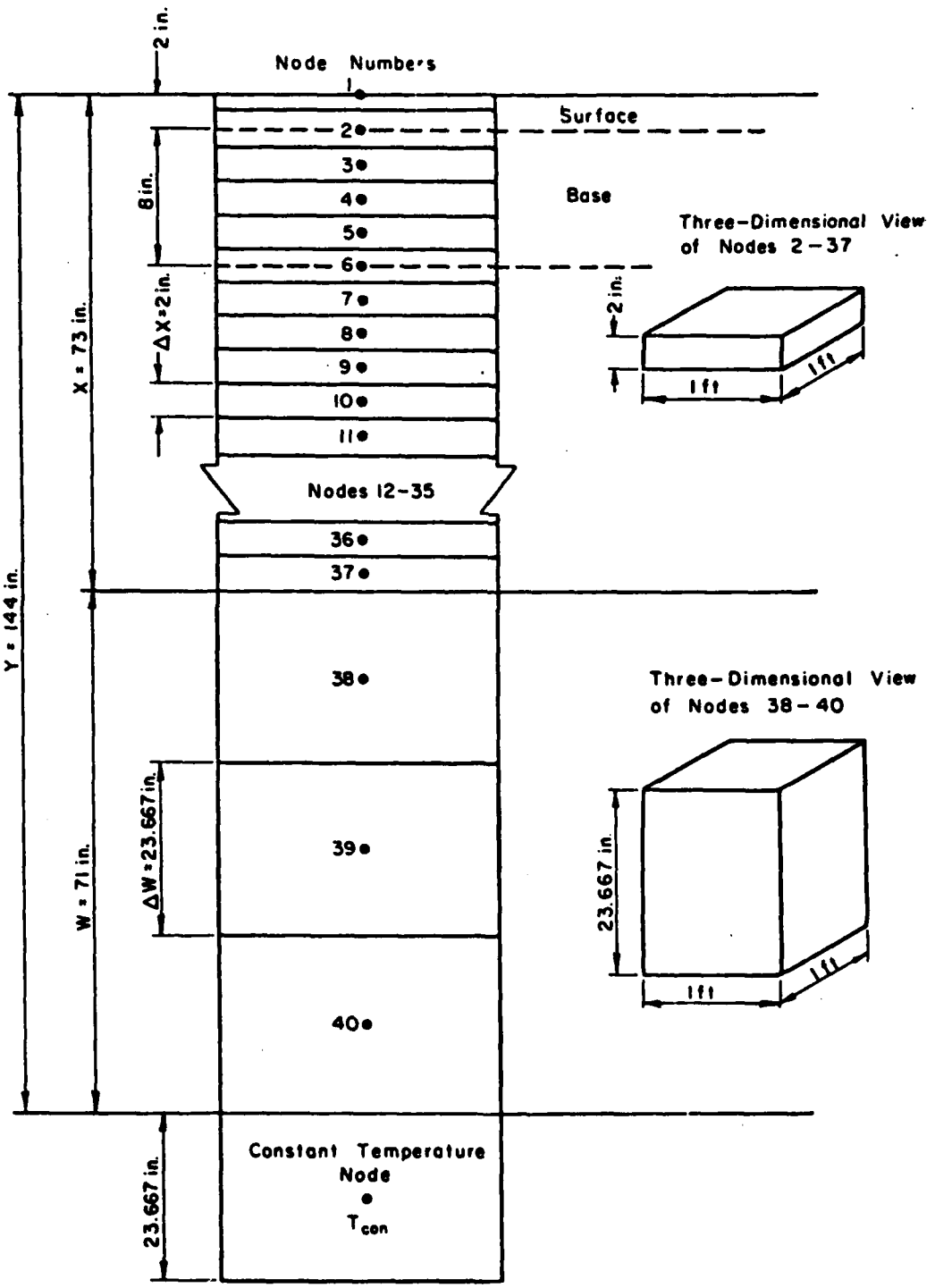

Figure 24. Typical Finite Difference Pavement System.

the thermal properties of these nodes correspond in part to the thermal properties of the adjacent pavement layers.

Node 1 consists of one-half of a normal node so that the nodal center will lie on the pavement surface. Node 1 at the pavement surface is the node at which the meteorological parameters are introduced and an energy balance is achieved.

Nodes 38, 39, and 40 are termination nodes and their purpose is to reduce computational time. The termination nodes replace the smaller nodes and reduce the total number of nodes in the finite difference pavement system with only a small increase in the finite difference error. Also, because the temperature variations decrease with increasing depth in the pavement, the increased depth of the bottom nodes, W, will not cause a large increase in the computational error.

b. Climatic Data Input

The most important parameters involved in the climatic model for ALRS are those related to the surface node of the pavement system. The meteorological heat transfer at the pavement surface was modeled from the energy balance relationship given by Equation (12) and shown in Figure 21.

A more thorough discussion of the climatic input procedures can be found in previous work by Dempsey (Reference 28) and Dempsey and Thompson (Reference 29).

c. Thermal Properties of Pavement Materials

The most important intrinsic factors considered in pavement temperature and frost action are the thermal properties of the materials, which include thermal conductivity, heat capacity, and latent heat of fusion. The climatic model recognizes three different sets of

thermal properties, depending on whether the pavement material is in an unfrozen, freezing, or frozen condition.

The procedures for determining the thermal properties of the pavement materials have been described in detail by Dempsey (Reference 28). The thermal properties of the surface materials such as concrete and asphalt concrete are determined from tables of physical properties or from previous research.

The methods developed by Kersten (Reference 54) are used for determining the thermal properties of the base, subbase, and subgrade soils.

The heat capacity of a pavement material during freezing is determined from the latent heat of fusion of the moisture in the material. When the moisture in the pavement freezes, the portion that is about to change phase remains at a constant temperature, the freezing temperature, until the latent heat of fusion is released. The time lag caused by this process retards the rate of frost penetration. The latent heat effect is incorporated into the finite difference equations by using a freezing zone. The freezing zone is a small, hypothetical temperature range over which freezing takes place. Because only moisture effects are considered in this range, the freezing heat capacity in the freezing zone is a function of the moisture content, dry density, and the small freezing temperature range. Although the freezing zone is a variable input to the climatic model, a temperature range between 30°F and 32°F is normally used for granular materials.

d. Validity of Climatic Model

The validity of the climatic model has been well established by comparing predicted and measured data from laboratory and field studies (References 28,29). Figures 25 and 26 provide typical comparisons between temperatures predicted by use of the climatic model and those measured in the field.

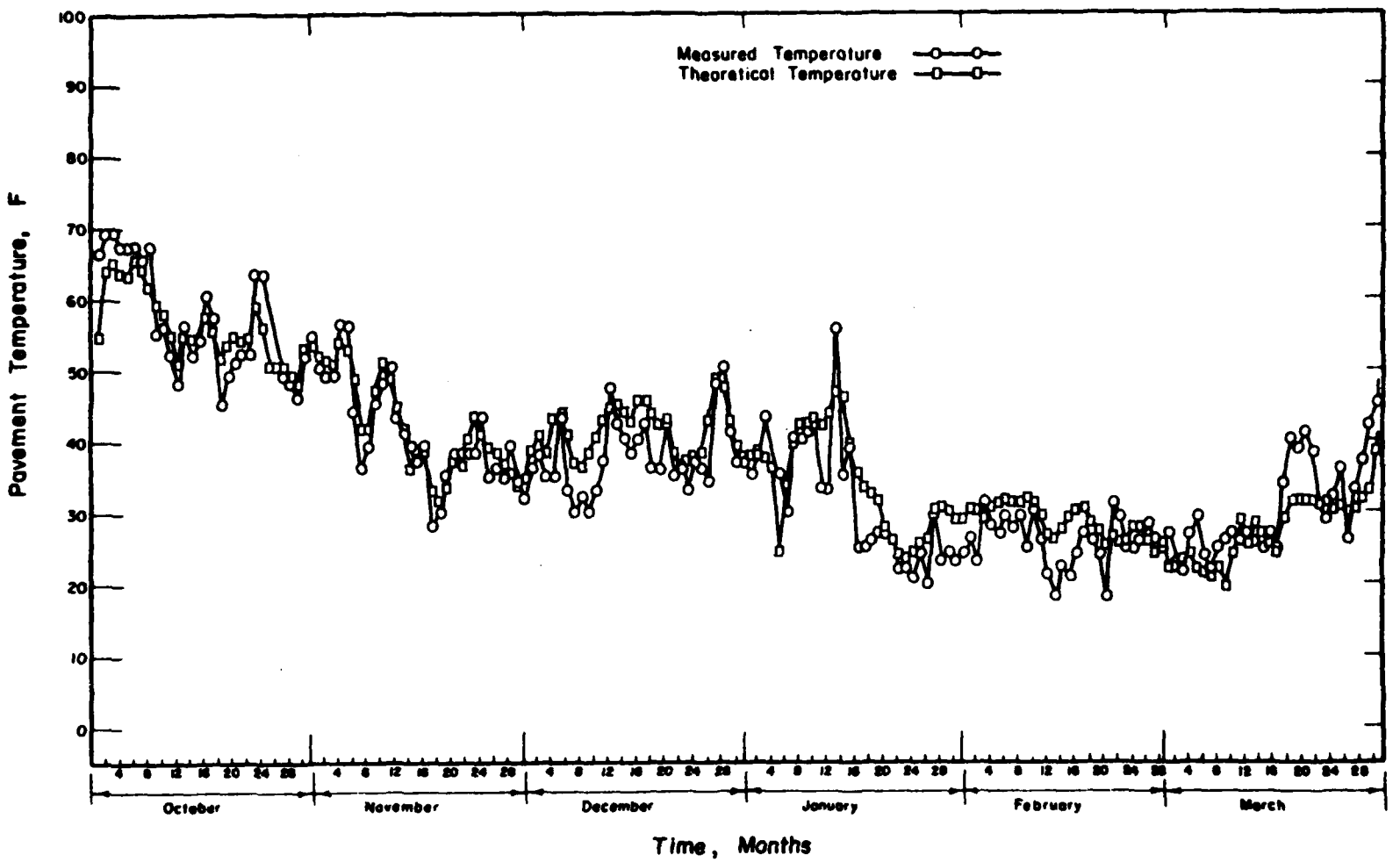

Figure 25. Comparison of Measured and Theoretical Temperatures at the 6-inch Depth of a 6-inch Asphalt Concrete Pavement at 0600 Hours, AASHO Road Test 1959 to 1960.

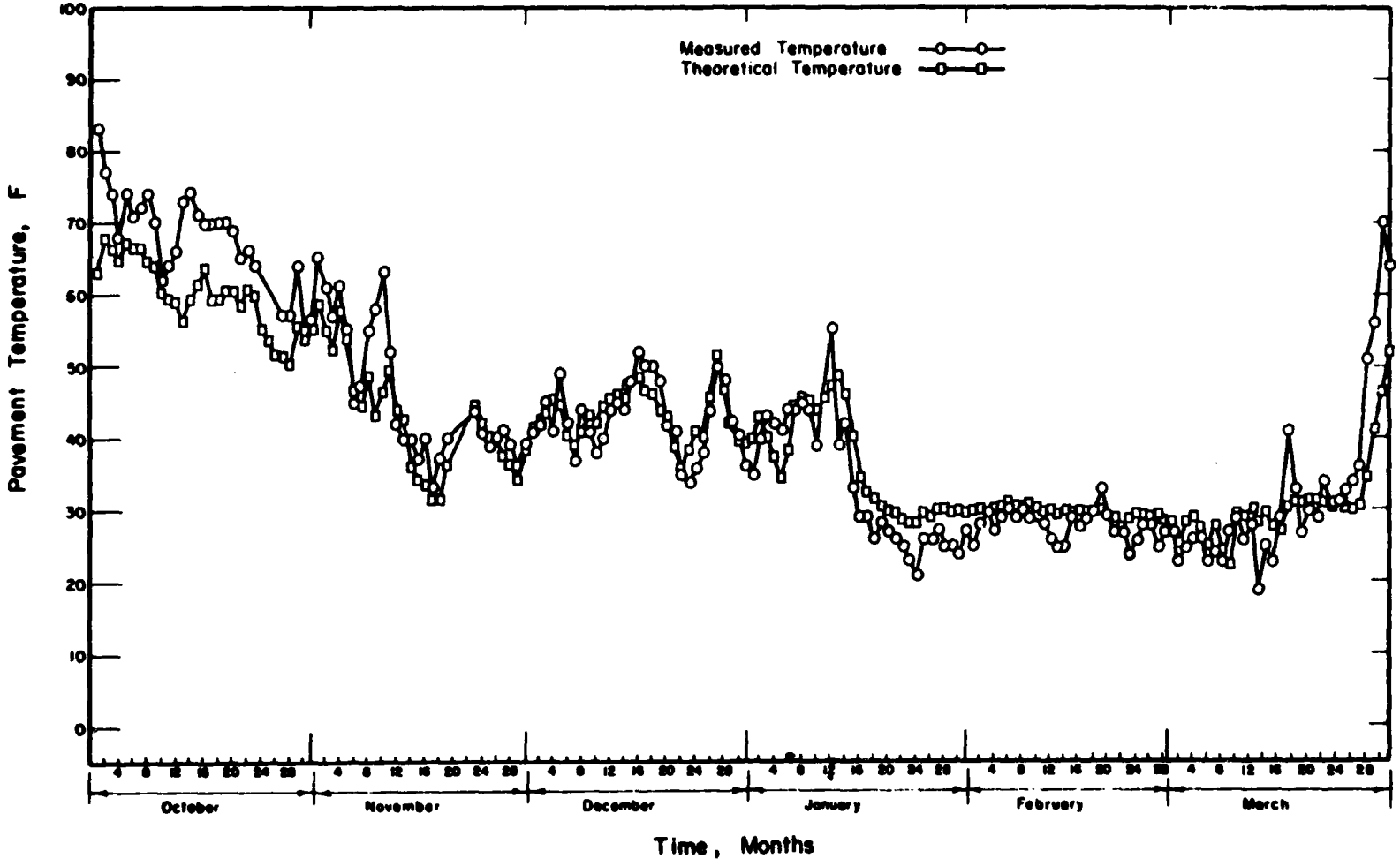

Figure 26. Comparison of Measured and Theoretical Temperatures at the 6-inch Depth of a 6-inch Asphalt Concrete Pavement at 1500 Hours, AASHO Road Test 1959 to 1960.

2. Moisture Modeling for ALRS

Moisture is of primary importance in ALRS design and performance. The shear strength of soil is very sensitive to change in moisture content. Black (Reference 55) has shown California Bearing Ratio, which is a measure of relative shear strength, to be inversely proportional to moisture content. Thus, the shear strength of a given subgrade can be expected to vary as moisture content changes with climate.

Thompson and Robnett (Reference 56) found that the dynamic or resilient modulus of unsaturated soils depends on moisture content. As the moisture content increased, the resilient modulus decreased. They have shown that the resilient modulus decreases with the percentage of saturation for a broad range of soils, Figure 27. Simonsen and Ajalmarsson (Reference 57) have found that the average resilient modulus for base course sections was a function of the water table depth and decreased as the water table depth decreased, Figure 28.

Moisture is a major factor on frost heaving and freeze-thaw effects in pavement systems. Taber (Reference 58) states that the amount of frost heaving that takes place is limited by the supply of available water. This water can either be already present in the soil or be drawn up from points below the depth of freezing. However, the rate of water flow in an unsaturated soil is controlled by the unsaturated hydraulic conductivity, which decreases substantially with a decrease in moisture content (Reference 59). Therefore, moisture content influences frost heaving directly as readily available water and indirectly by affecting the unsaturated hydraulic conductivity.

Figure 29 shows the influence of water table depth on the frost heave of a sandy gravel subgrade (Reference 60).

Thompson and Dempsey (Reference 61) have shown that the resilient behavior of fine-grained cohesive soils is greatly affected by

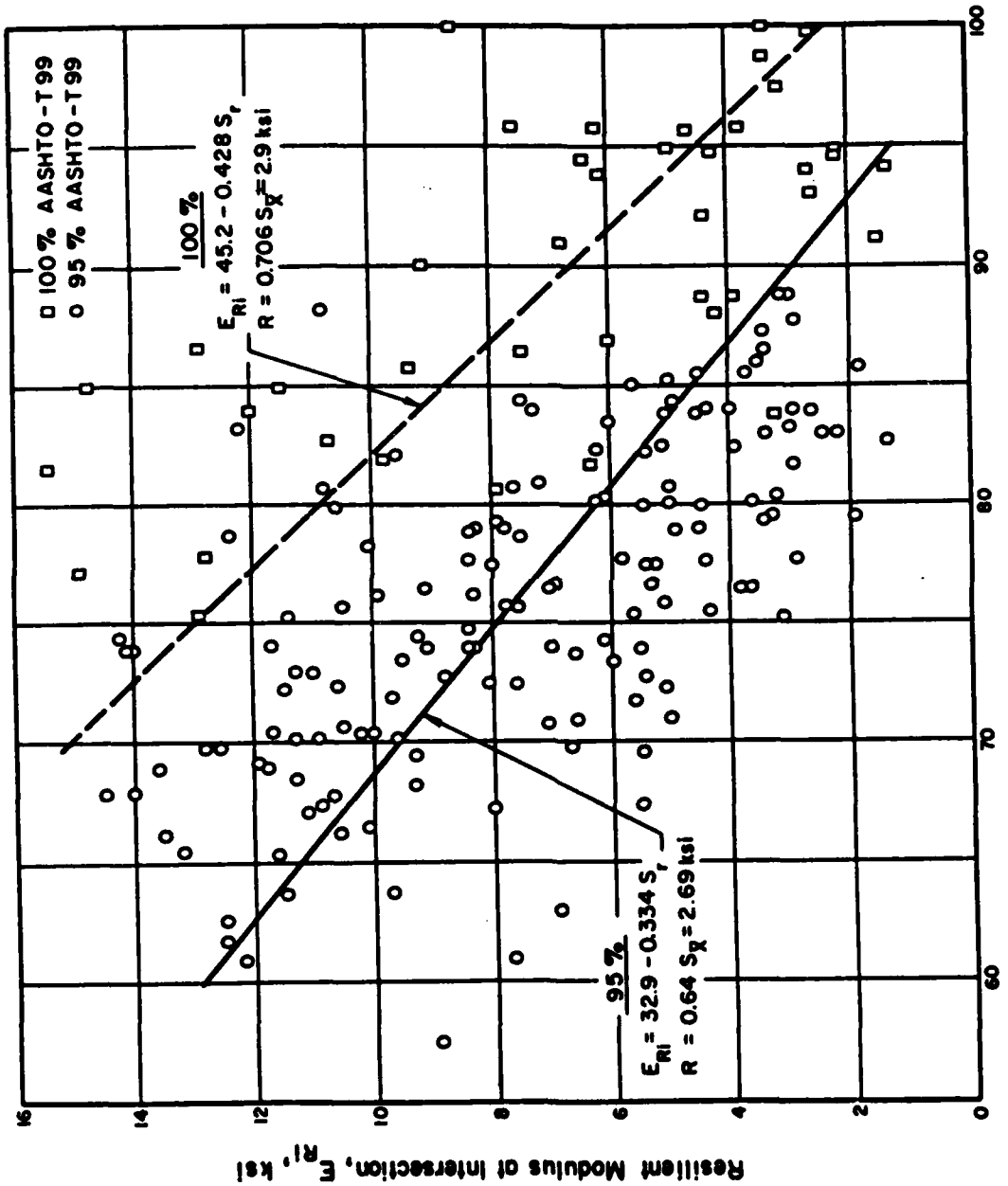

Figure 27. Resilient Modulus Versus Percent Saturation Relations for 95- and 100-Percent Compaction.

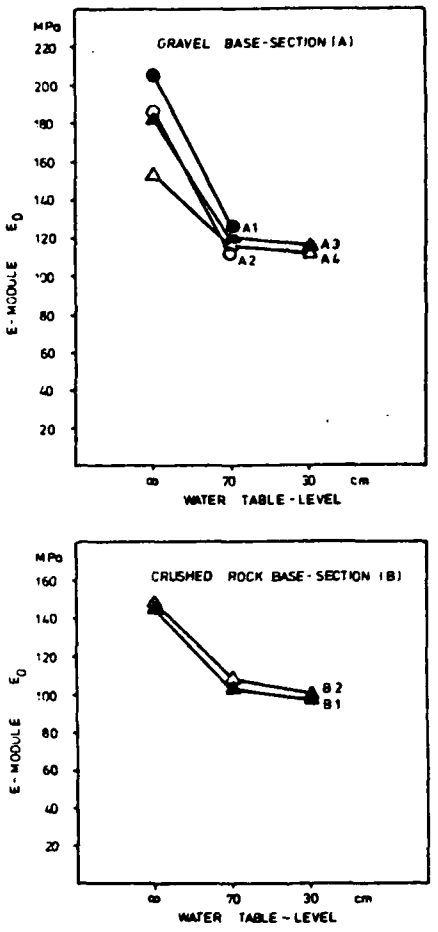

Figure 28. Mean E-Module From FWD-Tests for Different Levels of the Water Table.

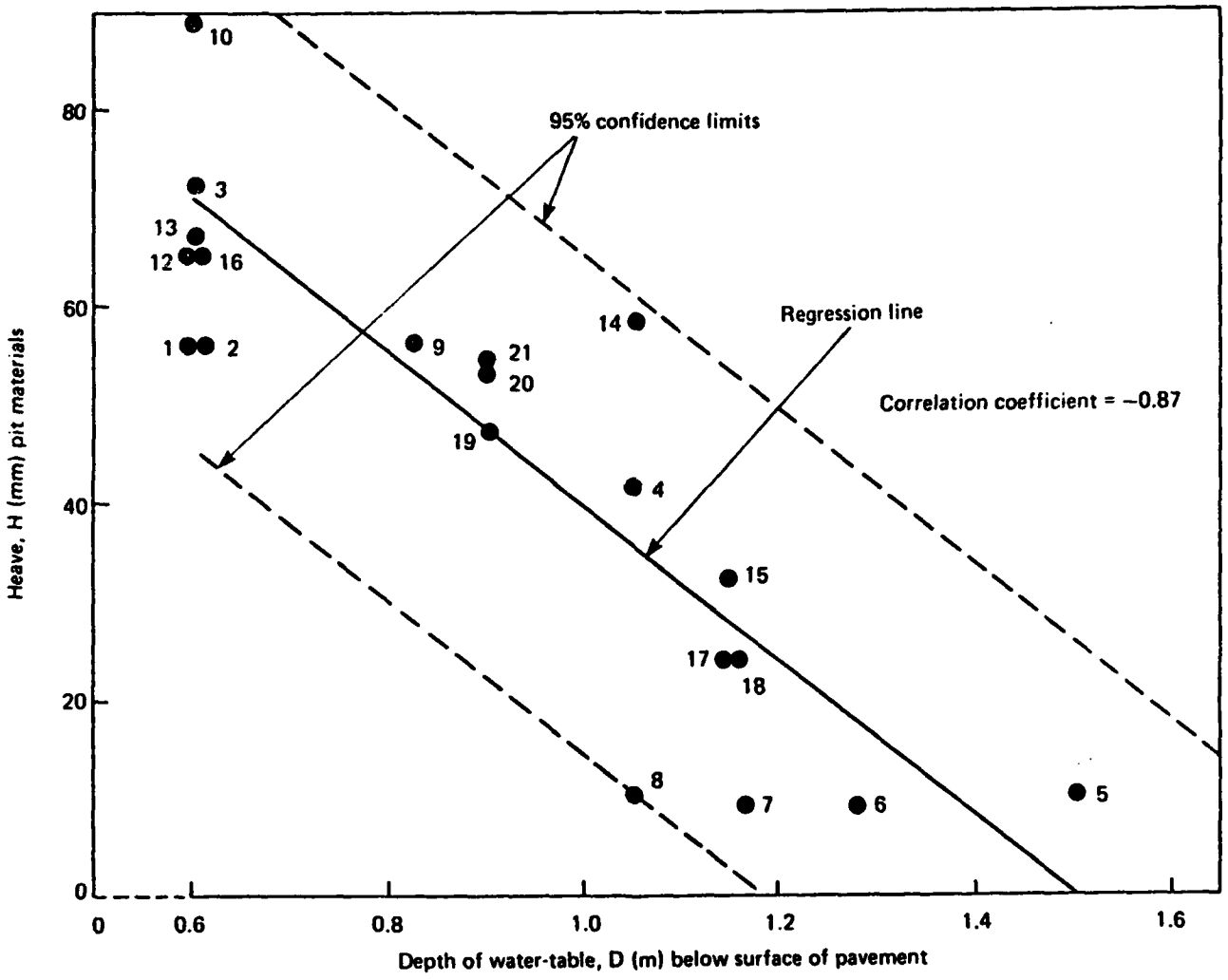

Figure 29. Correlation between Heave and Water Table Depth.

cyclic freeze-thaw action, Figure 30. Their study revealed that substantial decreases in resilient modulus were caused by the imposition of a small number of freeze-thaw cycles even though there was no change in the gross moisture content of the soil.

Just as subgrade strength properties are important inputs in pavement design, so should moisture content and moisture distribution be important inputs in subgrade strength evaluation. Although the moisture content of a subgrade at compaction is generally known, the field moisture content after a few years can be completely different. Dempsey (Reference 55) and Janssen and Dempsey (Reference 53) have listed numerous cases in which subgrade soils under in-service pavements were at other than optimum moisture content. A significant number of soils with high clay contents were well above optimum moisture content.

Subgrade moisture content is influenced by climate and seasonal fluctuations in the water table (Reference 53). In the ALRS design,the most detrimental moisture conditions should be considered. These conditions would be expected during periods of high water table which would cause the pavement materials to be near saturation and frost action effects to be most severe. For climatic areas similar to Ramstein AB, the most critical conditions are in the spring. Moisture content has the strongest influence on the thermal properties of the subgrade; even a stronger influence than type of soil (Reference 54).

C. APPLICATION OF THE CLIMATIC MODEL TO ALRS

The major application of the climatic model to ALRS is to determine the temperature as a function of pavement depth and time. Two standard pavement sections (2-inch asphalt concrete surface with either 8- or 16-inch stabilized base course) were analyzed. The 8-inch base section is shown in Figure 31. The thermal properties of the materials are shown in Table 15. Climatic input data for a 16-year period (1952-1968) were provided by the USAF Weather Service (Reference 62).

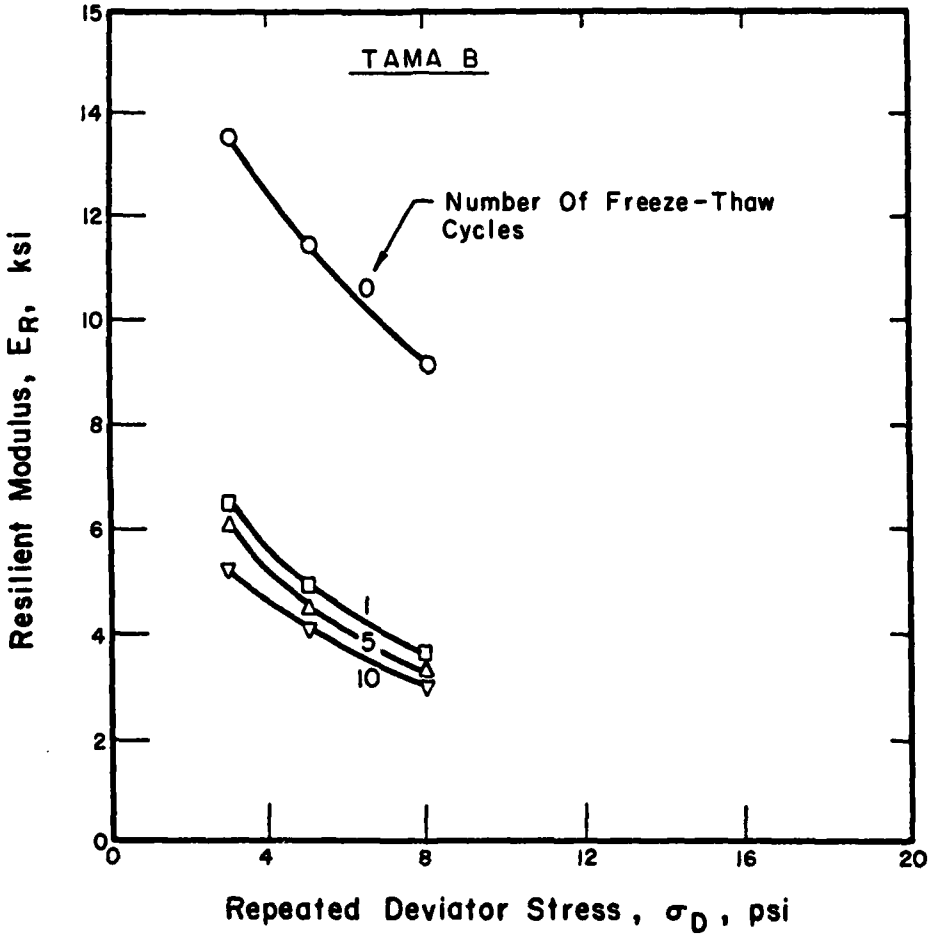

Figure 30. Influence of Cyclic Freeze-Thaw on the Resilient Behavior of a Fine-Grained Soil [AASHTO A-7-6(27)].

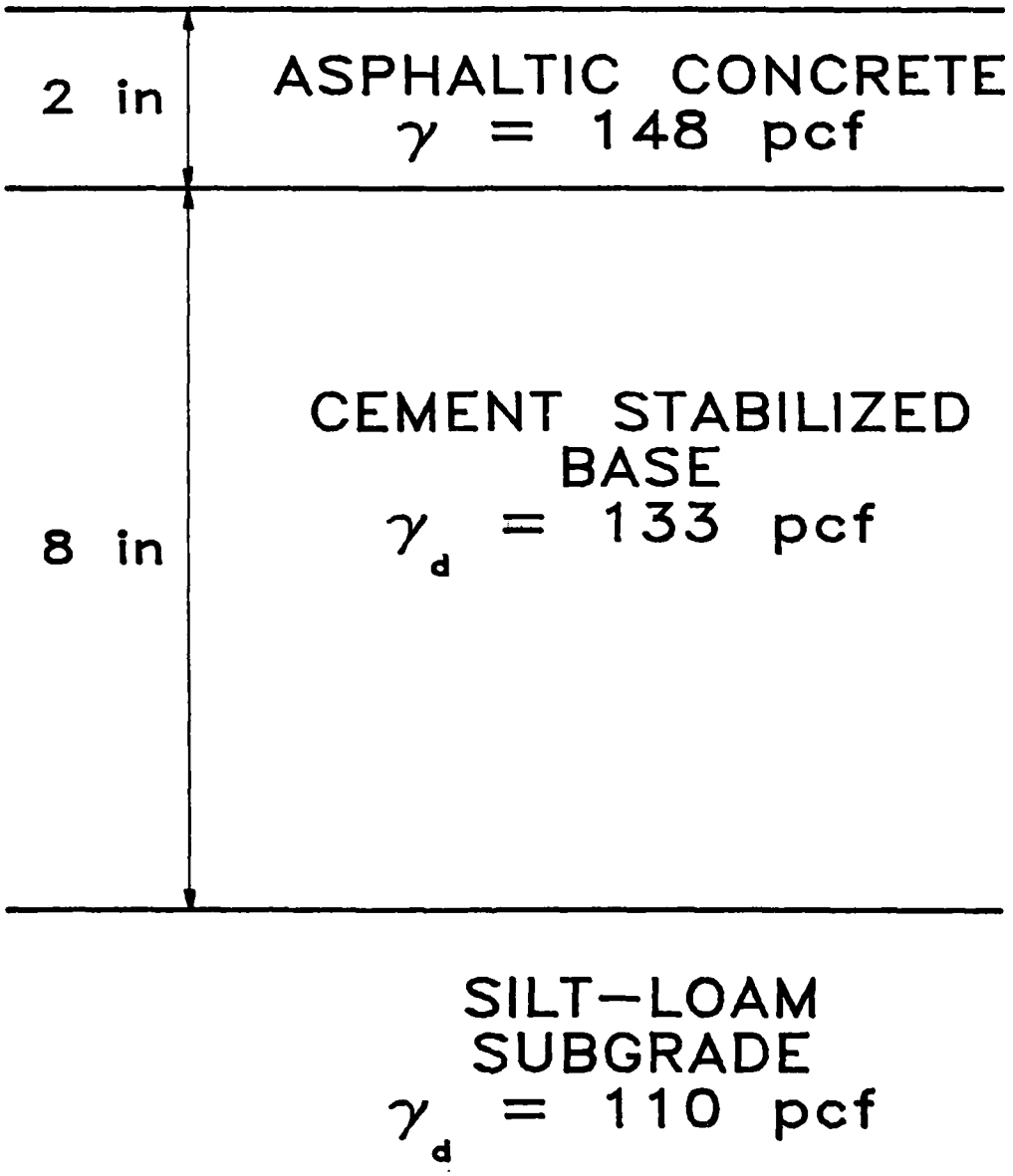

Figure 31. Pavement Section with 8-inch Base.

TABLE 15. MATERIAL THERMAL PROPERTIES

Thawed Condition

Layer	Thermal Conductivity (Btu/hr-ft-°F)	Heat Capacity (Btu/lb-°F)	Unit Weight (pcf)	Water Content (percent)
AC Surface	.70	.22	145.0	2.0
StabBase	1.92	.24	133.0	9.4
Subgrade	.92	.29	110.0	17.0

Freezing Condition

Layer	Thermal Conductivity (Btu/hr-ft-°F)	Heat Capacity (Btu/lb-°F)	Unit Weight (pcf)	Water Content (percent)
AC Surface	.70	1.44	145.0	2.0
StabBase	2.22	6.19	133.0	9.4
Subgrade	1.02	10.49	110.0	17.0

Frozen Condition

Layer	Thermal Conductivity (Btu/hr-ft-°F)	Heat Capacity (Btu/lb-°F)	Unit Weight (pcf)	Water Content (percent)
AC Surface	.70	.22	145.0	2.0
StabBase	2.52	.19	133.0	9.4
Subgrade	1.13	.22	110.0	17.0

Comparisons of temperature profiles generated by the heat transfer program for Ramstein AB, West Germany agree well with actual soil temperature data supplied by the Air Force (Reference 63). This indicates that the heat transfer program, with proper climatic inputs and thermal properties, adequately simulates actual field conditions.

By analyzing the temperature at a specified depth in the pavement system as a function of time, it is possible to establish a characteristic freeze-thaw cycle similar to the one shown in Figure 32 for Illinois conditions. Thompson and Dempsey (Reference 64) have utilized this procedure to describe the quantitative freeze-thaw environment of various pavement layers for a broad range of climatic conditions. The freeze-thaw cycle shown in Figure 33 is an important input for laboratory durability testing of pavement materials. The freeze-thaw cycle for testing the durability of stabilized base material for ALRS was derived by using the output from the climatic model and various analysis procedures.

The depth of the freezing isotherm at any time can also be determined from the generated temperature data.

1. Freeze-Thaw Parameters

To conduct realistic freeze-thaw durability tests on stabilized materials, the pertinent freeze-thaw parameters must be evaluated (Figure 32). Dempsey and Thompson (Reference 65) conducted parameter studies and determined that cooling rates and temperatures below freezing were very important in causing freeze-thaw damage. They also found that the length of the freezing period needed only to be long enough to permit complete freezing of the specimen. The temperature above freezing affected strength gain after thawing due to continued curing of cemented materials. If the temperatures above freezing are conducive to increased curing, as in many conventional freeze-thaw tests, the strength gain due to continued curing can offset the actual freeze-thaw damage.

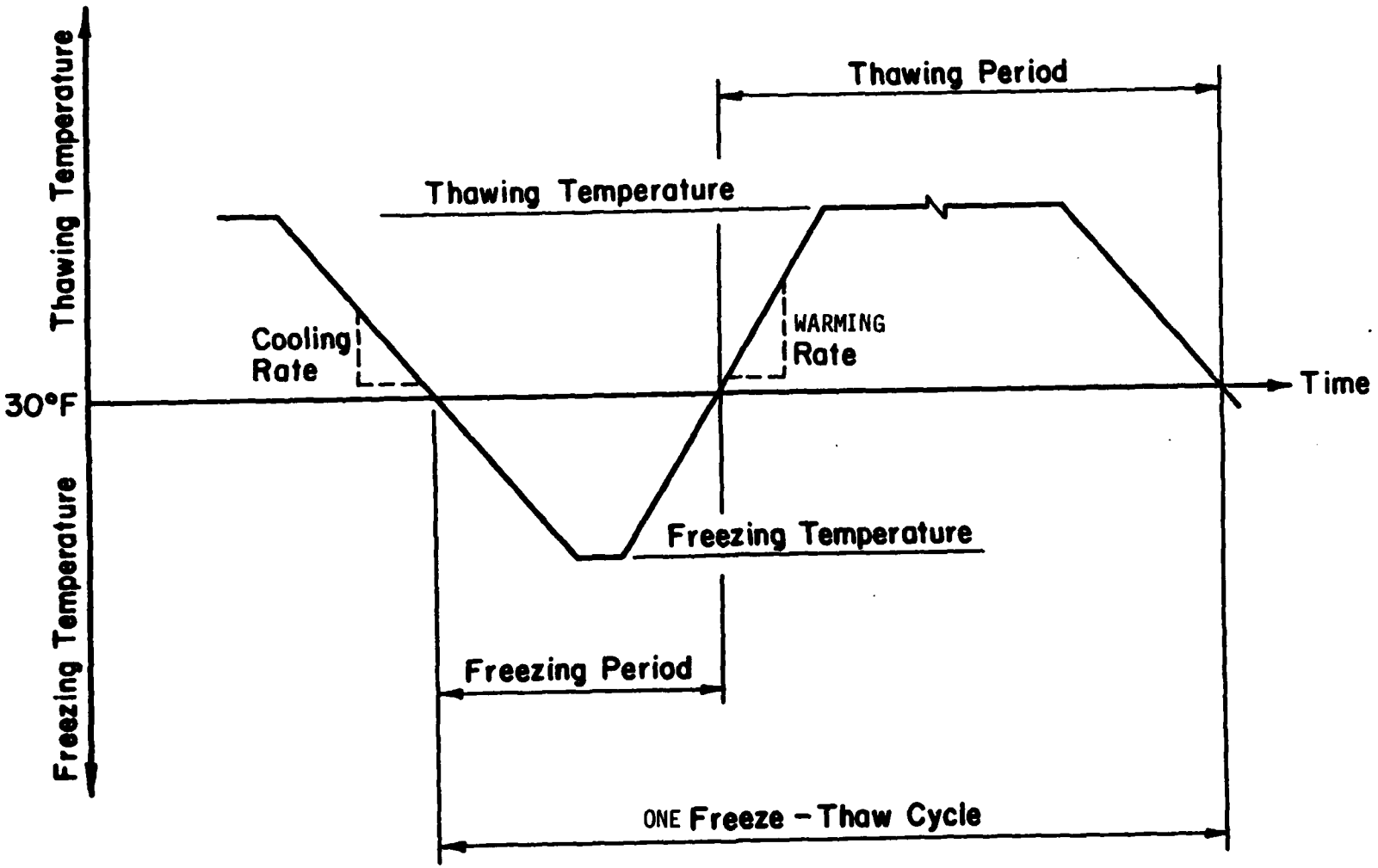

Figure 32. Idealized Freeze-Thaw Cycle.

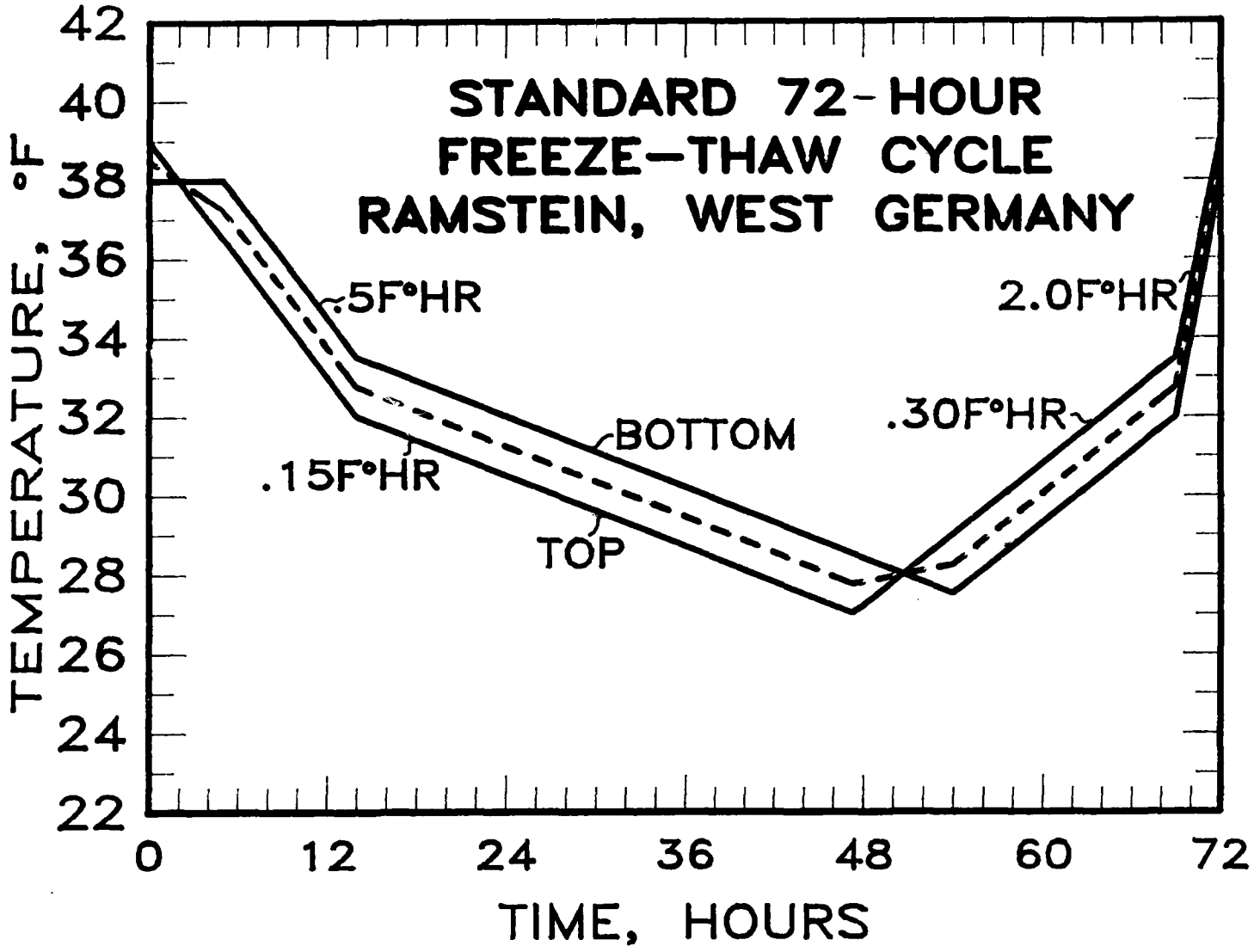

Figure 33. Standard Freeze-Thaw Cycle for Ramstein AB, West Germany.

Dempsey and Thompson (Reference 66) found substantial variability in the important frost action parameters from month to month and from year to year. Because a valid laboratory testing procedure should be representative of actual field conditions, a considerable amount of field data should be analyzed in order to determine representative values for the important parameters. Table 16 shows the monthly means of the freeze-thaw parameters as determined from 16 years of temperature data generated for Ramstein AB, West Germany by the heat transfer program previously discussed. These values were determined for a point 4 inches below the surface (2 inches into the stabilized layer) in the pavement section shown in Figure 31 . The mean temperature difference is the difference in temperature between the top and the bottom of a 4-inch thick sample. Freeze-thaw cycling occurs only during December, January and February, with the greatest number of cycles in January. The favored averages shown are for the three frost action months, with preference given to January. The values for the most important parameters have also been rounded to the nearest significant figure.

In the development of an accelerated laboratory freeze-thaw durability test, it is desirable to change some of the frost action parameters so that the period of time required to complete a freeze-thaw cycle can be shortened for laboratory use. However, any changes made in the cycle should not substantially alter its representation of the frost action that actually occurs in the field pavement system.

2. Freeze-Thaw Cycle

The typical freeze-thaw cycle developed for Ramstein AB, West Germany is shown in Figure 33. This figure shows the temperatures for the top and bottom of a 4-inch long specimen. The dashed line is the temperature at the center of the specimen, for which the frost action parameters have been evaluated. The temperature difference between the top and the bottom of the specimen is maintained at 1.5°F .

TABLE 16. FROST ACTION PARAMETERS

Month	Frost Action Parameters			
	Cooling Rate, °F /hr	Below Freezing T, °F	Duration of Freezing, days	Mean Temperature Difference, °F
November	0.24	none	none	1.75
December	0.15	28.49	0.39	1.28
January	0.12	28.34	0.79	1.31
February	0.24	26.71	0.83	2.10
March	0.46	none	none	3.51
Weighted Average	0.15	28.00	0.67	1.50

Month	Frost Action Parameters			
	Warming Rate, °F /hr	Above Freezing T, °F	Duration of Thawing, days	No. of F-T Cycles/month
November	0.35	44.88	29.94	0.00
December	0.21	38.10	26.00	0.94
January	0.20	35.17	19.78	2.19
February	0.40	39.59	24.34	0.81
March	0.80	50.52	30.88	0.00
Weighted Average	0.27	38.00	23.37	-

The cooling rate is accelerated above 32°F in order to save time. However, once 32 °F is reached, the rate is slowed to 0.15 °F /hour. The temperature below freezing is 28°F. The warming rate is 0.30°F /hour, until the specimen is above freezing. The rate is then accelerated. The final temperature above freezing is about 38°F. The entire cycle is completed in 72 hours.

3. Recurrence Interval

Another important parameter in a freeze-thaw durability study is the number of freeze-thaw cycles to be expected in a given year. Thompson and Dempsey (Reference 67) found that the number of Illinois freeze-thaw cycles per year are quite variable. This is also true for the Ramstein, AB, West Germany area. Table 17 shows the number of freeze-thaw cycles per year for the 16 years of data analyzed in this study. These values are for a point 2 inches below the top of the stabilized layer. The number of cycles ranged from a high of 13 cycles to a low of 0. Using hydrologic statistical concepts developed by Chow (Reference 68), a relationship can be developed between the number of freeze-thaw cycles and the recurrence interval (in years). A plot of this relation for the Ramstein AB data is shown in Figure 34. The equation for the regression line is:

$$N = 4.9K + 3.6 \qquad (14)$$

In Equation (14), N is the maximum number of expected freze-thaw cycle and K is given by:

$$K = -(1.1 + 1.80 \text{ Log } (\text{Log}Y - \text{Log } (Y-1))) \qquad (15)$$

Y is the return period, in years. Using the recurrence interval concept, it is possible to determine in a rational manner the number of freeze-thaw cycles that should be considered for durability evaluation. For a recurrence interval of 4 years, six freeze-thaw cycles would be exceeded on the average only once every 4 years, (Figure 34).

TABLE 17. NUMBER OF FREEZE-THAW CYCLES PER YEAR

Winter Period	Pavement System: 2" AC Surface 8" Stab Base	2" AC Surface 16" Stab Base	0" AC Surface 8" Stab Base
	Number of F-T Cycles 2" into StabBase		
1952-1953	0	0	-
1953-1954	6	7	-
1954-1955	0	0	-
1955-1956	7	8	-
1956-1957	2	3	-
1957-1958	0	0	-
1958-1959	0	0	-
1959-1960	3	3	-
1960-1961	0	0	-
1961-1962	4	5	-
1962-1963	12	13	21
1963-1964	13	15	16
1964-1965	0	1	-
1965-1966	5	6	-
1966-1967	0	0	-
1967-1968	2	2	-

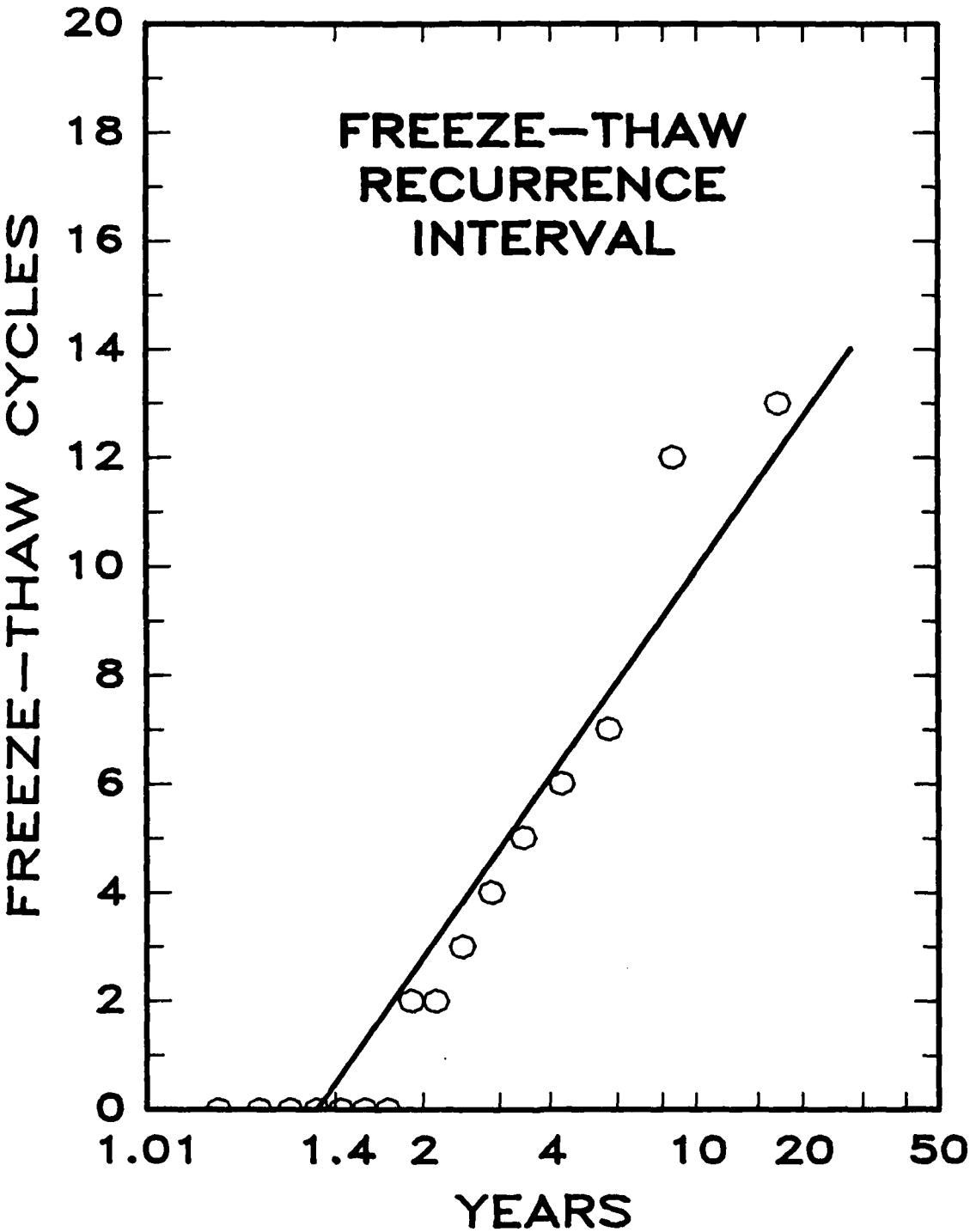

Figure 34. Freeze-Thaw Cycle Recurrence Interval.

4. Effects of Different Pavement Sections

Table 17 shows the number of freeze-thaw cycles for a pavement system with a 16-inch stabilized base instead of the 8-inch stabilized base. The effect of increasing the stabilized base thickness is to slightly increase the number of freeze-thaw cycles at a point 2 inches into the stabilized base. The increase is effected by the difference in thermal properties of the stabilized base and the subgrade soil which is replaced by the extra stabilized base.

Table 17 also shows the effect of reducing the asphalt surface thickness from 2 inches to 0 inches. (A thin asphalt surface treatment applied to waterproof the surface and aid in curing the stabilized base is considered to have 0 thickness for heat flow in pavement systems.) Only the two worst winter periods (1962-63 and 1963-64) were run to predict the maximum number of freeze-thaw cycles that could be expected to occur. Thompson and Dempsey (Reference 67) suggest that for Illinois conditions the number of freeze-thaw cycles expected on the average should be multiplied by a factor of 2 when changing from 2 inches of asphalt surface to a surface treatment. This is a conservative estimate and should also be valid for the Ramstein area.

5. Frost Penetration

During some of the colder winters the frost penetrates through the stabilized base and into the subgrade, Table 18. Figures 35, 36 and 37 show depth of frost penetration for December, 1963 and January and February, 1964. The frost line is taken as the 30°F isotherm. These are for the pavement section shown in Figure 31. The dashed lines in the frost depth graphs are the thawing lines. During warm winter days it is possible for the pavement system to be thawing from the top while it is still frozen at greater depths. These graphs show how a particular depth in the pavement system can cycle between frozen and unfrozen many times during a winter season.

TABLE 18. MAXIMUM DEPTH OF FROST PENETRATION EACH YEAR

Winter Period	Pavement System: 2" AC Surface 8" StabBase	2" AC Surface 16" StabBase	0" AC Surface 8" StabBase
	Maximum Depth of Frost Penetration		
1952-1953	3.1	3.2	-
1953-1954	15.9	19.9	-
1954-1955	3.4	3.5	-
1955-1956	17.4	21.5	-
1956-1957	5.8	5.8	-
1957-1958	2.6	2.7	-
1958-1959	3.0	3.0	-
1959-1960	7.9	8.0	-
1960-1961	3.7	3.8	-
1961-1962	9.6	9.4	-
1962-1963	23.5	28.0	25.4
1963-1964	13.2	14.7	14.0
1964-1965	4.0	4.6	-
1965-1966	14.7	18.3	-
1966-1967	2.9	2.9	-
1967-1968	6.0	7.0	-

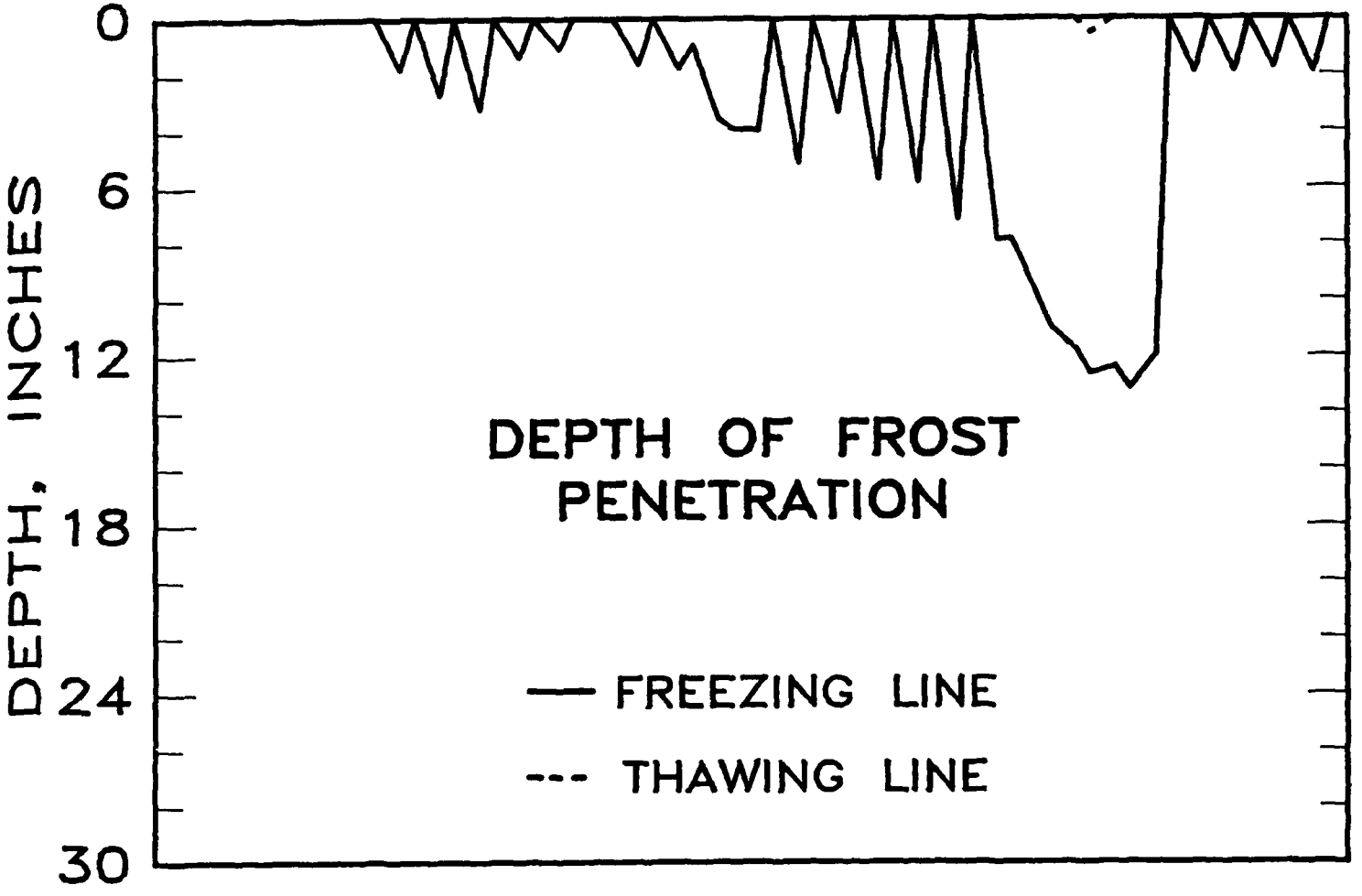

Figure 35. Frost Penetration for December, 1963.

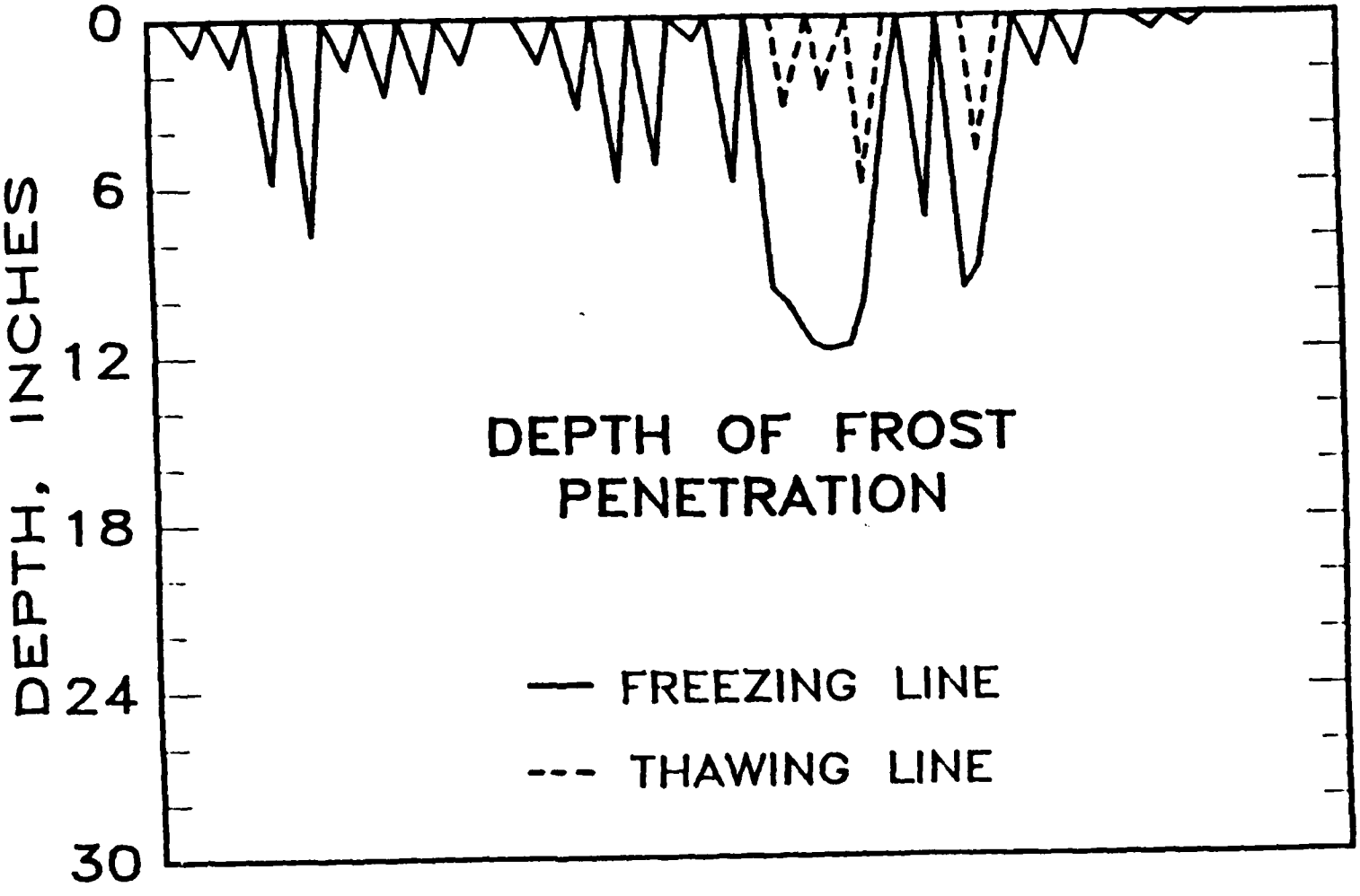

Figure 36. Frost Penetration for January, 1964.

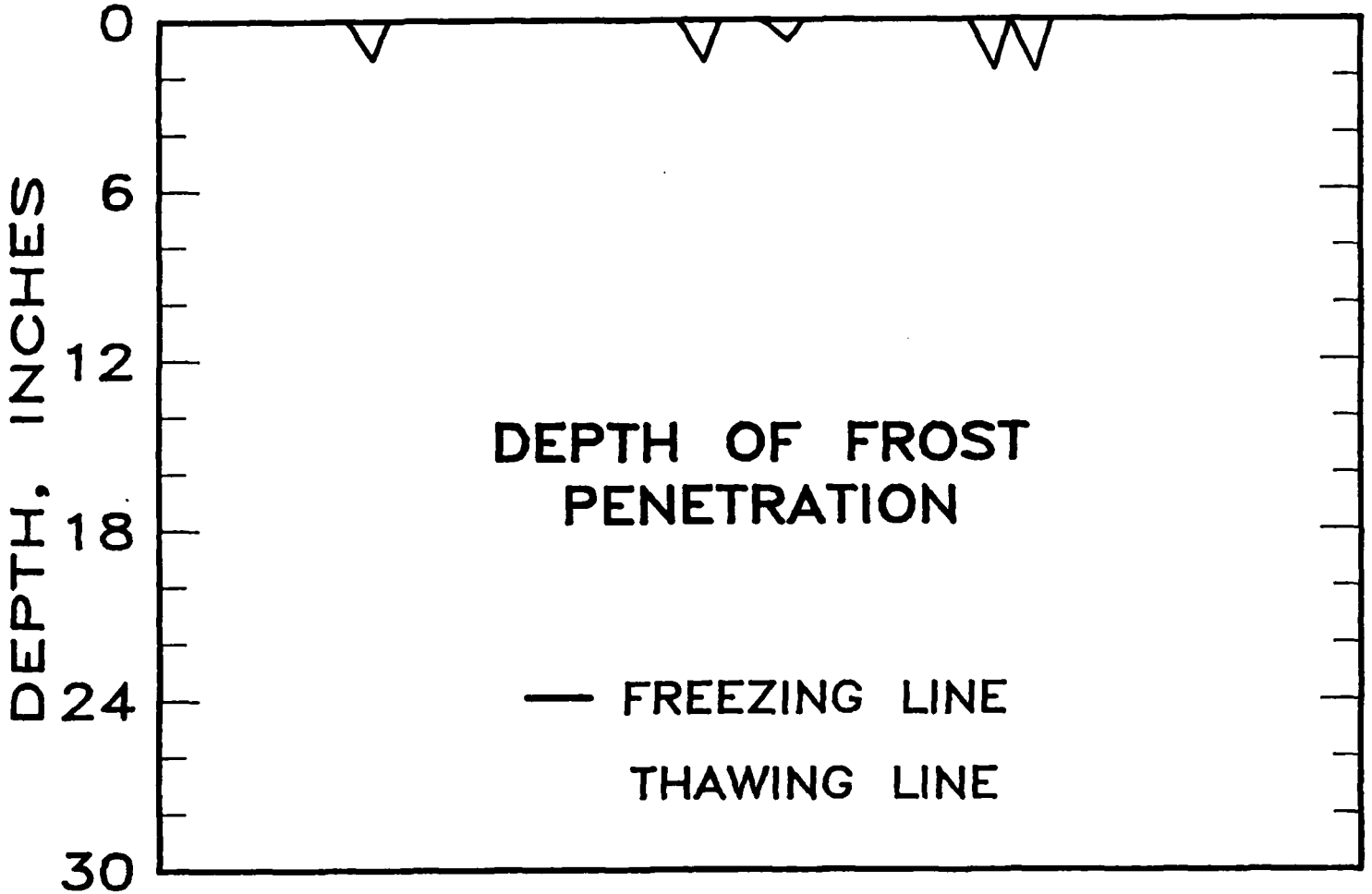

FEBRUARY, 1964

Figure 37. Frost Penetration for February, 1964.

Table 18 shows the maximum depths of frost penetration for the 16 years studied and for the three pavement sections considered. When the thickness of the stabilized base is increased, the depth of frost penetration is usually also increased. This is caused by the different material thermal properties.

D. LABORATORY FREEZE-THAW TESTING

1. Freeze-Thaw Testing Unit

Freeze-thaw durability testing was conducted in a special testing unit previously designed and constructed at the University of Illinois (Reference 69). The freeze-thaw testing unit accurately simulates the frost action data generated by the heat-transfer model previously discussed. Figure 38 shows a diagram of the freeze-thaw testing unit with the temperature controller and data logger. Figure 39 is a photograph of the inside of the cabinet showing samples with transducers to measure heave.

Time-temperature control of the freeze-thaw testing unit is maintained by an electronic digital controller. Temperature can either be kept constant with respect to time, or varied at a constant rate of change. The entire freeze-thaw cycle can then be programmed as a series of linear segments. Separate control for the top and bottom of the cabinet is possible, so a temperature difference can be maintained across the sample. The controller can also be programmed to trigger a data logger to take readings of sample length change at appropriate times (through transducers attached to some of the samples). For the ALRS testing series, readings were taken at 5-hour intervals with additional readings being taken at changes of slope in the freeze-thaw cycle, (Figure 33).

Experience to date indicates that the testing unit is very dependable, provides excellent temperature control, and requires little maintenance. Its versatility and temperature range capability make the

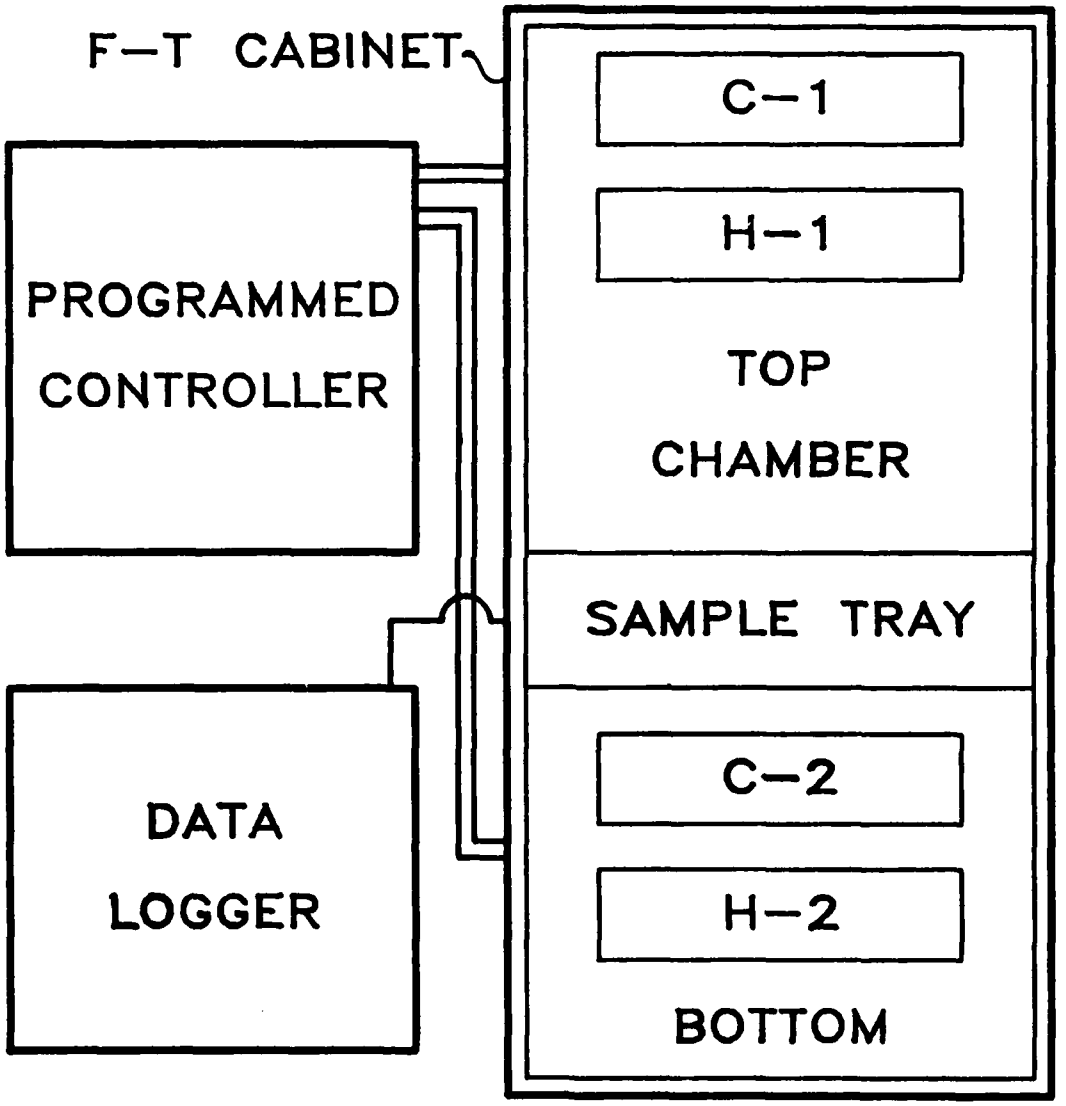

Figure 38. Schematic of Freeze-Thaw Testing Unit.

Figure 39. Inside of Freeze-Thaw Testing Unit.

unit ideal for studying the influence of frost action on paving materials. The specimen tray in the freeze-thaw cabinet can accommodate 12 Proctor-sized (4-inch diameter) specimens at once. The water control system incorporated the unit permits the bottom of the specimens to remain moist to simulate worst condition field conditions.

2. Materials

The Waterways Experiment Station, Vicksburg, Mississippi provided samples of the sandy-gravel and Portland Cement (Type 1) used in constructing the ALRS stabilized test section pavements. (Reference 70). Gradation data for the sandy gravel are presented in Table 19. Only the fraction passing the 3/4-inch sieve was used in the laboratory testing program.

3. Sample Preparation

ASTM 558-82 procedure (Method B) was used to establish the moisture-density relations for a 5 percent cement (dry weight of soil basis) treatment level. Maximum dry density was 132.9 pcf and the optimum moisture content was 8 percent. The 5-percent moisture-density relation was assumed to be representative of the 3-, 5-, 7-, and 9-percent mixtures.

The required amounts of cement and soil passing the No. 4 sieve were initially dry mixed with a Lancaster mortar mixer for approximately 1 minute. After dry mixing, water was added to bring the mixture to the optimum moisture content and mixing continued for approximately 2 minutes. The material passing the 3/4-inch sieve but retained on the No. 4 sieve was then added and mixing continued for an additional 3 minutes. Compaction of the soil-cement mixture proceeded immediately after mixing was completed. Samples were compacted in standard Proctor-sized molds (4-inch diameter by 4.59 inches) in accordance with ASTM D 560-82.

TABLE 19. WES SANDY GRAVEL GRADATION DATA*

WES Sandy Gravel Gradation Data

Sieve	% Passing
1-inch	97.6
3/4-inch	93.5
1/2-inch	82.5
3/8-inch	75.0
#4	61.8
#10	52.1
#16	48.2
#40	28.1
#80	10.2
#200	7.7

* "Washed" analysis

Ten samples were compacted for each cement content (3,5,7, and 9 percent cement by dry weight of soil). Compaction moisture contents were maintained within + 1 percent of the optimum and the dry densities were maintained within + 3 pcf of maximum dry density. Compaction data are presented in Table 20.

After 1 day of moist curing at 70°F the samples were extruded from the molds and moist cured an additional 6 days at 70 °F.

4. Sample Testing

Four of the specimens were tested in compression immediately following curing. The freeze-thaw specimens were labeled and wrapped in at least three layers of polyethylene to prevent evaporation from the sides of the specimens.The tops of the specimens were then covered with a layer of hot asphalt. The bottoms of the specimens were not covered in any way, in order to permit the sample to absorb water during the freeze-thaw testing. The specimens were then placed in the freeze-thaw cabinet for five or 10 freeze-thaw cycles. A detailed description of the testing procedure is given by Dempsey and Thompson (Reference 66).

Compressive strength tests (ASTM D1633-79) were conducted following the initial 7-day moist cure and five and 10 freeze-thaw cycles. Length and moisture content changes were determined for the specimens subjected to freeze-thaw. Test data are summarized in Table 20.

Figures 40 through 47 show measurements of sample heave versus freeze-thaw cycles for the different cement contents tested. It is quite apparent that some heave is occurring during sample freezing. This heave lasts only while the sample is frozen. While quantitative relationships between sample heave and acceptable freeze-thaw performance are difficult to establish (Reference 65), heave during freezing of a stabilized material is usually accompanied by a strength decrease.

TABLE 20. SUMMARY OF FREEZE-THAW TEST RESULTS

Cement Content %	Compaction Data ave γ_d, pcf	w%	Compressive Strength, psi 0 cycles	5 cycles	10 cycles
3	129.9	8.2	246	189	194
5	131.1	8.0	481	353	332
7	131.9	8.0	743	456	403
9	132.2	8.0	803	528	538

Cement Content %	Maximum Heave %	Moisture Content 0 cycles	5 cycles	10 cycles
3	.49	6.9	7.7	7.2
5	.46	6.3	6.3	6.7
7	.30	4.4	5.8	6.5
9	.40	4.9	6.1	5.8

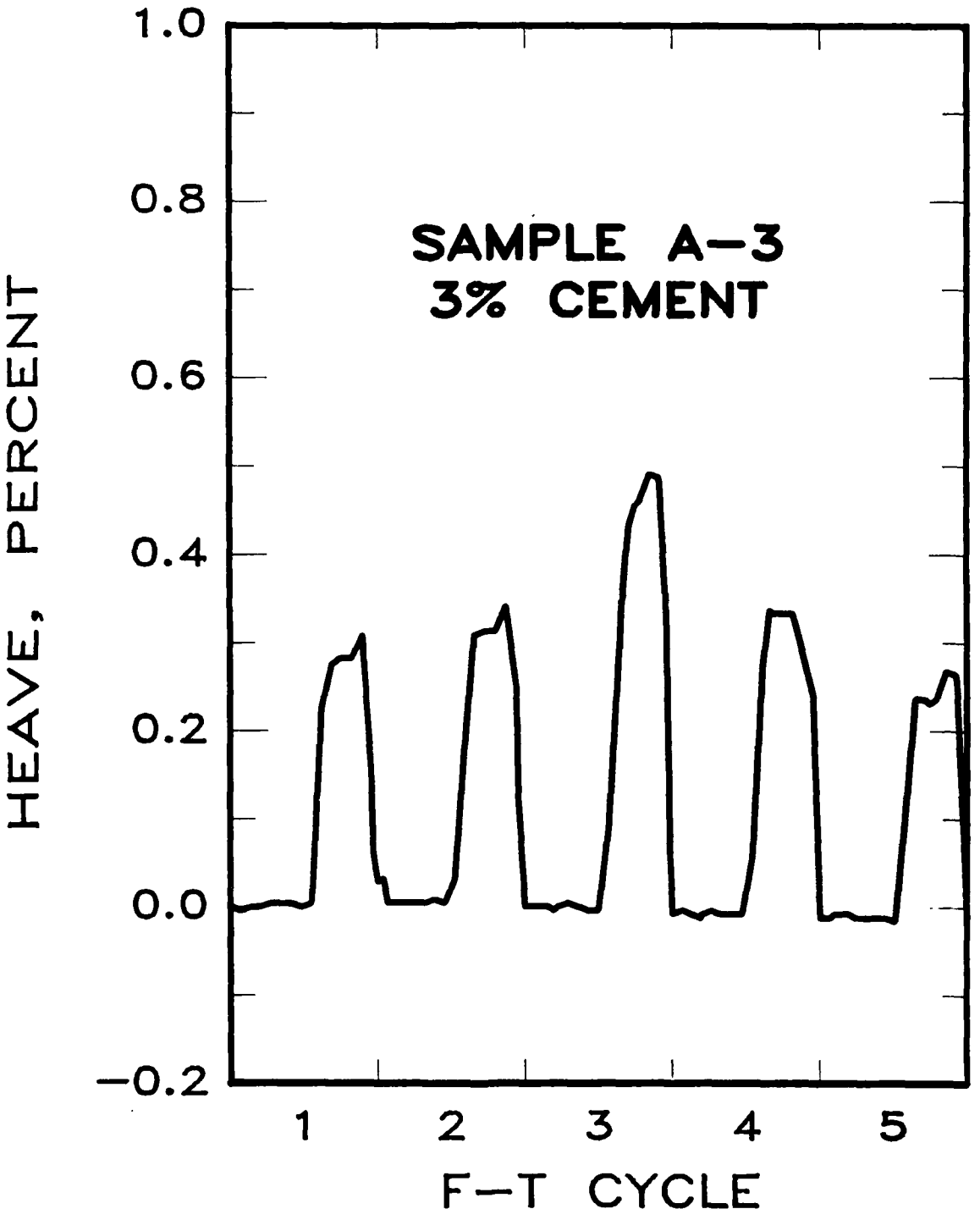

Figure 40. Frost Heave for 3-Percent Cement Sample, First Five Cycles.

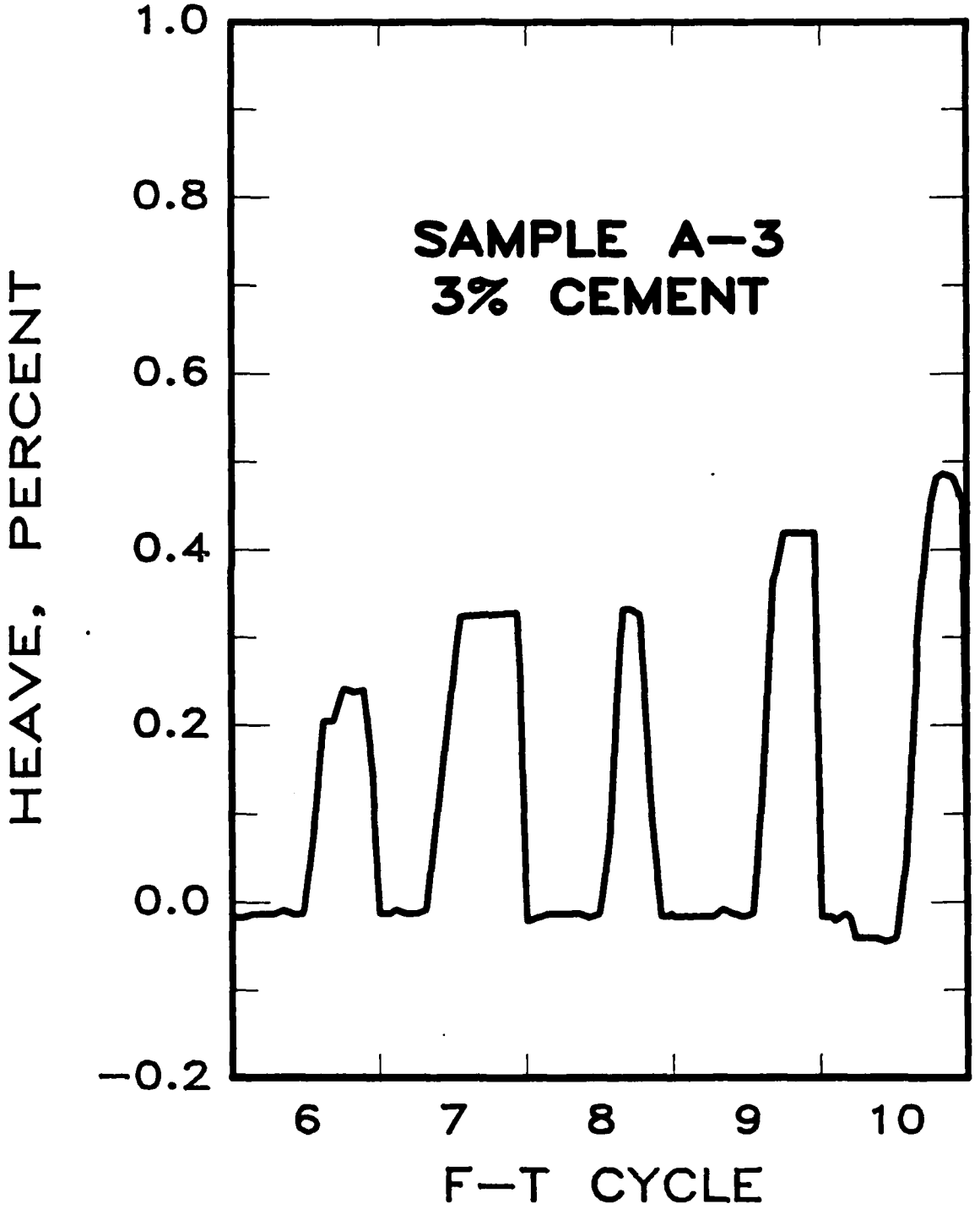

Figure 41. Frost Heave for 3-Percent Cement Sample, Last Five Cycles.

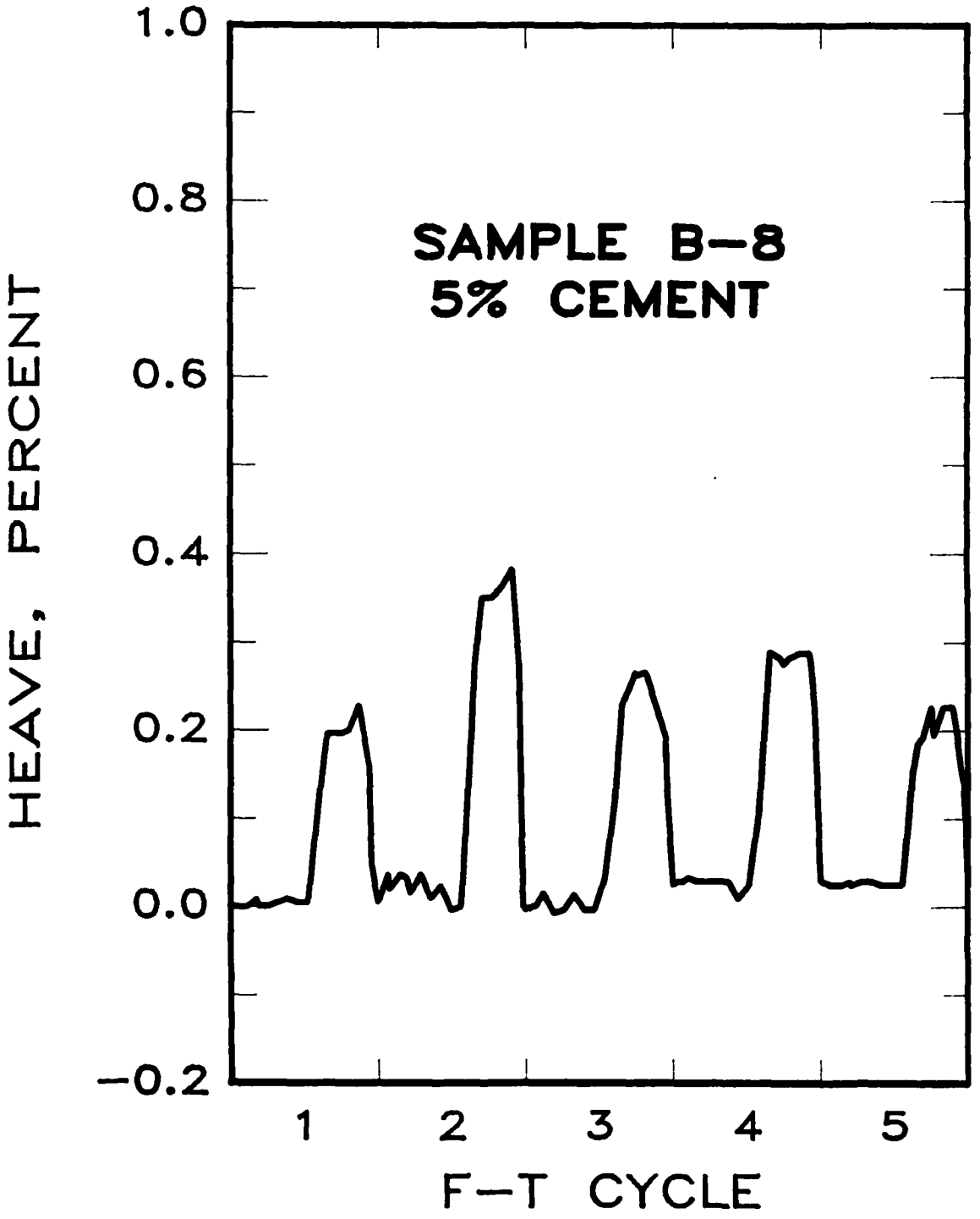

Figure 42. Frost Heave for 5-Percent Cement Sample, First Five Cycles.

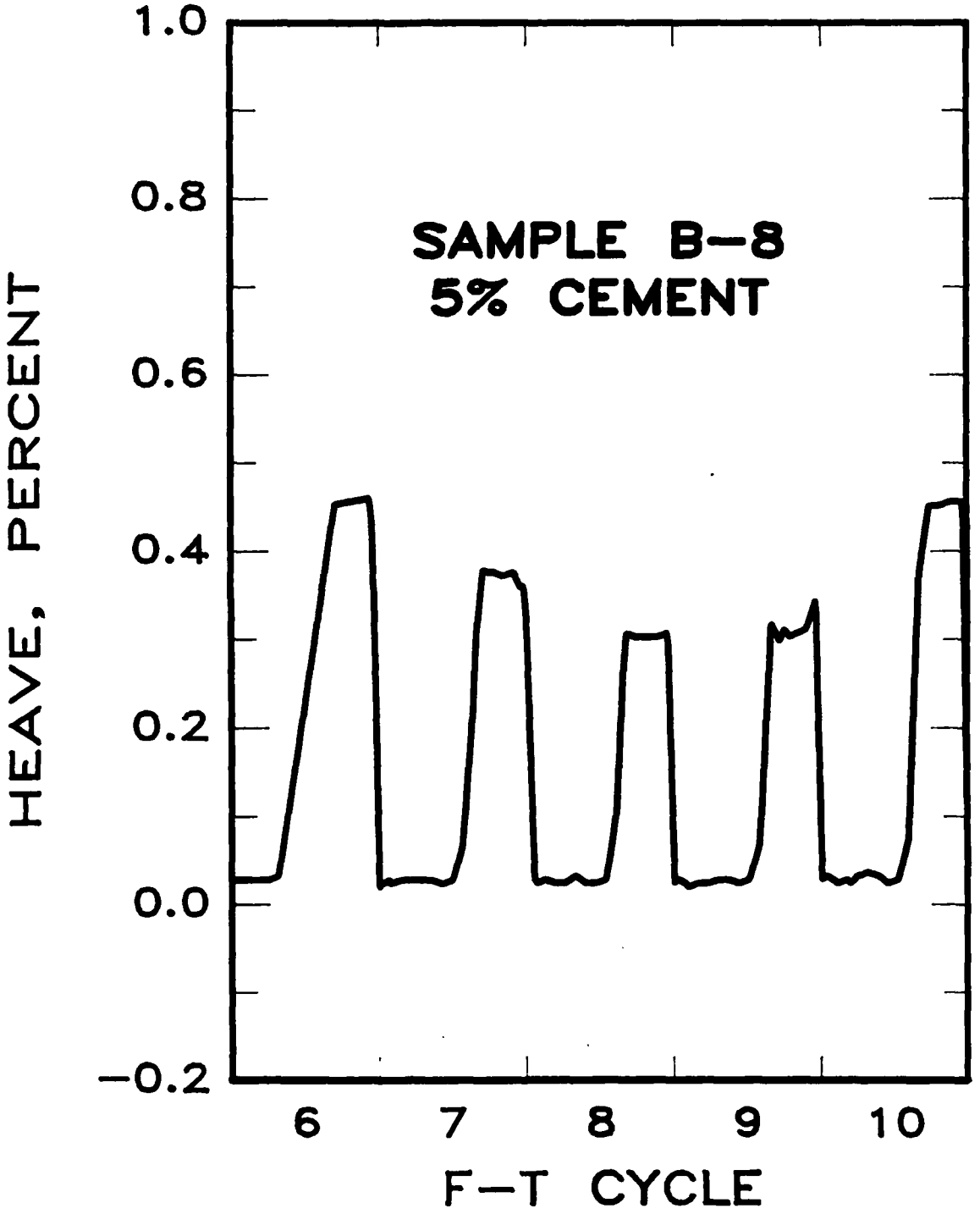

Figure 43. Frost Heave for 5-Percent Cement Sample, Last Five Cycles.

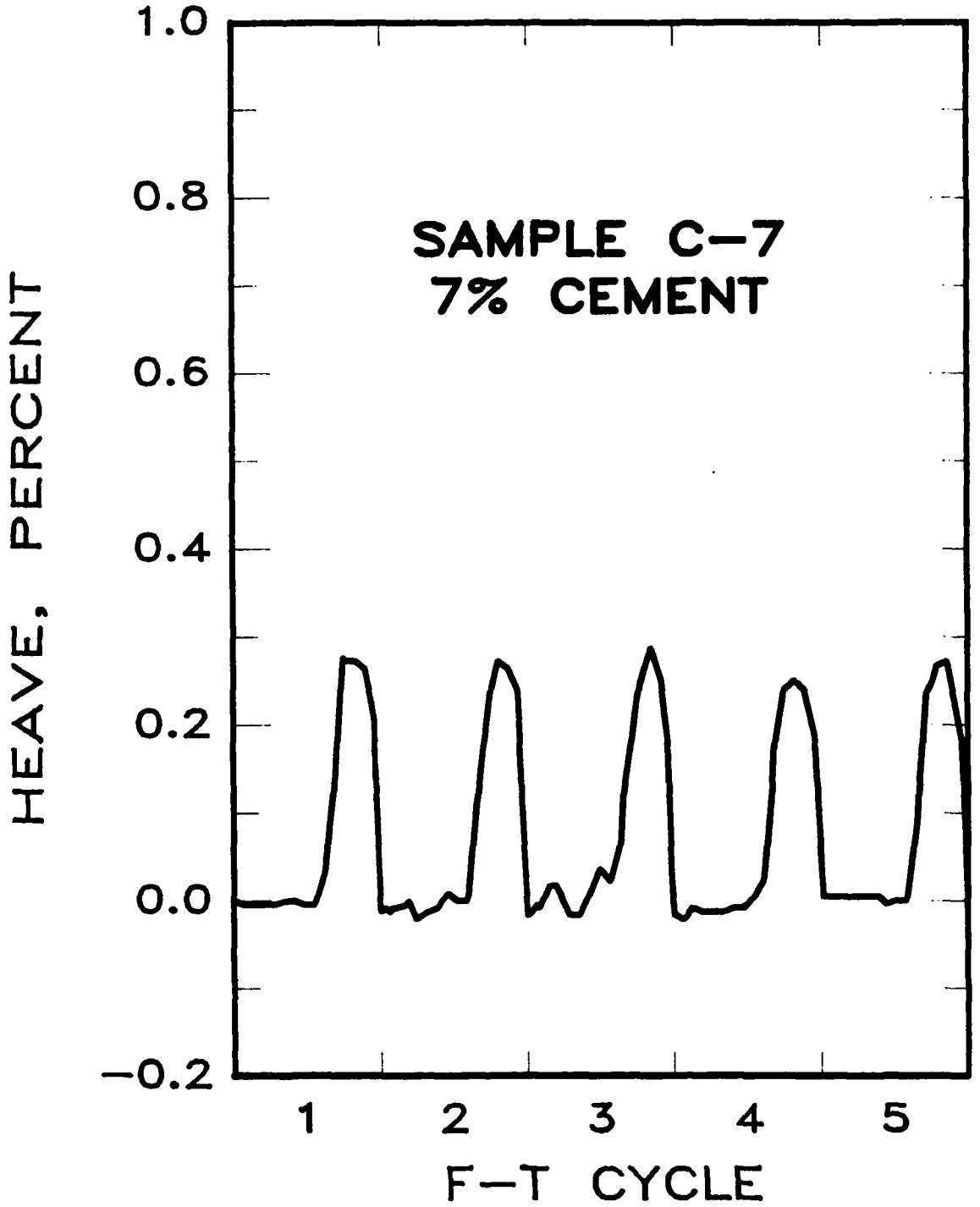

Figure 44. Frost Heave for 7-Percent Cement Sample, First Five Cycles.

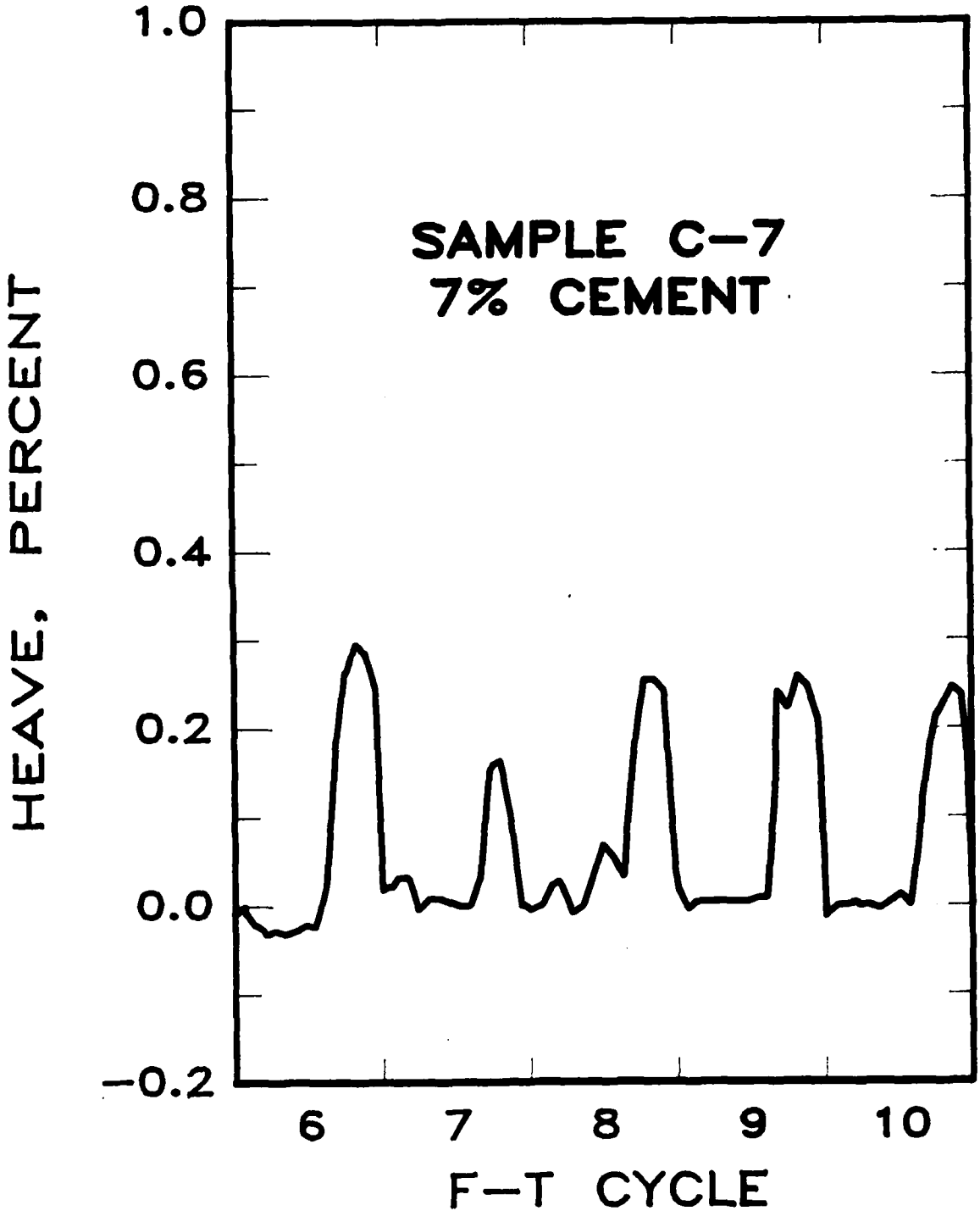

Figure 45. Frost Heave for 7-Percent Cement Sample, Last Five Cycles.

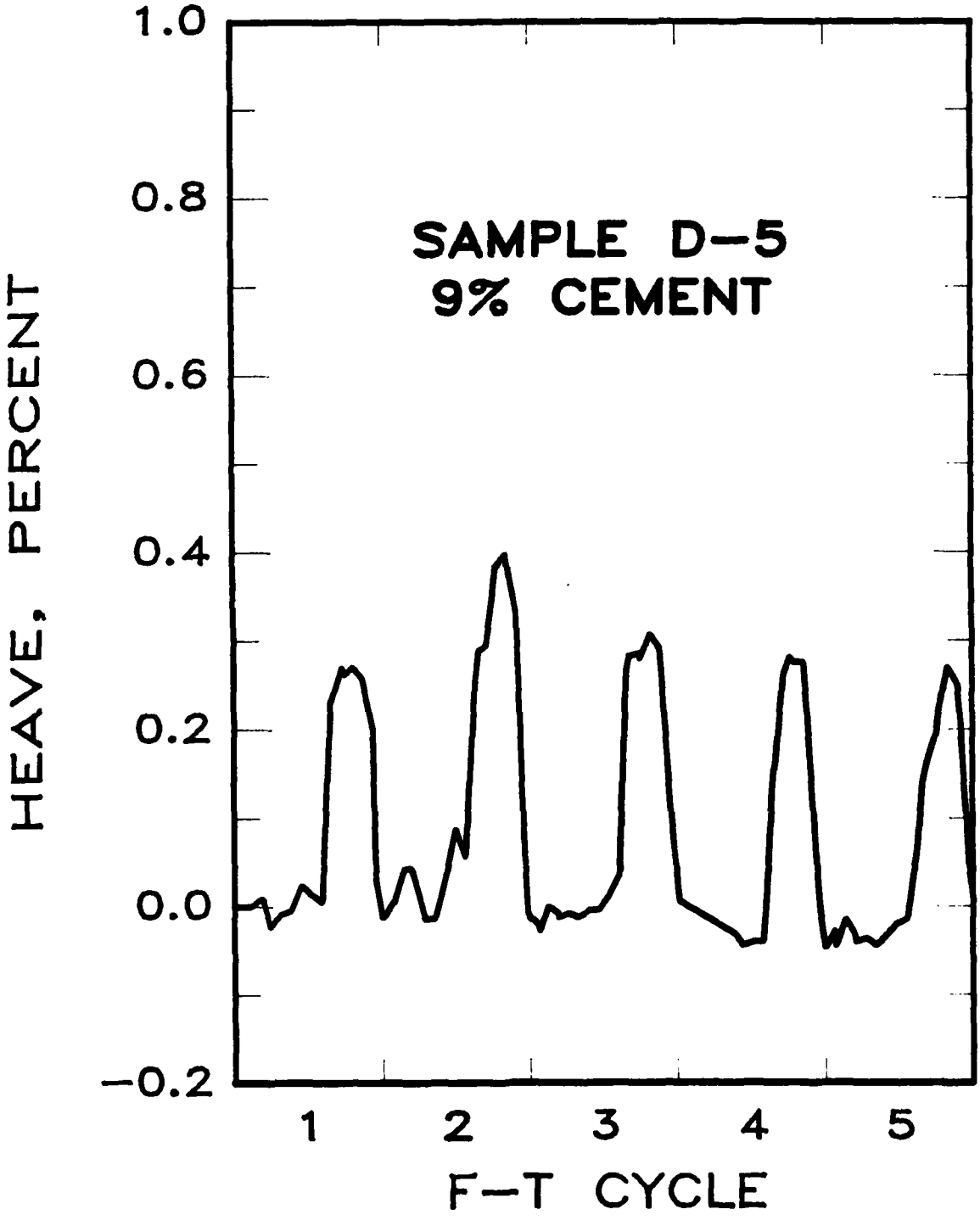

Figure 46. Frost Heave for 9-Percent Cement Sample, First Five Cycles.

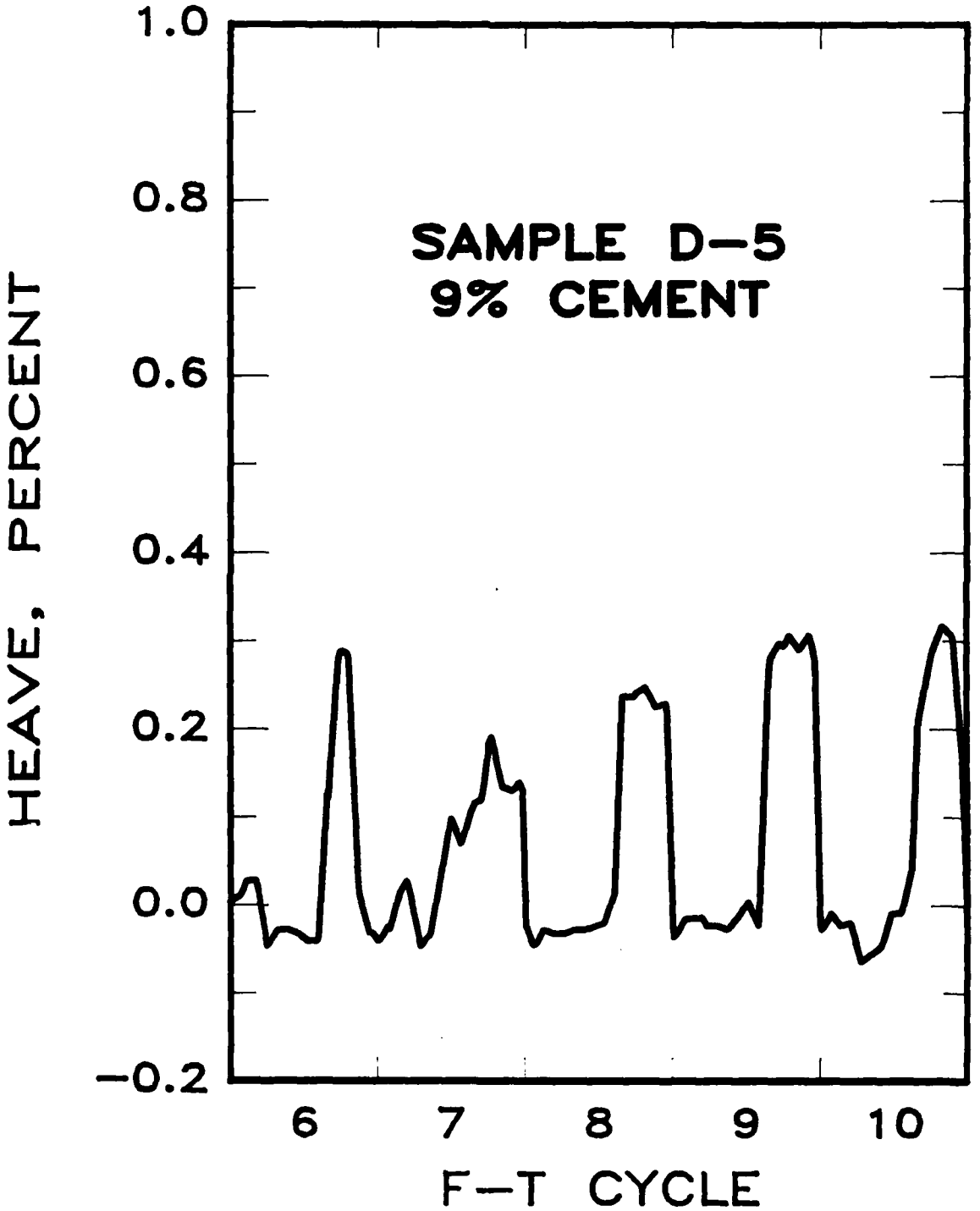

Figure 47. Frost Heave for 9-Percent Cement Sample, Last Five Cycles.

Figure 48 shows moisture contents versus the number of freeze-thaw cycles for the stabilized materials included in this testing program. It is generally assumed that a substantial increase in moisture content is indicative of a decrease in strength of a material subjected to freeze-thaw cycling.

Residual strength after freeze-thaw cycling is an important indicator of expected field durability performance. Residual strength is considered to be the compressive strength remaining after the sample has been subjected to a given number of freeze-thaw cycles. Thompson and Dempsey (Reference 67) suggest that the stabilized material residual strength after the first winter period must be adequate to withstand loading during the following season. Strength gain due to additional curing the following summer will enable the material to withstand subsequent winter periods. Figure 49 shows residual strengths as a function of the number of freeze-thaw cycles.

E. DISCUSSION OF LABORATORY TESTING RESULTS

Even though the higher initial strength samples show a greater magnitude of strength loss, they still show a higher residual strength than the lower initial strength samples. Also important is the fact that most of the strength loss occurs in the first five cycles. Thus an error in predicting the expected number of freeze-thaw cycles in the field has a decreasing significance as the number of freeze-thaw cycles increases.

Figure 50 shows a graph of residual strength versus initial strength for the 5 and 10 freeze-thaw cycle samples. The equation for the line in Figure 50 is:

$$RS = 0.55\ (IS) + 61 \qquad (16)$$

RS is the residual strength and IS is the initial strength. These results are similar to those presented by Dempsey and Thompson (Reference 66) for stabilized materials in the Illinois climate. The ALRS samples

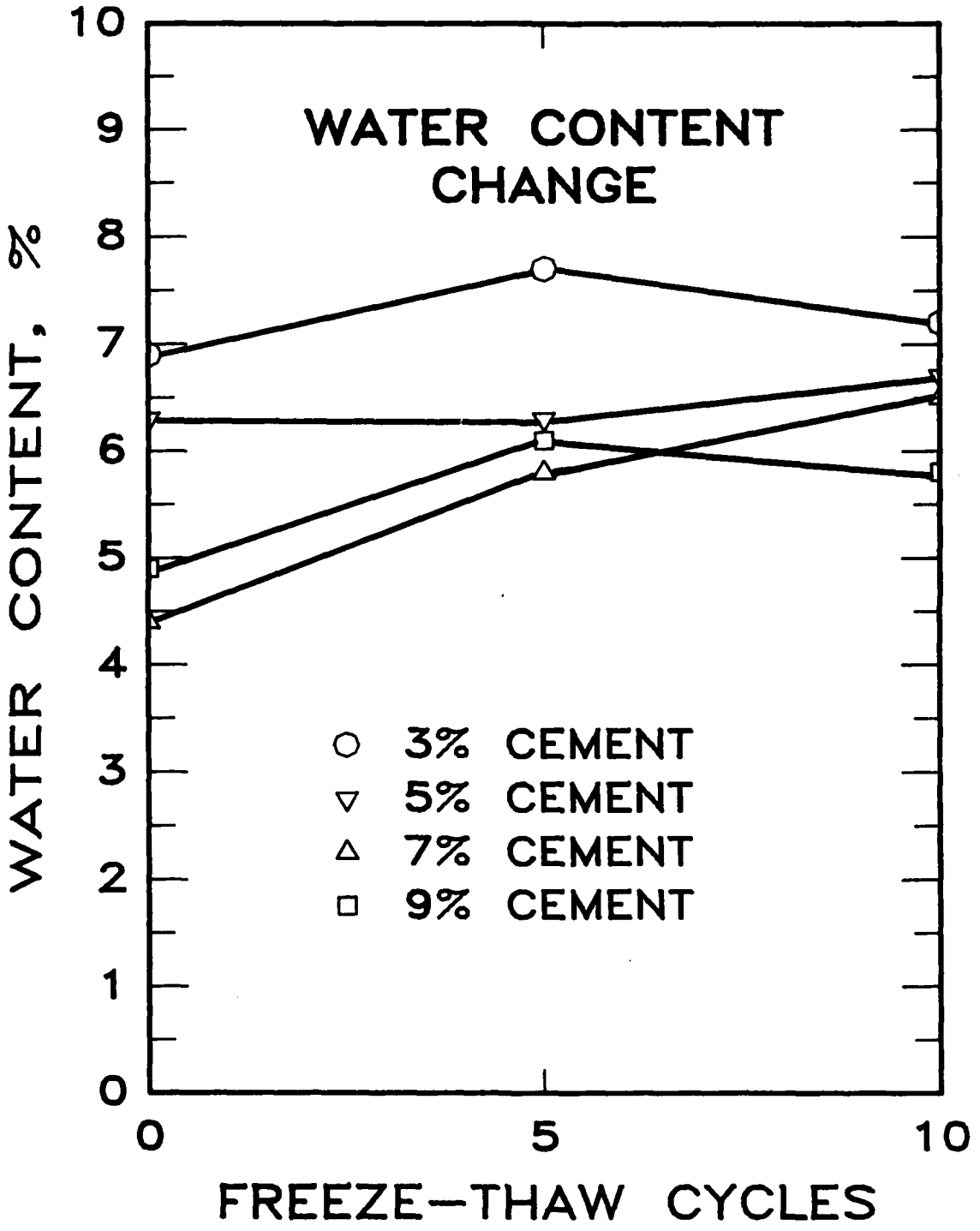

Figure 48. Water Content vs Number of F-T Cycles.

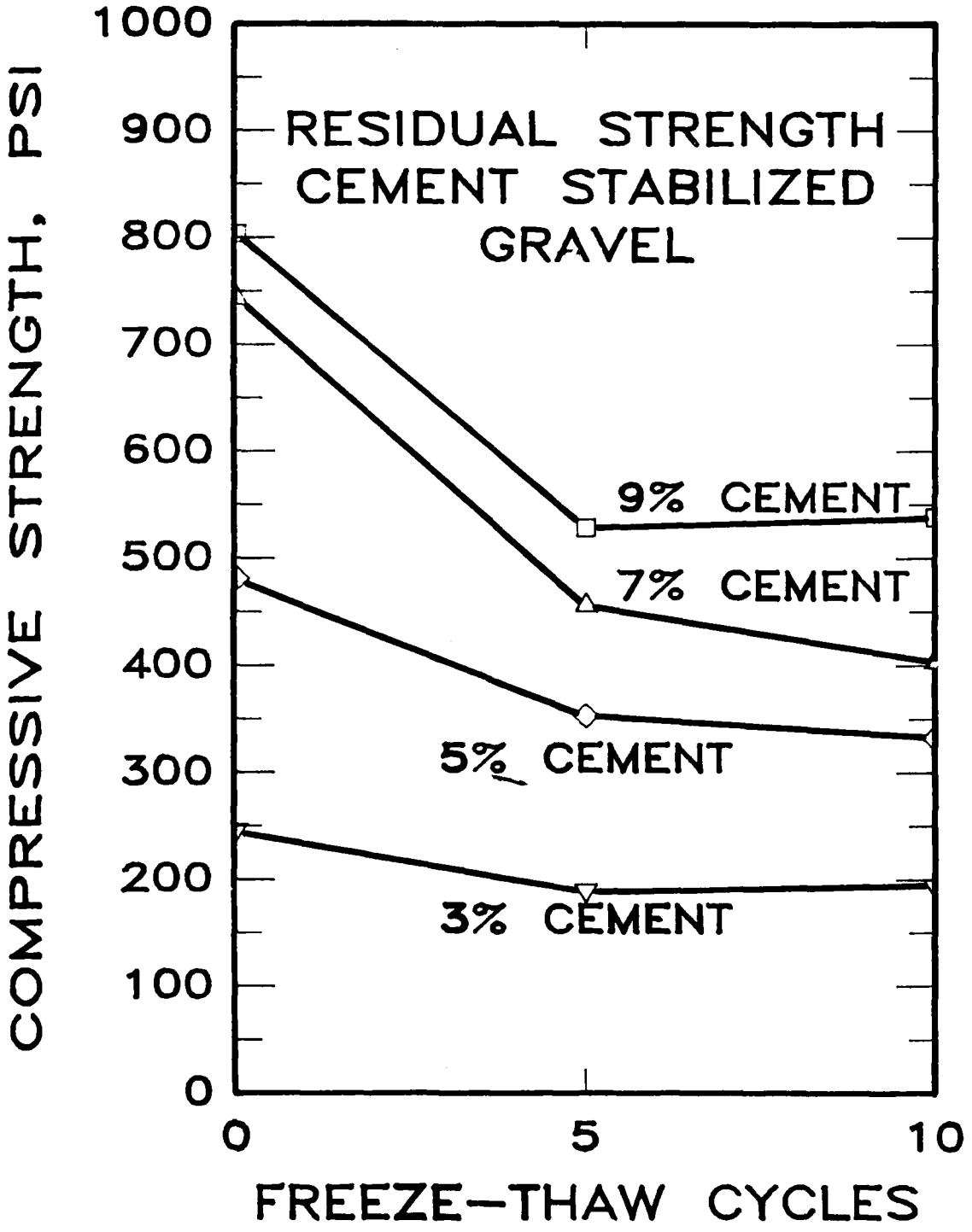

Figure 49. Residual Strength vs Number of F-T Cycles.

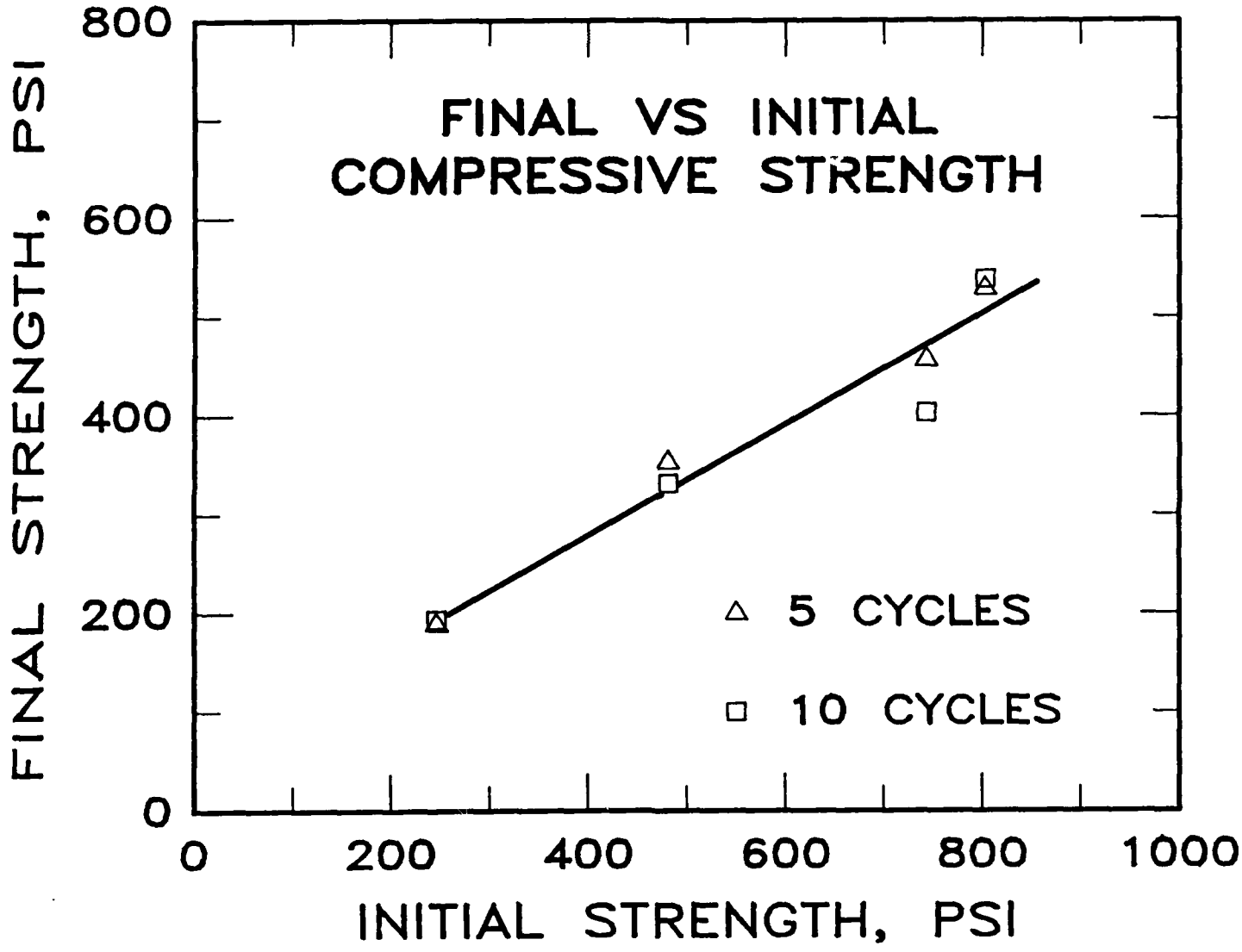

Figure 50. Residual Strength vs Initial Strength

show a greater strength loss for the higher initial strength materials than the Illinois tests. This is expected due to the slower freezing rate for the ALRS tests than for tests simulating the Illinois climate. The slower freezing rate permits more freeze-thaw damage to occur.

Vacuum saturation tests were not run on the ALRS samples because freeze-thaw testing gives more exact results.

F. SUMMARY

Heat transfer and moisture transfer equations were presented and the application of these equations to a climatic model for ALRS was discussed. The intrinsic and extrinsic parameters important to climatic modeling were described. Data were presented which indicated that pavement temperature predicted by the climatic model compared well with temperatures measured in the field.

Based on the use of the climatic model a characteristic freeze-thaw cycle for ALRS was developed for Ramstein AB, West Germany weather data. The freeze-thaw cycle was programmed into a freeze-thaw testing unit for the purpose of evaluating the durability properties of a cement stabilized base material which would meet the design criteria for ALRS. Test results showing compressive strength, heave and moisture content changes in samples with varying cement contents were determined after 5 and 10 freeze-thaw cycles.

The effects of different climates can be evaluated using the heat transfer model to determine values for the important freeze-thaw parameters of cooling rate, temperature below freezing and the number of freeze-thaw cycles. The effects of these parameters are discussed in the literature. (References 64, 65 and 66).

The effect of changing the soil being stabilized would only be a change in cured strength and could be evaluated using the results from this study. A change in the stabilizing agent, however, could affect the

nature of the cementing matrix, and would have to be evaluated with further testing.

The study indicated that the freeze-thaw testing procedure developed during this research phase would provide the necessary durability data for designing ALRS in various climates.

SECTION IV

STABILIZED PAVEMENT ANALYSIS SYSTEM

A. INTRODUCTION

Proposed procedures for designing ALRS-stabilized pavement sections are presented in this section. Details relating to stabilized material properties, structural analyses, structural response, pavement performance, and environmental factors are presented in other sections of this report.

Inputs required to establish a stabilized base thickness for an ALRS pavement (F-4 loading) are the field strength of the stabilized material and the E_{Ri} (measure of resilient modulus) of the subgrade. Only stress-softening (E_{Ri} decreases with increasing stress) fine-grained subgrades are considered.

B. STABILIZED MATERIAL STRENGTH

The unconfined compressive strength of the cured stabilized material is indicative of the modulus of elasticity and flexural strength of the material (see Appendix A).

1. Curing

The curing conditions should reflect local field - curing temperature conditions. Typical laboratory mixture design - curing conditions are:

Soil Cement - 7-or-28 day moist cure @ 73°F
Soil-Lime - 28 days in a sealed container @ 72°F
Lime-Fly Ash Aggregate - 14 days in a sealed container @ 72°F

Strength-degree-day relations are frequently used to extrapolate strength data for differing curing times. Field strength will generally increase with curing time. For climates with cyclic freeze-thaw, the maximum curing that can be achieved during the first year is from the time of construction to the onset of cold pavement temperatures (<40 °F) in the Fall.

In addition to curing considerations, adjustment factors (reductions) should be applied to the cured laboratory strength data to account for the difference between laboratory and field conditions and construction variability. Thompson and Dempsey (Reference 67) suggested mixing efficiency factors (field strength/laboratory strength) of 0.85 for plant-mixed material, 0.75 for mixed in-place stabilized granular material, and 0.65 for mixed in-place stabilized fine-grained soils. Suggested (Reference 67) coefficients of variation for the field strength of stabilized materials are 15 percent for plant-mixed material and 25 percent for mixed in-place material.

Density has a very pronounced impact on stabilized material-cured strength. Cured strength estimates should be based on "comparable densities" (laboratory vs field).

2. Residual Strength

The field-cured stabilized material will experience freeze-thaw strength loss. The residual strength (strength following the first winter of cyclic freeze-thaw action) is the field-cured strength (prior to experiencing freeze-thaw action) minus freeze-thaw strength loss.

Freeze-thaw strength loss is a function of the number of freeze-thaw cycles experienced. Residual strength-freeze-thaw cycle relations for the Ramstein AB, Germany area are shown in Figure 49 for several cement-aggregate mixtures evaluated in this study.

C. SUBGRADE RESILIENT MODULUS

The stabilized base flexural stress-base thickness-subgrade resilient modulus algorithms developed in Section II show that the major factor influencing the flexural stress is base course thickness. The effect of subgrade-resilient modulus is of little significance relative to stabilized base flexural stress. If the stabilized base section "breaks up" and loses its slab action characteristics, subgrade strength and modulus become the major factors influencing pavement response and performance. Chou (Reference 71) indicates that Corps of Engineers rigid pavement field and test section experience shows that slabs on weak subgrade ($k < 200$ psi/in.) develop multiple cracking and differential displacement shortly after initial slab cracking. Current Corps of Engineers design concepts (Reference 71) are based on "initial slab cracking" for weak subgrades but multiple slab cracking for stronger subgrades.

In the proposed "intact slab" thickness design approach the stabilized base thickness is established to prevent "break-up." Thus, the lowest anticipated subgrade E_{Ri} value should be utilized in the thickness design process.

The major factors influencing the resilient moduli of fine-grained soils are texture, plasticity, and moisture content. Freeze-thaw drastically reduces (sometimes by a factor of 2 to 4) the resilient modulus. Thompson and Dempsey (Reference 61) have considered subgrade soil inputs to concrete pavement design in detail. Silty and lower PI soils (ML, MH, CL, ML-CL) are more moisture-susceptible and CH type soils suffer a larger resilient modulus loss with freeze-thaw action. Thus, for "worst-scenario" conditions, all fine-grained soils should be assigned a "low" E_{Ri} value for the ALRS pavement design process. Suggested E_{Ri} values for various Unified soil classes, water table conditions, and frost effects, are shown in Table 21.

TABLE 21. SUGGESTED SUBGRADE VALUES FOR ALRS DESIGN

Unified Soil Class	Design Subgrade E_{Ri} ksi			
	High Water Table*		Low Water Table**	
	With Frost Penetration	Without Frost Penetration	With Frost Penetration	Without Frost Penetration
ML,MH,CL,ML-CL	2.0	4.0	3.0	6.0
CH	2.0	5.0	3.5	7.0

* Water table seasonally within 24 inches of subgrade surface.

** Water table seasonally within 72 inches of subgrade surface.

D. STABILIZED BASE THICKNESS

1. Design Inputs

The design compressive strength should be the lowest expected field strength anticipated for the facility during the specified ALRS design life. If the pavement is to be utilized immediately after construction, the appropriate curing condition may be limited to a short time period. In most cases, the lowest expected strength for German conditions will be the residual strength following the first winter of freeze-thaw exposure. Selection of the design compressive strength should be based on consideration of a combination of USAF design and construction policies and stabilized material technology.

Use the design compressive strength value to select a stabilized material modulus from Figure 51. Estimate the stabilized material design flexural strength as 20 percent of the design compressive strength.

The design subgrade E_{Ri} is selected from Table 21. As an alternative, the value can be established based on the results of more extensive field investigation and laboratory testing. Moisture-density and freeze-thaw softening effects can be quantified from repeated loading laboratory testing.

2. Base Thickness Determination

Stabilized base thickness is established by comparing the stabilized material design flexural strength with the estimated F-4 edge load condition flexural stress. The estimated edge load flexural stress is 50 percent greater than the ILLI-PAVE interior stress calculated from Equations (1), (2), (3), or (4).

Use the stress ratio (edge load flexural stress/design flexural strength) to predict the fatigue life from Figure 1. If the fatigue life is sufficient (greater than anticipated traffic), the thickness is

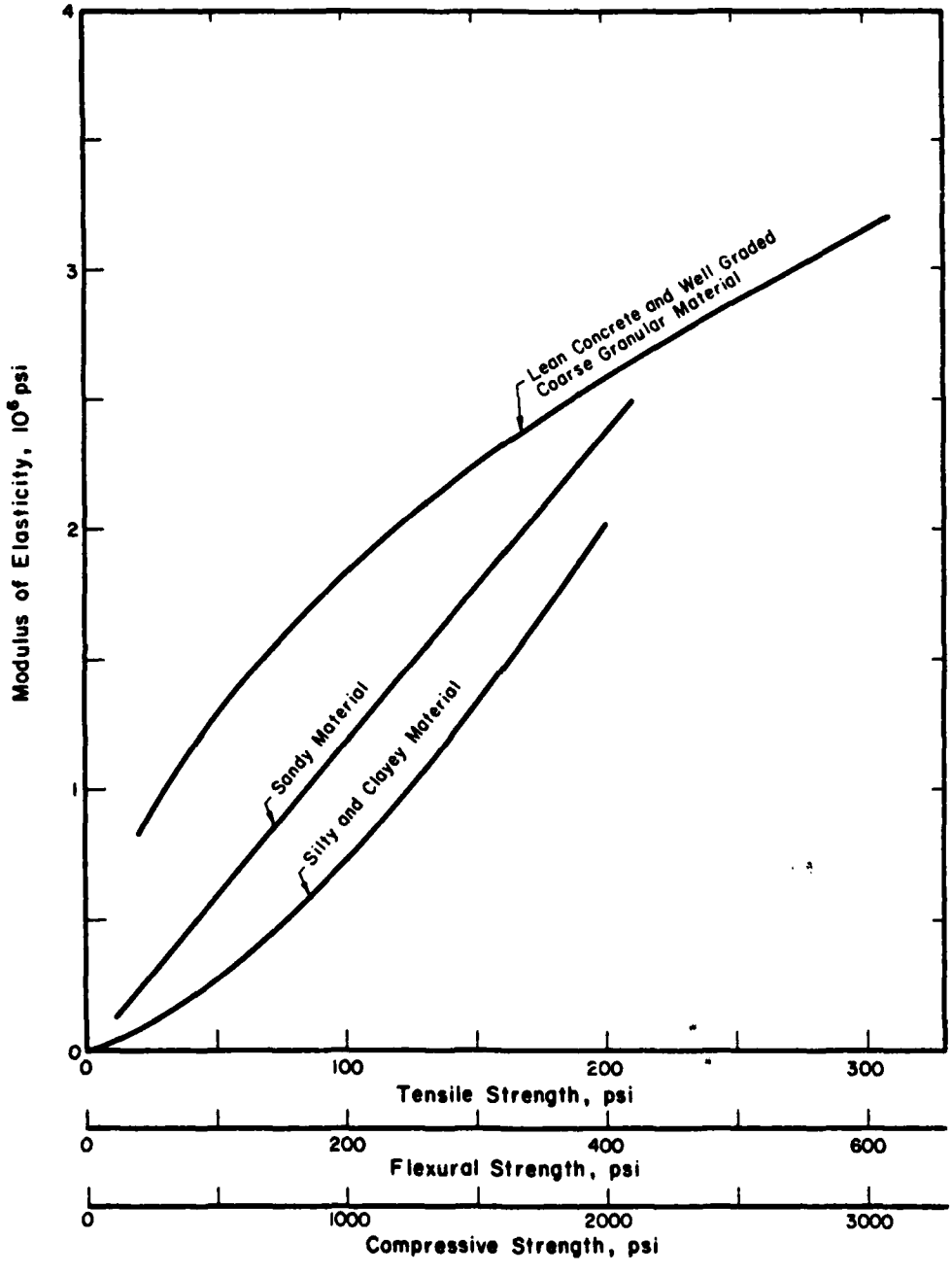

Figure 51. Recommended Modulus-Strength Relations for Cement-Stabilized Materials.

satistactory. In no case should the stress ratio exceed 0.65 (factor of safety = 1.5).

If an AC surface course is to be considered as a structural layer, the required stabilized base thickness can be reduced. AC surface thickness in excess of 2 inches is not normally required. A thickness less than 1 inch is of little structural value. For a 2-inch AC surface the stabilized base thickness can be reduced by 1 inch.

As a final design check, calculate the Meyerhof ultimate load-carrying capacity (edge-loading condition, Appendix C). The pavement thickness is the thickness of the stabilized base or the stabilized base thickness plus 1 inch if a 2-inch AC surface is utilized. The ultimate load (F-4 conditions) should be at least 40 kips.

3. Inverted Pavement Section Design

For combined thicknesses of AC surface and granular base of at least 6 inches, stabilized base flexural stress is approximately 65 percent of the stress estimated in Section IV.D for the stabilized base thickness only. For inverted pavement design, use the design concept presented in Section IV.D modified for the stress reduction affected by the AC and granular base layers. The controlling design parameters are still the stabilized base flexural stress and fatigue.

4. C-130 and F-15 Considerations

ALRS stabilized pavement sections designed in accordance with the proposed F-4 procedures will accommodate the limited (25 passes) C-130 traffic included in current ALRS requirements. Increased C-130 passes should be considered in a more detailed structural analysis.

Increased F-15 loading (30-kip and 36-kip wheel loads) will decrease the 1.5 factor of safety recommended for the F-4 design section. The approximate factors of safety (based on the limited F-15 data presented in Table 2) for the F-15 are 1.3 for 30-kip loading and

1.1 for 36-kip loading. Limited F-15 traffic can be accommodated by an ALRS section designed for F-4 traffic.

E. MATERIALS TESTING

1. General

Materials testing is required to develop mixture design recommendations, stabilized material compressive strength, and subgrade soils data. The thickness design procedure proposed is relatively insensitive to subgrade soil resilient modulus (E_{Ri}). Stabilized material strength has a great impact on pavement performance under repeated loading. Stress ratio (repeated flexural stress/flexural strength) and ultimate load-carrying capacity are directly related to the stabilized material strength. The major emphasis in materials testing should be directed to the stabilized material(s).

2. Stabilized Materials Testing

Relevant portions of AFM 88-6 should be used for soil stabilizer selection and mixture design guidance. Bituminous stabilization options are not included in the current ALRS-stabilized pavement study.

3. Soils Investigation and Testing

Routine site soils investigation and testing as per the appropriate AF guides and manuals are sufficient to provide the essential data for stabilized pavement thickness design. Unified soil classification and water table depth data are needed to select subgrade design E_{Ri} from Table 2 1.

F. SUMMARY

A preliminary stabilized pavement analysis system (SPAS) is proposed.

F. SUMMARY

SPAS F-4 design thicknesses seem realistic, but validation activities are needed. An extension of this project has been approved for considering pavement structural response and performance data developed in the ALRS Stabilized Test Section Project conducted at the Waterways Experiment Station, Vicksburg, MS.

The SPAS system can be readily calibrated to field performance by adjusting the stress ratio and ultimate edge load-carrying capacity requirements presented in Section IV.D.2.

SECTION V

CONCLUSIONS AND RECOMMENDATIONS

A preliminary ALRS Stabilized Material Pavement Analysis System (SPAS) is presented. Stabilized material properties (strength, modulus, fatigue), structural modeling and behavior concepts, and environmental factors (freeze-thaw, frost depth) are utilized in the SPAS development.

A. CONCLUSIONS

Inputs required to establish a stabilized base thickness for an ALRS pavement (F-4 loading) are the field strength of the stabilized material and the E_{Ri} (measure of resilient modulus) of the fine-grained subgrade. A properly designed ALRS pavement for F-4 loading can accommodate a limited number of C-130 and F-15 load applications. The SPAS thickness design concepts (based on an intact slab approach) are applicable to a broad range of cementitious-stabilized materials (soil-cement, lime-fly ash-aggregate, soil-lime mixtures, similar high strength and modulus materials). SPAS F-4 thickness requirements appear reasonable.

B. RECOMMENDATIONS

Further research and development is required to validate SPAS. Data and analyses related to the USAF ALRS Stabilized Test Section Project (Reference 70) at the Waterways Experiment Station will be useful.

It is emphasized that adequate material quality control and construction procedures must be developed and implemented for field construction. Stabilized mixture uniformity (percent stabilizer, thoroughness of mixing, moisture content, etc.), placement (layer thickness, compacted density), and curing (time, temperature, moisture maintenance) are some critical specification items.

REFERENCES

1. Hay, D. R., Aircraft Characteristics for Airfield Pavement Design and Evaluation, Technical Report AFWL-TR-69-54, Air Force Weapons Laboratory, Kirtland Air Force Base, New Mexico, October, 1969.

2. Tayabji, S. D., Nussbaum, P. J., and Ciolko, A. T., Evaluation of Heavily Loaded Cement-Stabilized Bases, Record 839, Transportation Research Board, 1982.

3. Thickness Design of Soil-Cement Pavements for Heavy Industrial Vehicles, Publication No. IS187, Portland Cement Association, 1975.

4. Raad, L., "Design Criteria for Soil-Cement Bases," Ph.D. Thesis, Department of Civil Engineering, University of California, Berkeley, 1976.

5. Maree. J. H., and Freeme, C. R., The Mechanistic Design Method Used to Evaluate the Pavement Structures in the Catalogue of the Draft TRH4 1980, Technical Report RP/2/81, National Institute for Transport and Road Research, CSIR, South Africa, March, 1981.

6. Suddath, L. P. and Thompson, M. R., Load-Deflection Behavior of Lime-Stabilized Layers, Technical Report M-118, U. S. Army, Construction Engineering Research Laboratory, Champaign, IL, January, 1975.

7. Horfman, M. S., and Thompson, M. R., Mechanistic Interpretation of Nondestructive Pavement Testing Deflections," Civil Engineering Studies, Transportation Engineering Series No. 32, University of Illinois at Urbana-Champaign, June, 1981.

8. Tabatabaie, A. M., and Barenberg, E. J., Longitudinal Joint Systems in Slip-Formed Rigid Pavements - Volume III - Users Manual, Report No. FAA-RD-79-4, November, 1979.

9. Thompson, M. R., Ioannides, A. M., Fischer, J. M., and Barenberg, E. J., Development of a Stress-Dependent Finite Element Slab Model, Report AFOSR-TR-83-1061, Air Force Office of Scientific Research (AROSR), 1983.

10. Westergaard, H. M., "Stresses in Concrete Pavements Computed by Theoretical Analysis," Public Roads, Vol. 7, No. 2, April, 1926. (Also in Highway Research Board, Proceedings, 5th Annual Meeting, 1925 published 1926, Part I, under title "Computation of Stresses in Concrete Roads").

11. Westergaard, H. M., "New Formulas for Stresses in Concrete Pavements of Airfields," ASCE, Transactions, Vol. 113, 1948. (Also in ASCE Proceedings, Vol. 73, No. 5, May, 1947).

12. Bradbury, R. D., Reinforced Concrete Pavements, The Wire Reinforcing Institute, 1938.

13. Ahlberg, H. L., and Barenberg, E. J., Pozzolanic Pavements, Bulletin 473, University of Illinois at Urbana-Champaign, 1965.

14. Barenberg, E. J., Evaluating Stabilized Materials, NCHRP Report, Project 63-4, Department of Civil Engineering, University of Illinois, Urbana, Illinois, 1967.

15. Meyerhof, G. G., "Load-Carrying Capacity of Concrete Pavements," Journal, Soil Mechanics and Foundations Division, ASCE, Vol. 88, No. SM3, June, 1962.

16. Mitchell, J. K., et al, Behavior of Stabilized Soils Under Repeated Loading; Report 6, A Summary Report with a Suggested Structural Pavement Design Procedure, Contract Report No. 3-145, Report 6, Waterways Experiment Station, U. S. Army Corps of Engineers, Vicksburg, MS, October, 1974.

17. Pretorius, P. C., "Design Considerations for Pavements Containing Soil Cement Bases," Ph.D. Thesis, Department of Civil Engineering, University of California, Berkeley, 1970.

18. Otte, E., Analysis of a Cracked Pavement Base Layer, Record 725, Transportation Research Board, 1979.

19. Brown, S. F., Design of Pavements with Lean-Concrete Base Courses, Record 725, Transportation Research Board, 1979.

20. Dempsey, B. J., Climatic Effects on Airport Pavement Systems: State of the Art, Final Report, U. S. Army Corps of Engineers and Federal Aviation Administration, Washington, D. C., 1976.

21. Dusinberre, G. M., Numerical Analysis of Heat Flow, McGraw-Hill Book Company, Inc., New York, 1949.

22. Berg, R. L., "Thermoinsulating Media Within Embankments on Perennially Frozen Soil," Ph.D. Thesis, University of Alaska, Department of Civil Engineering, Fairbanks, Alaska, 1973.

23. Carroll, C., Schenck, H., Jr., and Williams, W., "Digital Simulation of Heat Flow in Soils," Journal of the Soil Mechanics and Foundations Division, ASCE, Vol. 92, No. SM4, 1966.

24. Schenck, J., Jr., FORTRAN Methods in Heat Flow, The Ronald Press Company, New York, 1963.

25. Straub, A. L., Schenck, H. N., Jr., and Przybycien, F. E., Bituminous Pavement Temperature Related to Climate, Record No. 256, Highway Research Board, 1968.

26. Corlew, V. S., and Dickson, P. F., "Methods for Calculating Temperature Profiles of Hot-Mix Asphalt Concrete as Related to the Construction of Asphalt Pavements," Proceedings, The Association of Asphalt Paving Technologists, 1968.

27. Christison, J. T., and Anderson, R. O., "The Response of Asphalt Pavements to Low Temperature Climatic Environments," Proceedings, Third International Conference on the Structural Design of Asphalt Pavements, Vol. 1, London, England, 1972.

28. Dempsey, B. J., "A Heat-Transfer Model for Evaluating Frost Action and Temperature Related Effects in Multilayered Pavement Systems," Ph.D Thesis, University of Illinois, Department of Civil Engineering, Urbana, Illinois, 1969.

29. Dempsey, B. J., and Thompson, M. R., A Heat-Transfer Model for Evaluating Frost Action and Temperature-Related Effects in Multilayered Pavement Systems, Record No. 342, Highway Research Board, 1970.

30. Johnson, A. W., and Lovell, C. W., Jrs., Frost Action Research Needs, Bulletin 71, Highway Research Board, 1953.

31. Bouyoucos, G. J., "Effect of Temperature on the Movement of Water Vapor and Capillary Moisture in Soils," Journal, Agricultural Research, Vol. 5, 1915.

32. Hutchinson, H. P., Dixon, I. S., and Denbigh, K. G., "The Thermo-osmosis of Liquids Through Porous Materials," Discussion, Faraday Society, Vol. 3, 1946.

33. Philip, J. R., and de Vries, D. A., "Moisture Movement in Porous Materials Under Temperature Gradients," Transactions, American Geophysical Union, Vol. 38, The American Geographical Union of the National Academy of Sciences, National Research Council, Washington, D. C., 1957.

34. Taylor, S. A., and Cary, J. W., "Linear Equations for the Simultaneous Flow of Matter and Energy in a Continuous Soil System," Proceedings, Soil Science Society of America, Vol. 28, 1964.

35. Taylor, S. A., and Cary, J. W., "Soil Water Movement in Vapor and Liquid Phases," Methodology of Plant Eco-System, UNESCO Arid Zone Research, Vol. 25, 1905.

36. Cassel, D. K., Soil-Water Behavior in Relation to Imposed Temperature Gradients," Ph.D. Thesis, University of California, Davis, California, 1968.

37. Cary, J. W., "Soil Moisture Transport Due to Thermal Gradients: Practical Aspects," Proceedings, Soil Science Society of America, Vol. 30, 1966.

38. Hoekstra, P., "Moisture Movement in Soils Under Temperature Gradients, with Cold-Side Temperature Below Freezing," Water Resources Research, Vol. 2, 1966.

39. Jumikis, A. R., Experimental Studies on Moisture Transfer in a Silty Soil Upon Freezing as a Function of Porosity, Cushing-Malloy, Inc., Ann Arbor, Michigan, 1969.

40. Dempsey, B. J., "A Mathematical Model for Predicting Coupled Heat and Water Movement in Unsaturated Soil," Vol. 2, International Journal for Numerical and Analytical Methods in Geomechanics, John Wiley and Sons, New York, New York, 1977.

41. Jumikis, A. R., Amount of Soil Moisture Transferred in a Therosmotic Process of Freezing as a Function of Porosity of Soils, Record No. 209, Highway Research Board, 1967.

42. Harlan, R. L., "Ground Conditioning and the Groundwater Response to Winter Conditions," International Symposia on the Role of Snow and Ice in Hydrology, Symposium on Properties and Processes, Banff, Alberta, 1972.

43. Hoekstra, P., The Physics of Water and Ice in Soil, Monograph II-D2, Corps of Engineers, U. S. Army, Cold Regions Research and Engineering Laboratory, Hanover, New Hampshire, 1972.

44. Berg, R. L., Guymon, G. L., and Johnson, T. C., Mathematical Model to Correlate Frost Heave of Pavements with Laboratory Predictions, Report No. FAA-RD-79-109, U. S. Army, Corps of Engineers, Cold Regions Research and Engineering Laboratory, Hanover, NH, 1980.

45. Dempsey, B. J., and Thompson, M. R., Durability Properties of Lime-Soil Mixtures, Record No. 235, Highway Research Board, 1968.

46. Dirksen, C., "Water Movement and Frost Heaving in Unsaturated Soil Without an External Source of Water," Ph.D. Thesis, Cornell University. Ithaca, New York, 1964.

47. Dempsey, B. J., and Elzeftawy, A., A Mathematical Model for Predicting Moisture Movement in Pavement Systems, Record No. 612, Transportation Research Board, 1977.

48. Scott, R. F., "Heat Transfer at the Air-Ground Interface with Special Reference to Freezing and Thawing Problems Below Airfield Pavements," Thesis, Massachusetts Institute of Technology, 1955.

49. Berg, R. L., Energy Balance on a Paved Surface, Technical Report 226, Corps of Engineers, U. S. Army, Cold Regions Research and Engineering Laboratory, Hanover, New Hampshire, 1974.

50. Hamon, R. W., Weiss, L. L., and Wilson, W. T., "Isolation as an Empirical Function of Daily Sunshine Duration," Monthly Weather Review, Vol. 82, No. 6, U. S. Weather Bureau, Washington, D. C., 1954.

51. Baker, D. G., and Hanes, D. A., Solar Radiation and Sunshine Duration Relationships in the North-Central Region and Alaska, Technical Bulletin 262, Agricultural Experiment Station, University of Minnesota, 1969.

52. Pochop. L. O., Shanklin, M. D., and Horner, D. A., "Sky Cover Influence on Total Hemispheric Radiation During Daylight Hours," Journal of Applied Meteorology, Vol. 7, No. 3, American Meteorological Society, Hartford, Connecticuit, 1968.

53. Janssen, D. J., and Dempsey, B. J., Soil Water Properties of Subgrade Soils, Department of Civil Engineering, University of Illinois, Urbana-Champaign, Transportation Engineering Series 27, Illinois Cooperative Highway and Transportation Series 184, April, 1980.

54. Kersten, M. S., Thermal Properties of Soils, Bulletin No. 28, University of Minnesota, Engineering Experiment Station, Minneapolis, MN, 1949.

55. Black, W.P.M., "A Method of Estimating the California Bearing Ratio of Cohesive Soils from Plasticity Data," Geotechnique, Dec. 1962.

56. Thompson, M. R., and Robnett, Q. L., Final Report, Resilient Properties of Subgrade Soils, Department of Civil Engineering, University of Illinois, Urbana-Champaign, Transportation Engineering Series No. 14, Illinois Cooperative Highway and Transportation Series 160, June 1976.

57. Simonsen, P., and Ajalmarsson, S. O., "Influence of the Ground Water Table-Level on the Bearing Capacity," Road Drainage, Organization for Economic Cooperation and Development, Paris, 1978.

58. Taber, S., "Frost Heaving," Journal of Geology. Vol. 37, 1929.

59. Dempsey, B. J., Moisture Movement and Moisture Equilibria in Pavement Systems, Final Report, Transportation Engineering Series No. 25, Illinois Cooperative Highway and Transportation Series No. 129, Urbana, Illinois, 1979.

60. Burns, J., The Effect of Water-Table on the Frost Susceptibility of a Roadmaking Material, Report 305, Transport and Road Research Laboratory, England, 1977.

61. Thompson, M. R., and Dempsey, B. J., "Subgrade Soils: An Important Factor in Concrete Pavement Design," Proceedings, International Conference on Concrete Pavement Design, Purdue University, 1977.

62. USAFETAC DATSAV Data Base for Ramstein 1952-1968, United States Air Force Air Weather Service (MAC), USAF Environmental Technical Applications Center, Scott Air Force Base, Illinois.

63. Zimmerman, Michael, J., Major, USAF, Miscellaneous Climate Data, Correspondence, November 22, 1982.

64. Thompson, M. R., and Dempsey, B. J., "Quantitative Characterization of Cyclic Freezing and Thawing in Stabilized Pavement Materials," Record No. 304, Highway Research Board, 1970.

65. Dempsey, B. J., and Thompson, M. R., Effects of Freeze-Thaw Parameters on the Durability of Stabilized Materials, Record No. 379, Highway Research Board, 1972.

66. Dempsey, B. J., and Thompson, M. R., Interim Report- Durability Testing of Stabilized Materials, Civil Engineering Studies, Transportation Engineering Series No. 1, Illinois Cooperative Highway Research Program Series No. 132, University of Illinois at Urbana-Champaign, September, 1972.

67. Thompson, M. R., and Dempsey, B. J., Durability Testing of Stabilized Materials - Final Report, Transportation Engineering Series No. 11, Department of Civil Engineering, Engineering Experiment Station, University of Illinois, Urbana, Illinois, 1974.

68. Chow, Ven Te, Frequency Analysis of Hydrologic Data with Special Application to Rainfall Intensities," University of Illinois Engineering Experiment Station, Bulletin Series No. 44, University of Illinois at Urbana-Champaign, July, 1953.

69. Dempsey, B. J., "A Programmed Freeze-Thaw Durability Testing Unit for Evaluating Paving Materials," Vol. 7, No. 2, American Society for Testing and Materials, Philadelphia, Pennsylvania, 1972.

70. Styron, C. R., Performance Data for F-4 Operations on Alternate Launch and Recovery Surfaces, Geotechnical Laboratory, U. S. Army, Waterways Experiment Station, Vicksburg, MS, August, 1983 (Draft Report to AFESC, Tyndall AFB, FL).

71. Chou, Y. T., "Subgrade Contact Pressures Under Rigid Pavements," Journal, Transportation Engineering, ASCE, Vol. 109, No. 3, May, 1983.

(The reverse of this page is blank)

APPENDIX A

THE SELECTION OF
STRESS-STRAIN, STRENGTH, AND FATIGUE RELATIONSHIPS
FOR USE IN MECHANISTIC PAVEMENT DESIGN PROCEDURES

APPENDIX A

THE SELECTION OF STRESS-STRAIN, STRENGTH, AND FATIGUE RELATIONSHIPS FOR USE IN MECHANISTIC PAVEMENT DESIGN PROCEDURES

A. INTRODUCTION

The mechanistic design of a pavement requires a knowledge of the stress-strain relationships for each of the materials to be used. Ideally, tests would be conducted as a part of the design to identify these relationships. This approach, however, is rarely practical both because the testing is costly and time-consuming and because the exact sources of all materials are frequently not known at the time of design. Therefore generalized relationships between the required properties and the properties normally specified for construction control are needed for the mechanistic approach to be useful for routine design.

This appendix presents a review of the literature to identify stress-strain relationships for cementitious-stabilized materials. Cementitious-stabilized materials are defined as fine-and coarse-grained soils and aggregates that have been bound together by a stabilizing agent so as to produce a hard, rigid mass. These include soil-cement, soil-lime mixtures, lime-fly ash aggregate mixtures, cement aggregate mixtures, and the various stabilization processes that incorporate a combination of cement, fly ash, and/or lime.

The relationships presented herein are quite general with no distinction being made for the effects of specific test conditions. For example, the compressive-to-tensile strength relationship is discussed without regard to such details as the length-to-diameter (L/D) ratio of the compressive test specimens. This is because the relationships reported are so divergent that the influence of these details become obscured. This, however, does not prevent these generalized

relationships from being quite useful for design purposes; nor does it negate the importance of noting and controlling such details in routine material testing programs.

B. STRENGTH RELATIONSHIPS

The strength of the stabilized material is a fundamental property required for design, often specified and used for construction control. The types of tests frequently used for control are the flexure (beam) test, the split tension test, and the unconfined compression test with the latter being perhaps the most common because of its relative simplicity. Since each of these provide a different measure of the "true" strength of the material, some relationship between the different measures is required for them to have equal value to the design process.

The tensile strength of the material is required for most design purposes. Of the various tests, all except the unconfined compression test provide a measure of this property. However, numerous investigators have found that the tensile strength obtained for a given material will vary depending upon which type of test is used. Sherwood (Reference 1) for example found that the flexural strength was generally about 1.5 times (and in some cases more than two times) the split tensile strength. Similarly, data reported by Pretorious and Monismith (Reference 2) suggest that flexural strength is about twice the direct tensile strength. The direct tension test is generally believed to provide the truest measure of tensile strength.

Raad (Reference 3) has demonstrated that these apparent strength differences are because the modulus of elasticity of these materials is not the same in both compression and tension. He made a detailed analysis of the various tensile strength tests using finite element theory and varying the compression and tension moduli of elasticity. In the analyses he demonstrated that the tensile strengths from the split tensile test and the direct tension test are about equal, but that the

tensile strength from the flexure test can be more than double the direct tension strength. The validity of the analysis is subsequently demonstrated through comparisons of direct tension, split tension, and flexural strengths.

From these, it seems reasonable to assume for design purposes that both the direct tension and split tension tests provide a direct measure of the tensile strength; and that the strength obtained from the flexural (beam) test is double the "true" tensile strength.

Relationships between unconfined compressive strength and the various measures of tensile strength have been reported by many investigators. Felt and Abrams (Reference 4) found that flexural strength of soil cement was about 20 percent of the compressive strength. Other investigators have reported similar percentages- 22.4 by Scott (Reference 5), 13 to 25 by Yrjanson and Packard (Reference 6), 14 to 16 by Sherwood (Reference 1), and 25 by Barenberg (Reference 7). Mitchell and Monismith (Reference 8) have recommended a more complex relationship:

$$FS = 0.5(CS)^{0.88}$$

where:

FS = flexural strength, psi

CS = unconfined compressive strength, psi.

For compressive strengths ranging from 500 psi to 3000 psi, this equation is equivalent to using compressive strength percentages ranging from 23.7 to 19.1.

Similar percentages have been reported for other cementitious stabilized materials. Thompson (Reference 9) found that the flexural strength of lime soil mixtures was about 25 percent of the unconfined compressive strength. Barenberg (Reference 10) reported flexural

strengths for lime fly ash aggregate mixtures that were 18 to 20 percent of the corresponding compressive strengths.

Relationships between split tensile strengths and unconfined compressive strength have also been investigated. Sherwood (Reference 1) found that the split tensile strength of cement-stabilized material was about 10 percent of the compressive strength; and Thompson (Reference 11) found that the split tensile strength of lime-stabilized soil was 13 percent of the unconfined strength. Kennedy et al. (Reference 12) reported the relationship:

$$ST = -11.38 + .1662\ CS$$

where:

ST = split tensile stength, psi
CS = unconfined compressive strength, psi.

For compressive strengths ranging from 500 psi to 3000 psi, this is equivalent to percentages of 14.3 to 16.1.

These suggest that flexural strength is generally about 20 to 25 percent of the unconfined compressive strength and that the split tensile strength is about 10 to 15 percent. These percentages are consistent with the 2:1 flexural to split tension relationship noted earlier and are reasonably conservative for design purposes. They are also consistent with relationships identified by Price (Reference 13) and reported by Neville (Reference 14) for concrete having compressive strengths between 1000 and 3000 psi.

From the data reported in the literature the following general conclusions are made regarding the relationships between the various measures of strength for cementitious stabilized material.

1. Both the direct tension test and the split tension test provide a reasonable measure of the "true" tensile strength of a cementitious stabilized material.
2. The tensile strength determined from a flexural (beam) test is significantly greater than the "true" tensile strength, often by as much as a factor of two.
3. The unconfined compression test can be used to approximate the tensile strength of a cementitious stabilized material. An acceptable conservative estimate is that the tensile strength is 10 percent of the compressive strength.

From the conclusions the following strength relationships are recommended for use in design.

$$TS = ST$$
$$TS = .5\ FS$$
$$TS = .1\ CS$$
$$FS = .2\ CS$$

where:

TS = tensile strength (direct tension)
ST = split tension strength
FS = flexural strength
CS = compressive strength.

C. STRESS-STRAIN RELATIONSHIPS

The stress-strain behavior of a pavement material is normally expressed in terms of an elastic or resilient modulus. For cementitious-stabilized materials, the selection of an appropriate modulus value to represent the material for design is complicated not only because of the difficulty in testing but also because 1) different test methods give

different values (Reference 5), 2) the relationship is generally nonlinear above about 60 percent of the strength of the material (Reference 15), and 3) the modulus is generally lower in tension than it is in compression (References 3, 15, 16). Because of these difficulties, Packard (Reference 17) recommended using a relationship between flexural strength and the modulus of elasticity in lieu of testing.

Numerous investigators have reported data relating strength and the modulus of elasticity of various cementitious-stabilized materials. Lilley and Williams (Reference 18) examined the data published by Felt and Abrams (Reference 4), Larsen and Nussbaum (Reference 19), Jones (Reference 20), and others. From their examination they concluded that different relationships exist, dependent upon the quality of the material being stabilized. They classified the material reported as lean concrete, cement-bound granular material, and fine-grained soil-cement. For a given strength level, they found the lean concrete to have the highest modulus and the fine-grained soil cement to have the lowest. Envelopes of the values found by Lilley and Williams are shown on Figure A-1.

Shen (Reference 21), Mitchell et al. (Reference 22), and Wang (Reference 23) investigated the stress-strain behavior of several soil cements. From their work an equation was developed (References 15, 24) that relates the resilient modulus in flexure to the compressive strength, cement content, and a material constant which must be established for each material. The equation is:

$$Er = Kf\ (10)^{m(CS)}$$

where:

Er = the resilient modulus in flexure in psi
Kf = a material constant
$m = 0.04(10)^{-0.186C}$
CS = the unconfined compressive strength in psi
C = the cement content in percent by weight.

This equation can be used in design if the constant Kf for the material is known.

Numerous other investigators have reported strength-modulus relationships for various cementitious-stabilized materials. Several of these are plotted on Figure A-2. Although they exhibit the general relationship of higher modulus with higher quality material that was noted by Lilley and Williams (Reference 18), the modulus values for lean concrete are lower than those shown in Figure A-1.

Also shown on Figure A-2 is a plot of the equation used for estimating modulus of elasticity in reinforced concrete design under the ACI Code (Reference 25). This equation is:

$$E = 33 * w^{3/2} * (CS)^{1/2}$$

where:

E = the modulus of elasticity in psi
CS = compressive strength in psi
w = unit weight of the concrete in pcf.

For a typical concrete unit weight of about 145 pounds per cubic foot the equation reduces to:

$$E = 57,500\ (CS)^{1/2}$$

This equation appears to be in reasonably close agreement with the relationships for lean concrete and coarse – grained stabilized material.

Based on an examination of these relationships, three strength-modulus relatonship curves are recommended for use in design when only the type of material to be stabilized and its specified or

expected strength are known. These are shown in Figure A-3, superimposed over the relationships plotted on Figure A-2, and separately on Figure A-4. As noted on the figures, the upper curve is recommended for use with lean concrete and high-quality, well-graded, coarse-grained material; the middle curve is for sandy material; and the lower curve is for silty and clayey fine-grained material. The equations governing these curves are:

For lean concrete and high-quality coarse-grained material:

$$E = 57{,}500\ (CS)^{1/2}$$

For lower-quality coarse-grained and sandy material:

$$E = 1200\ CS$$

For silty and clayey fine-grained material:

$$E = 440\ CS + .28\ (CS)^2$$

where:

E = the modulus of elasticity in psi
CS = compressive strength in psi.

D. POISSON'S RATIO

Numerous investigators have determined Poisson's ratio for various cementitious stabilized materials. Felt and Abrams (Reference 4) tested four soil-cement mixtures with varying cement contents.

They reported ratios ranging from 0.22 to 0.36 for dynamic tests and 0.08 to 0.24 for static tests. In a discussion of Felt and Abrams work, Winterkorn (Reference 32) presents the results of tests on four additional soil cements in which values of 0.053 to 0.142 were obtained.

In a paper discussing the mechanistic design procedure developed for use in South Africa, Maree and Freeme (Reference 33) indicate that Poisson's ratio for cement treated materials can range from 0.1 to 0.5. A value of 0.35 is recommended for use in that design procedure.

Thompson (Reference 29) determined Poisson's ratio for four lime-soil mixtures. He found values ranging from 0.08 to 0.12 at low stress levels (less than 25 percent of ultimate) and from 0.27 to 0.37 at higher stress levels (50 to 75 percent of ultimate). Ahlberg and Barenberg (Reference 34) reported similar values and a similar relationship with increasing stress levels for lime-fly ash aggregate mixtures.

The FHWA User's Manual for Soil Stabilization in Pavement Structures (Reference 24) recommends the following ranges of values for the various cementitious stabilized materials:

MATERIAL	POISSON'S RATIO
Lime Soil	0.15 to 0.20
Lime-Fly Ash Materials	0.10 to 0.15
Cement-Stabilized Granular	0.10 to 0.20
Fine-Grained Soil-Cement	0.15 to 0.35

Based on these recommendations and an examination of the values reported in the literature, a Poisson's ratio of 0.15 has been selected as the appropriate value for use in general pavement design analyses. This value is the same as that normally used in the design of PCC pavements (37).

E. FATIGUE CHARACTERISTICS

The fatigue characteristics of cementitious stabilized materials have been studied in terms of radius of curvature, strain levels, stress

ratios, and strength reduction. One of the earliest studies of the fatigue characteristics of cement-stabilized materials was conducted by Larsen and Nussbaum (Reference 19). Their study attempted to duplicate pavement loading conditions by testing soil-cement beams supported on a simulated subgrade composed of neoprene pads. Variations in subgrade support were simulated by varying the number of pads. Three soil-cement mixtures were used in the tests. Two of these were coarse-grained predominantly gravel and sand) and one was fine-grained predominantly fine sand, silt and clay). Larsen and Nussbaum selected radius of curvature of the loaded beam as the basic response used to characterize the observed behavior. Their fatigue model was:

$$Rc/R = a\ N^{-b}$$

where:

Rc = critical radius of curvature, the radius of curvature that would cause failure due to a single load application.

R = the initial radius of curvature of the test beam under the fatigue test loading.

N = number of load applications to failure.

a & b = fatigue factors determined from the tests.

Failure was defined as the development of a visible crack.

An important conclusion from their study was that subgrade strength did not affect the fatigue characteristics (except, of course, as reflected in the radius of curvature). This shows that a more fundamental model based on stress or strain levels can be used to characterize the fatigue properties.

Pretorius (Reference 35) investigated the fatigue behavior of a single soil cement and examined three possible fatigue models: the Larsen

and Nussbaum curvature model. one based on initial tensile strain, and one based on intial tensile stress. He found general agreement with Larsen and Nussbaum's results but concluded that the initial strain model provided the "best" fit to his experimental data.

Pretorious also examined the strain history of the test specimens. He found that the strain induced by a given load remained relatively constant over most of the fatigue life but increased just prior to failure. Strains at failure were found to be between 130 and 170 microstrain regardless of the initial strain. By comparison, the failure strain for a single static load was found to be about 200 microstrain. Similar results have been reported by other investigators (Reference 27) with the average strain at failure being about 160 microstrain.

This behavior suggests a progressive weakening of the material with load repetitions. Raad (Reference 3) investigated this phenomenon and developed a fatigue model for soil-cement based on loss of tensile strength. His work indicates that failure occurs when the tensile strength becomes less than the applied stress.

Nevertheless, the majority of investigators have used a stress ratio model (applied stress/tensile strength) when studying the fatigue behavior of the various cementitious-stabilized materials. Consequently, the fatigue behavior of cementitious stabilized materials appears at this time to be most comprehensively defined by the stress ratio model. This model is also the one most generally used with portland cement concrete. As a result, the majority of practicing engineers are familiar with the stress model concept making it more readily understood and accepted in practice. A stress ratio model, therefore, has been selected for use in the mechanistic design procedure.

Stress ratio-fatigue relationships reported by various investigators are shown on Figure A-5. Included on the figure is the fatigue relationship recommended by the Portland Cement Association

(Reference 38) for use in the design of concrete pavements. This relationship closely approximates several of the relationships reported for the other cementitious materials. Since this curve is also close to the lower boundary of the reported relationships, it has been selected for use in design with one alteration.

For PCC pavement design, the PCA method allows an unlimited number of repetitions for stress ratios of 0.50 or less. This is represented by the horizontal portion of the curve shown on Figure A-5. For design of cementitious stabilized bases and subbases, the general slope of the PCA fatigue relationship is continued beyond the 0.50 stress ratio limit.

The fatigue relationship recommended for use in design is shown in Figure A-6. This relationship can also be represented by the equation:

$$\log (N) = (.9722 - S)/.0825$$

where:

N = allowable number of load repetitions
S = applied flexural stress/flexural strength ratio.

REFERENCES

1. Sherwood, P.T., The Properties of Cement-Stabilized Materials, RRL Report LR 205, Road Research Laboratory, England, 1968.

2. Pretorius, P.C. and Monismith, C.L., "The Prediction of Shrinkage Stresses in Pavements Containing Soil Cement Bases," Paper presented at the Annual Meeting of the Highway Research Board, Washington, D.C., 1971.

3. Raad, L., "Design Criteria for Soil-Cement Bases," Ph.D. Dissertation, Department of Civil Engineering, University of California, Berkeley, 1976.

4. Felt, E.J. and Abrams, M.S., Strength and Elastic Properties of Compacted Soil-Cement Mixtures, Special Technical Publication Number 206, American Society for Testing Materials, 1957.

5. Scott, J.L.M., Flexural Stress-Strain Characteristics of Saskatchewan Soil Cements, Technical Report 23, Saskatchewan Department of Highways and Transportation, Canada, 1974.

6. Yrjanson, W.A. and Packard, R.G., Econocrete Pavements: Current Practices, Record 741, Transportation Research Board, 1980.

7. Barenberg, E.J., Evaluating Stabilized Materials, National Cooperative Highway Research Program, Contract No. HR 63-4-1, Unpublished Report.

8. Mitchell, J.K. and Monismith, C.L., "A Thickness Design Procedure for Pavements with Cement Stabilized Bases and Thin Asphalt Surfacings," Fourth International Conference on the Structural Design of Asphalt Pavement, University of Michigan, 1977.

9. Thompson, M.R., "Engineering Properties of Lime-Soil Mixtures," Journal of Materials, Vol. 4, No. 4, American Society for Testing Materials, December, 1969.

10. Barenberg, E.J., Behavior of Pozzolanic Pavements Under Load, Record 112, Highway Research Board, 1966.

11. Thompson, M.R., The Split-Tensile Strength of Lime-Stabilized Soils, Record 92, Highway Research Board, 1966.

12. Kennedy, T.W., Moore, R.K., and Anagnos, J.N., Estimations of Indirect Tensile Strengths for Cement-Treated Materials, Record 351, Highway Research Board, 1971.

13. Price, W.H., Factors Influencing Concrete Strength, Journal of the American Concrete Institute, Number 47, February, 1951.

14. Neville, A.M., Properties of Concrete, John Wiley & Sons, Inc., New York, 1963.

15. Chou, Y.T., Engineering Behavior of Pavement Materials: State of the Art, Technical Report S-77-9, U.S. Army Engineer Waterways Experiment Station, 1977.

16. Bofinger, H.E., The Measurement of the Tensile Properties of Soil-Cement, RRL Report LR 365, Road Research Laboratory, England, 1970.

17. Packard, R.G., "Structural Design of Concrete Pavements with Lean Concrete Lower Course," 2nd Rigid Pavement Conference, Purdue University, 1981.

18. Lilley, A.A., Cement-Stabilized Materials in Great Britain, Record 442, Highway Research Board, 1973.

19. Larsen, T.J. and Nussbaum, P.J., Fatigue of Soil Cement, Bulletin D119, Portland Cement Association, 1967.

20. Jones, R., Measurement of Elastic and Strength Properties of Cemented Materials in Road Bases, Record 128, Highway Research Board, 1966.

21. Shen, C.K., "Behavior of Cement Stabilized Soils Under Repeated Loading," Ph. D. Dissertation, Department of Civil Engineering, University of California, Berkeley, 1965.

22. Mitchell, J.K., Fossberg, P.E., and Monismith, C.L., Behavior of Stabilized Soils Under Repeated Loading, Report 3: Repeated Compression and Flexure Tests on Cement and Lime Treated Buckshot Clay, Confining Pressure Effects in Repeated Compression for Cement-Treated Silty Clay, Contract Report 3-145, U.S. Army Engineer Waterways Experiment Station, 1969.

23. Wang, M.C., "Stress and Deflection in Cement-Stabilized Soil Pavements," Ph. D. Dissertation, University of California, Berkeley, 1968.

24. Terrel, R.L., Epps, J.A., Barenberg, E.J., Mitchell, J.K., and Thompson, M.R., Soil Stabilization in Pavement Structures, A User's Manual, Volume 2, Mix Design Considerations, Report No. FHWA-IP-80-2, Federal Highway Administration, 1979.

25. _____, Building Code Requirements for Reinforced Concrete, ACI Standard 318-77, American Concrete Institute, 1977.

26. Brown, S.F., Design of Pavements with Lean-Concrete Bases, Record 725, Transportation Research Board, 1979.

27. Walker, R.N., Paterson, W.D.O., Freeme, C.R., and Marais, C.P., "The South African Mechanistic Design Procedure," Fourth International Conference on the Structural Design of Asphalt Pavements, University of Michigan, 1977.

28. Ahlberg, H.L., and Barenberg, E.J., The University of Illinois Pavement Test Track - A Tool for Evaluating Highway Pavements, Record 13, Highway Research Board, 1963.

29. Thompson, M.R., Engineering Properties of Lime-Soil Mixtures, Project IHR-76, Illinois Cooperative Highway Research Program, University of Illinois, 1969.

30. Marshall, B.P. and Kennedy, T.W., Tensile and Elastic Characteristics of Pavement Materials, Research Report 183-1, Center for Highway Research, The University of Texas at Austin, 1974.

31. Lotfi, H. and Witczak, M.W., "Dynamic Characteristics of Cement-Treated Base/Subbase Materials," Paper Presented at Transportation Research Board Meeting, 1983.

32. Winterkorn, H.F., Discussion - Strength and Elastic Properties of Compacted Soil-Cement Mixtures, Special Technical Publication 206, American Society for Testing Materials, 1957.

33. Maree, J.H. and Freeme, C.R., The Mechanistic Design Method Used to Evaluate the Pavement Structures in the Catalogue of the Draft TRH 4 1980, Technical Report RP/2/81, National Institute for Transport and Road Research, CSIR, South Africa, 1981.

34. Ahlberg, H.L. and Barenberg, E.J., Pozzolanic Pavements, Bulletin 473, Engineering Experiment Station, University of Illinois, 1965.

35. Pretorius, P.C., "Design Considerations for Pavements Containing Soil-Cement Bases," Ph.D. Dissertation, Civil Engineering, University of California, Berkeley, 1970.

36. Ahlberg, H.L. and McVinnie, W.W., Fatigue Behavior of a Lime-Fly Ash-Aggregate Mixture, Bulletin 335, Highway Research Board, 1962.

37. Yoder, E.J. and Witczak, M.W., Principles of Pavement Design, Second Edition, John Wiley & Sons, Inc., New York, 1975.

38. _____, Thickness Design for Concrete Pavement, Portland Cement Association, 1966.

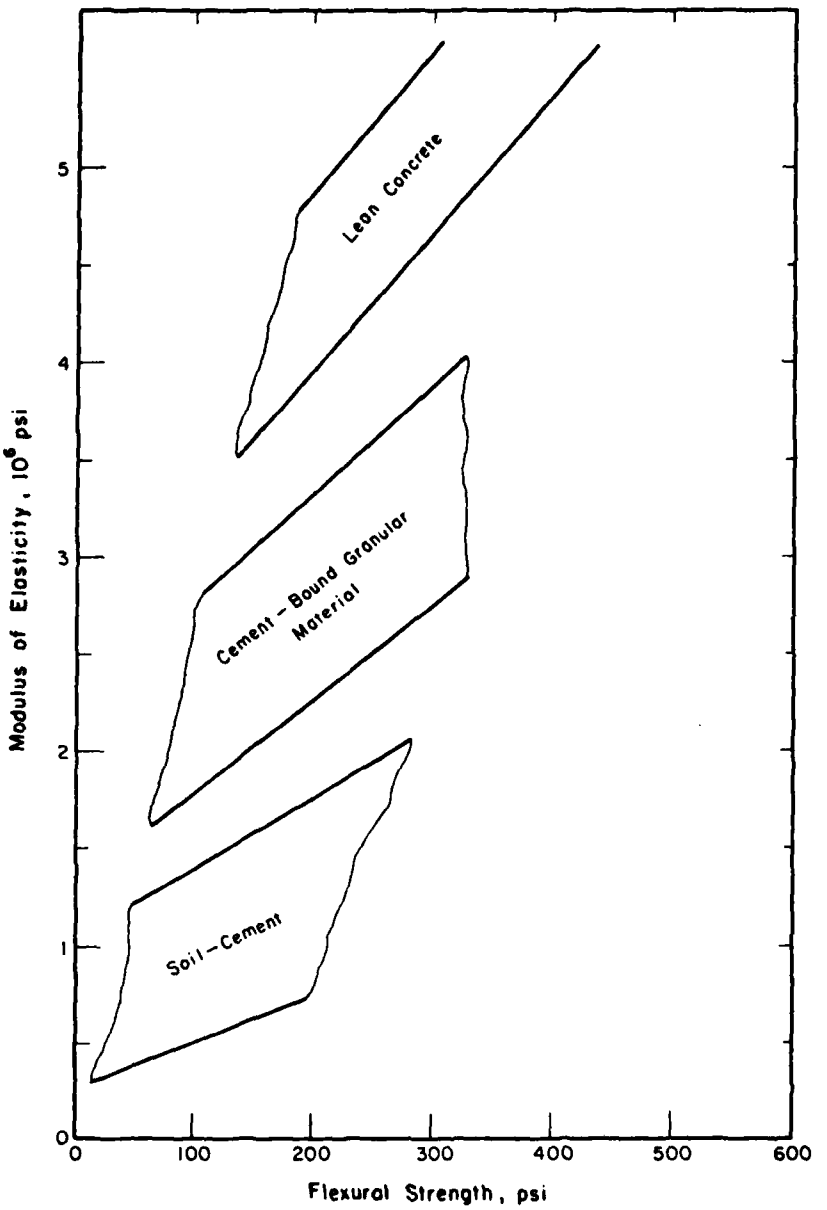

Figure A-1. Modulus of Elasticity-Envelopes of Strength Relations (Reference 18).

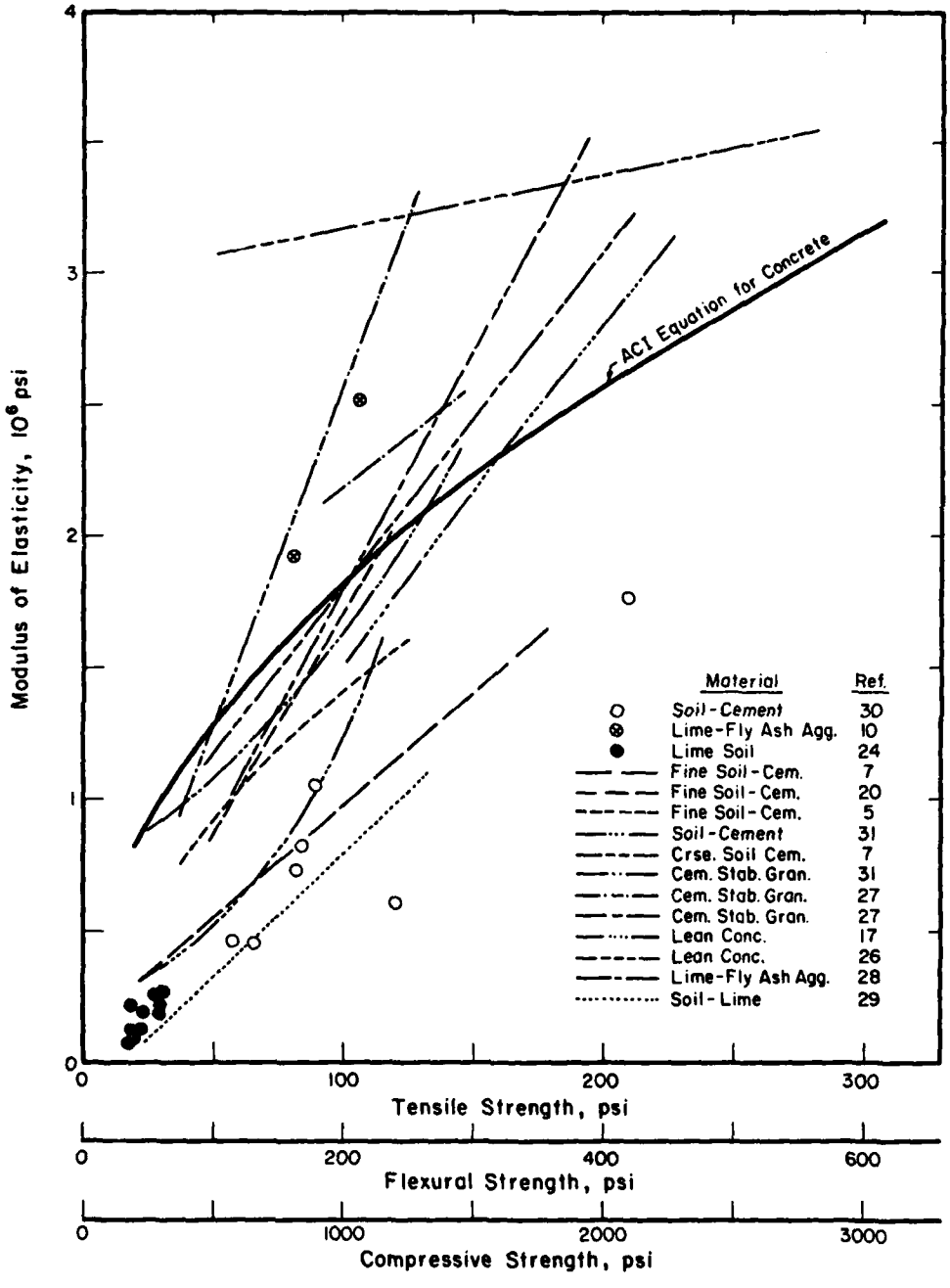

Figure A-2. Reported Modulus of Elasticity-Strength Relations.

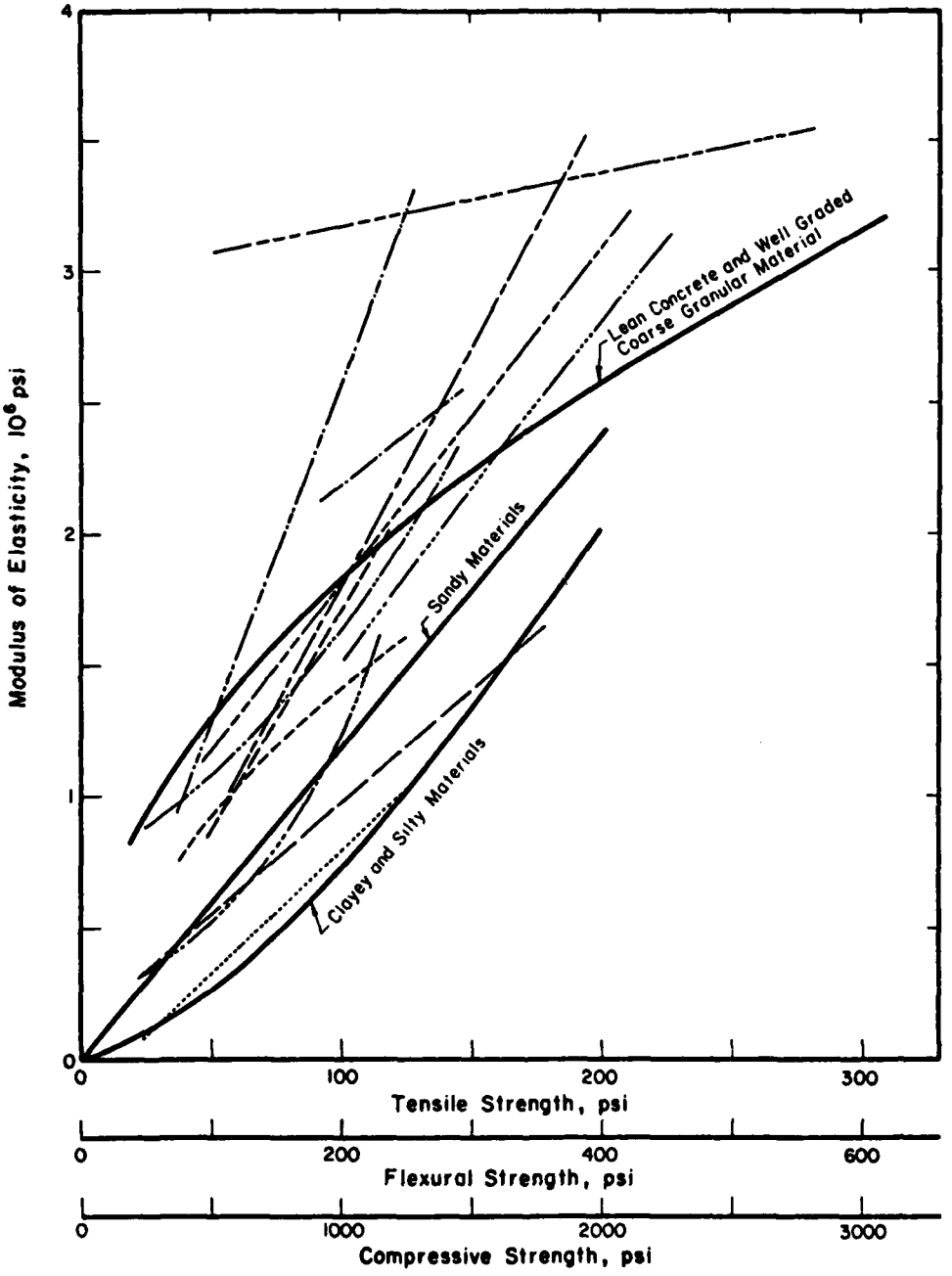

Figure A-3. Recommended Modulus-Strength Relations Superimposed on Reported Relations.

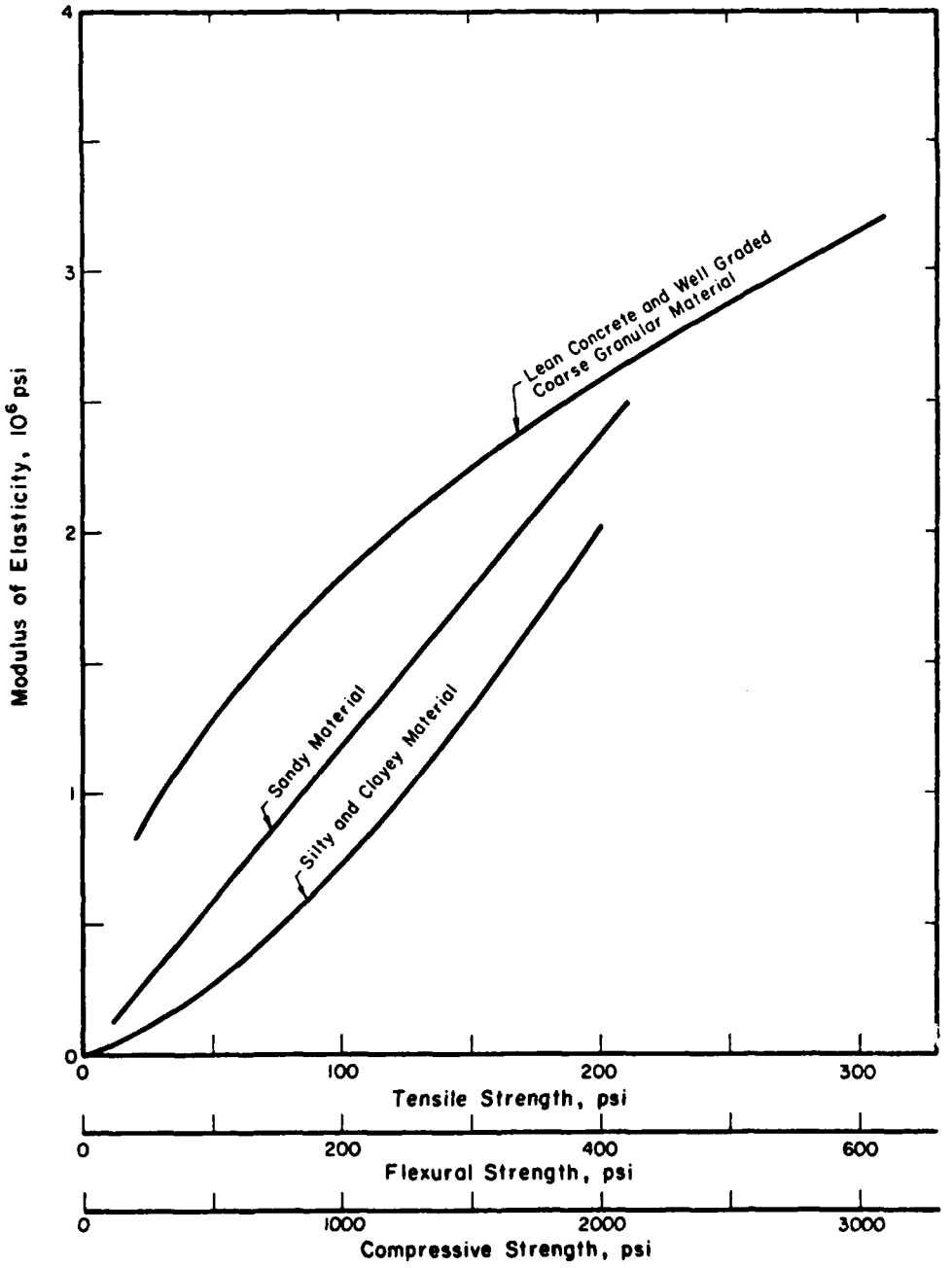

Figure A-4. Recommended Modulus-Strength Relations for Cementitiously Stabilized Materials.

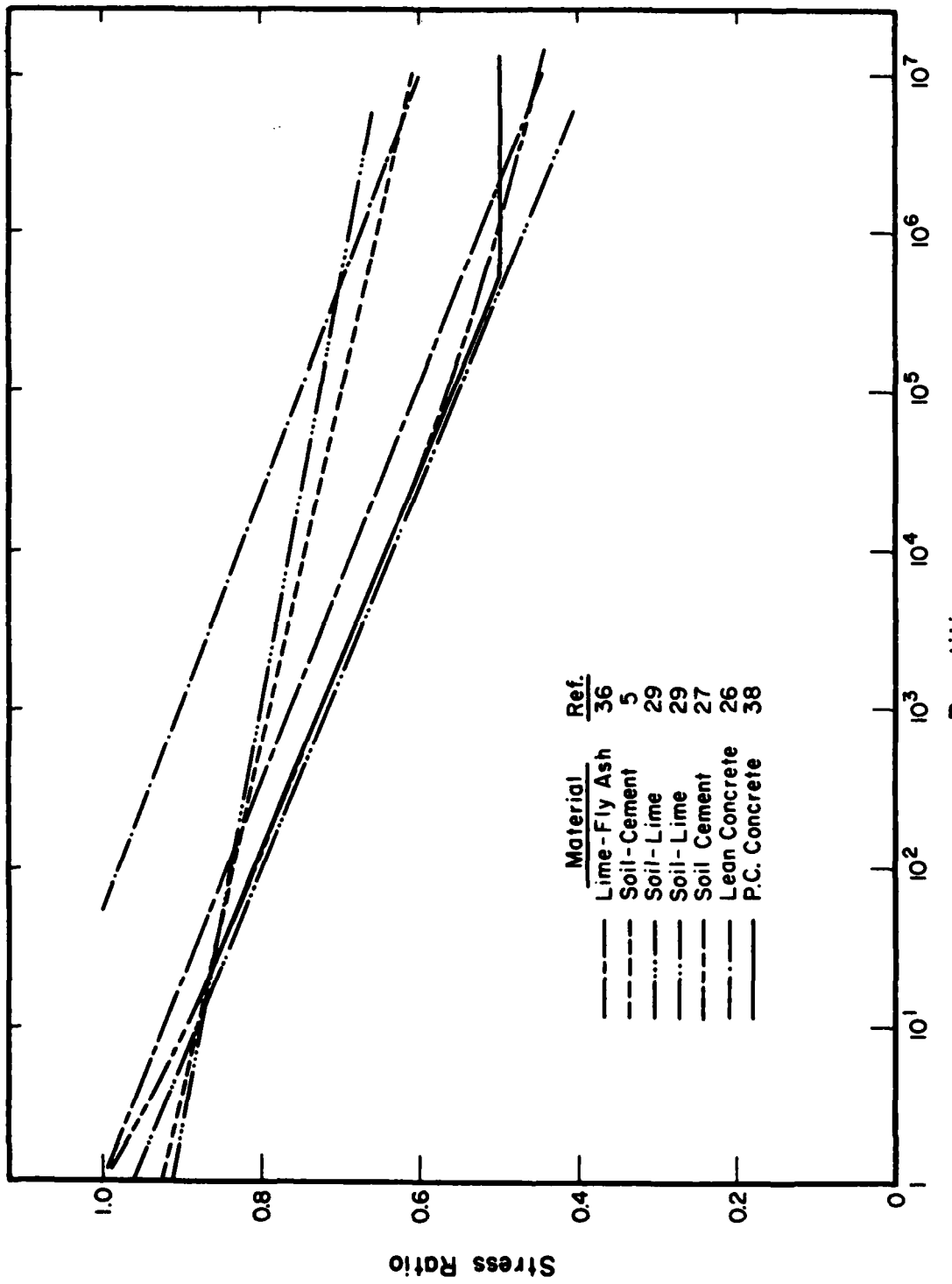

Figure A-5. Reported Stress Ratio-Fatigue Relations.

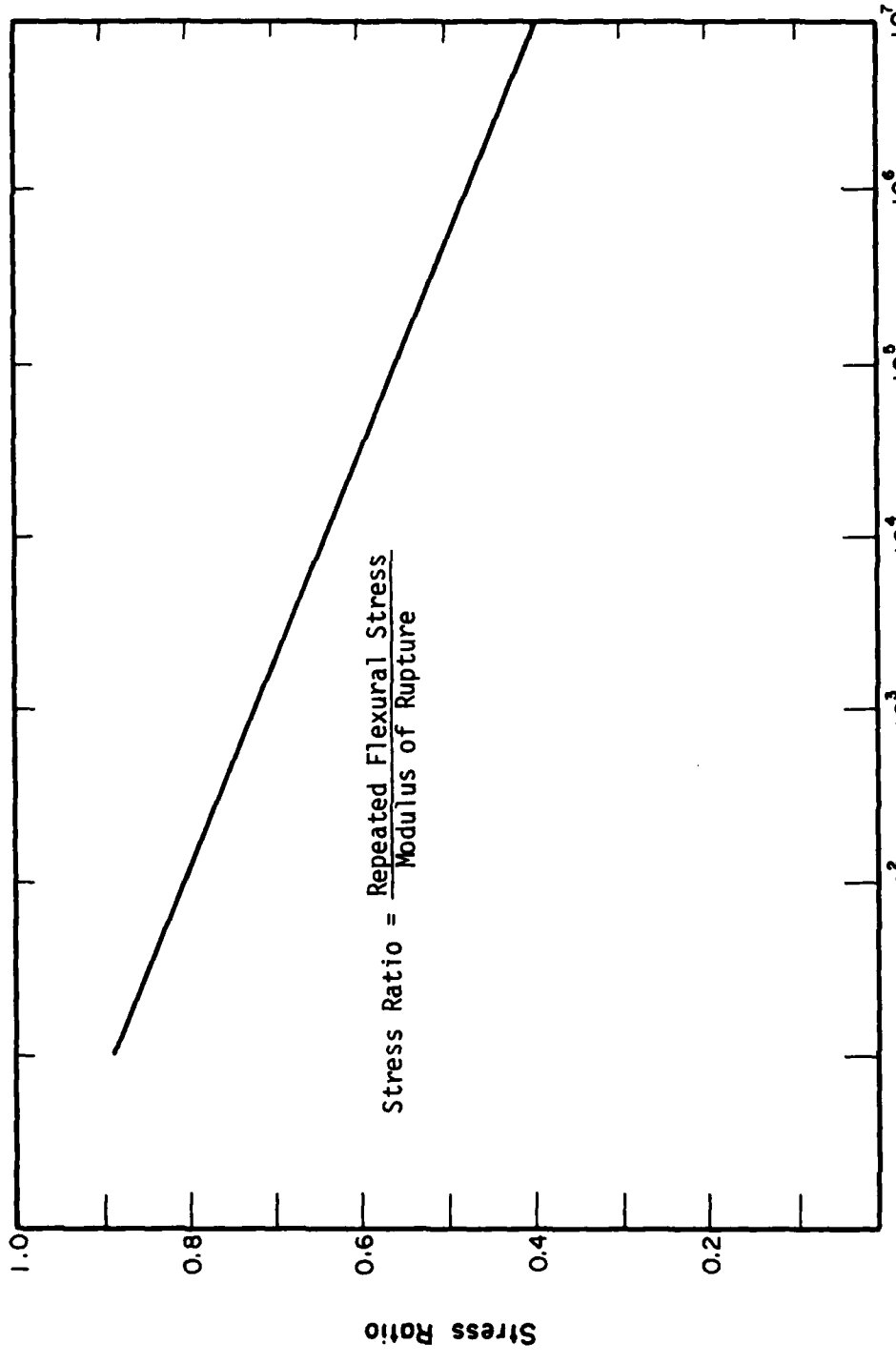

Figure A-6. Recommended Stress Ratio-Fatigue Relations for Cement-Stabilized Materials.

APPENDIX B

ILLI-PAVE DATA SUMMARY

F-4 LOADING

DESCRIPTION OF VARIABLES

	VARIABLE	UNIT
TST	THICKNESS OF STABILIZED LAYER	INCHES
EST	MODULUS OF ELASTICITY OF THE STABILIZED LAYER	KSI
ERI	SUBGRADE MODULUS AT THE INTERCEPT	KSI
MTST	MAXIMUM TENSILE STRESS AT BOTTOM OF STABILIZED LAYER	PSI
MEST	MAXIMUM RADIAL STRAIN AT BOTTOM OF STABILIZED LAYER	MICROSTRAIN
D0	DEFLECTION AT R = 0.0 IN. FROM LOAD	MILS
D1	DEFLECTION AT R = 12.0 IN. FROM LOAD	MILS
D2	DEFLECTION AT R = 24.0 IN. FROM LOAD	MILS
D3	DEFLECTION AT R = 36.0 IN. FROM LOAD	MILS
DS	DEFLECTION AT TOP OF THE SUBGRADE	MILS
EZ	MAXIMUM STRAIN AT TOP OF THE SUBGRADE	0.0001 IN/IN
SZ	MAXIMUM SUBGRADE NORMAL STRESS	PSI
TS	MAXIMUM SUBGRADE SHEARING STRESS	PSI
SDEV	MAXIMUM SUBGRADE DEVIATOR STRESS	PSI
AREA	DEFLECTION BASIN AREA	INCHES

TST	EST	ERI	AREA	DO	D1	D2	D3	DS	EZ	MEST	MTST	SZ	TS	SDEV
9.0	100	1.00	19.99	135.8	89.8	52.8	31.5	123.5	60.1	2166	249	9.4	2.9	5.8
9.0	200	1.00	22.63	88.7	64.4	43.6	29.8	82.6	27.4	1149	265	6.8	3.0	5.9
9.0	500	1.00	26.31	56.0	45.5	35.4	27.8	53.5	12.9	506	290	9.8	3.1	6.2
9.0	1000	1.00	29.05	42.5	37.0	31.3	26.7	41.3	7.9	274	314	6.8	1.8	3.7
9.0	2000	1.00	31.43	34.5	31.6	28.5	26.0	33.9	4.5	144	330	5.0	1.2	2.3
9.0	3000	1.00	32.55	31.5	29.5	27.4	25.6	31.1	3.2	98	337	4.2	0.9	1.8
12.0	100	1.00	21.15	98.4	65.4	43.9	29.8	83.2	36.7	1309	151	6.8	1.8	3.6
12.0	200	1.00	24.20	65.9	49.0	36.9	28.1	58.4	22.0	696	160	6.2	1.4	2.7
12.0	500	1.00	28.19	43.8	36.7	31.0	26.6	40.8	8.3	304	175	6.7	1.8	3.7
12.0	1000	1.00	30.89	35.0	31.4	28.3	25.8	33.5	4.7	161	185	5.1	1.2	2.4
12.0	2000	1.00	32.89	30.1	28.2	26.6	25.3	29.3	2.8	83	192	3.9	0.8	1.6
12.0	3000	1.00	33.74	28.4	27.1	26.0	25.1	27.8	2.1	56	194	3.5	0.6	1.2
15.0	100	1.00	21.83	79.0	52.1	38.0	28.2	61.9	25.2	840	96	5.9	1.2	2.5
15.0	200	1.00	25.18	54.2	40.5	32.7	26.9	45.6	12.6	444	102	7.1	1.8	3.5
15.0	500	1.00	29.35	37.7	32.0	28.5	25.7	34.2	5.4	194	111	5.4	1.4	2.7
15.0	1000	1.00	31.91	31.4	28.5	26.7	25.2	29.7	3.1	101	117	4.3	0.9	1.8
15.0	2000	1.00	33.69	28.0	26.6	25.6	24.8	27.2	2.0	52	120	3.6	0.6	1.2
15.0	3000	1.00	34.35	26.9	25.9	25.3	24.7	26.3	1.6	35	121	3.3	0.5	1.0
18.0	100	1.00	22.22	67.7	44.0	34.0	27.0	49.2	22.0	559	64	6.3	1.1	2.1
18.0	200	1.00	25.84	47.6	35.6	30.1	26.0	38.4	8.0	298	68	6.3	1.6	3.3
18.0	500	1.00	30.12	34.3	29.4	27.0	25.1	30.6	3.7	130	74	4.7	1.1	2.1
18.0	1000	1.00	32.55	29.4	27.0	25.7	24.7	27.6	2.3	67	77	3.9	0.7	1.4
18.0	2000	1.00	34.04	26.9	25.6	25.0	24.5	26.0	1.5	34	78	3.5	0.5	1.0
18.0	3000	1.00	34.71	26.0	25.2	24.8	24.4	25.4	1.3	23	79	3.4	0.4	0.8

TST	EST	ERI	AREA	DO	D1	D2	D3	DS	EZ	MEST	MTST	SZ	TS	SDEV
9.0	100	3.02	18.60	112.3	68.8	38.2	21.8	99.6	54.4	1956	224	17.0	5.0	10.0
9.0	200	3.02	21.32	75.7	52.3	33.5	21.7	69.5	30.0	1091	250	12.7	3.8	7.6
9.0	500	3.02	24.98	47.1	36.8	27.4	20.6	44.6	13.4	490	281	9.8	2.9	5.8
9.0	1000	3.02	27.78	34.8	29.4	23.9	19.7	33.6	7.6	266	305	7.8	2.2	4.3
9.0	2000	3.02	30.31	27.3	24.4	21.4	19.0	26.7	4.2	141	324	5.7	1.4	2.8
9.0	3000	3.02	31.70	24.4	22.5	20.4	18.7	24.0	3.0	96	332	4.8	1.1	2.2
12.0	100	3.02	19.78	83.7	52.2	33.2	21.4	68.2	31.1	1190	136	12.3	3.8	7.6
12.0	200	3.02	22.76	56.3	39.8	28.5	20.7	48.6	18.4	661	152	9.2	2.5	5.0
12.0	500	3.02	26.79	36.1	29.1	23.7	19.5	33.0	8.0	294	169	7.6	2.1	4.2
12.0	1000	3.02	29.68	27.9	24.3	21.3	18.9	26.4	4.4	157	181	5.7	1.5	3.0
12.0	2000	3.02	31.97	23.2	21.3	19.7	18.4	22.4	2.5	82	189	4.4	1.0	1.9
12.0	3000	3.02	33.01	21.5	20.2	19.1	18.2	21.0	1.9	56	193	3.8	0.7	1.5
15.0	100	3.02	20.32	68.2	42.0	29.1	20.6	50.8	21.7	771	88	9.6	2.7	5.4
15.0	200	3.02	23.61	46.0	32.5	25.1	19.8	37.4	12.3	425	97	8.0	2.0	3.9
15.0	500	3.02	27.95	30.5	24.9	21.5	18.8	27.1	5.1	189	108	6.1	1.6	3.2
15.0	1000	3.02	30.76	24.5	21.6	19.8	18.3	22.8	2.9	100	115	4.7	1.1	2.2
15.0	2000	3.02	32.94	21.2	19.8	18.8	18.0	20.4	1.7	52	119	3.8	0.7	1.4
15.0	3000	3.02	33.87	20.0	19.1	18.4	17.9	19.5	1.4	35	120	3.5	0.6	1.1
18.0	100	3.02	20.55	59.0	35.5	26.1	19.9	40.3	14.4	520	59	8.3	2.1	4.2
18.0	200	3.02	24.15	40.1	28.2	22.9	19.1	30.8	7.5	286	65	7.1	1.9	3.9
18.0	500	3.02	28.75	27.3	22.5	20.1	18.3	23.7	3.5	127	72	5.2	1.3	2.6
18.0	1000	3.02	31.54	22.6	20.2	18.9	18.0	20.8	2.0	66	76	4.2	0.8	1.7
18.0	2000	3.02	33.46	20.1	18.9	18.2	17.8	19.2	1.3	34	78	3.6	0.6	1.1
18.0	3000	3.02	34.13	19.3	18.4	18.0	17.7	18.7	1.1	23	79	3.4	0.5	0.9

TST	EST	ERI	AREA	DO	D1	D2	D3	DS	EZ	MEST	MTST	SZ	TS	SDEV
9.0	100	7.68	16.64	82.6	44.5	22.6	12.3	69.4	41.0	1577	178	29.7	9.9	19.9
9.0	200	7.68	19.35	57.5	36.2	21.3	12.9	51.0	24.5	939	214	21.8	7.2	14.5
9.0	500	7.68	23.04	36.2	26.6	18.4	12.8	33.7	12.2	452	258	13.7	4.2	8.5
9.0	1000	7.68	25.79	26.1	20.9	16.0	12.3	24.8	7.0	250	287	9.9	2.8	5.6
9.0	2000	7.68	28.47	19.6	16.8	14.0	11.8	19.0	4.0	136	311	7.2	1.9	3.8
9.0	3000	7.68	30.14	17.0	15.2	13.2	11.6	16.6	2.7	94	322	6.0	1.6	3.2
12.0	100	7.68	17.64	65.1	35.8	21.0	12.7	49.1	24.3	983	111	20.6	7.2	14.5
12.0	200	7.68	20.63	44.0	28.4	18.9	12.7	36.2	14.6	583	133	14.8	5.0	10.0
12.0	500	7.68	24.66	27.4	20.7	15.8	12.2	24.3	7.3	275	158	9.6	2.8	5.7
12.0	1000	7.68	27.65	20.2	16.7	13.9	11.7	18.7	4.1	150	173	7.2	2.0	4.0
12.0	2000	7.68	30.42	15.9	14.1	12.6	11.3	15.2	2.3	80	184	5.3	1.3	2.6
12.0	3000	7.68	31.76	14.3	13.1	12.0	11.2	13.8	1.6	55	189	4.5	1.0	2.0
15.0	100	7.68	18.02	55.0	29.8	19.0	12.6	37.2	15.7	650	73	15.1	5.3	10.7
15.0	200	7.68	21.25	36.4	23.3	16.8	12.3	27.7	9.6	384	87	11.0	3.6	7.1
15.0	500	7.68	25.61	22.8	17.3	14.1	11.7	19.3	4.6	178	102	7.6	2.2	4.4
15.0	1000	7.68	28.85	17.2	14.4	12.7	11.3	15.5	2.6	96	111	5.7	1.5	3.0
15.0	2000	7.68	31.53	14.1	12.7	11.8	11.0	13.3	1.5	50	116	4.4	1.0	1.9
15.0	3000	7.68	32.72	13.0	12.1	11.4	10.9	12.5	1.1	34	118	3.9	0.7	1.5
18.0	100	7.68	18.16	48.5	25.6	17.4	12.3	29.6	10.8	448	50	11.8	4.0	8.0
18.0	200	7.68	21.53	31.8	20.0	15.2	11.9	22.4	6.6	262	59	8.9	2.7	5.4
18.0	500	7.68	26.31	20.0	15.2	13.0	11.3	16.4	3.1	121	69	6.2	1.7	3.4
18.0	1000	7.68	29.46	15.6	13.1	11.9	11.0	13.7	1.8	64	74	4.9	1.1	2.3
18.0	2000	7.68	32.00	13.2	11.9	11.3	10.8	12.2	1.1	33	77	4.0	0.7	1.5
18.0	3000	7.68	33.27	12.3	11.5	11.1	10.7	11.7	0.8	23	78	3.7	0.6	1.2

TST	EST	ERI	AREA	DO	D1	D2	D3	DS	EZ	MEST	MTST	SZ	TS	SDEV
9.0	100	12.34	15.38	67.8	33.0	15.8	8.4	54.1	33.9	1334	148	38.9	13.7	27.4
9.0	200	12.34	18.05	47.5	27.8	15.4	9.0	40.9	20.9	829	187	28.6	10.2	20.4
9.0	500	12.34	21.74	30.2	21.1	13.9	9.2	27.7	10.8	418	238	17.7	6.0	12.0
9.0	1000	12.34	24.53	21.7	16.8	12.2	9.0	20.5	6.4	238	272	12.2	3.8	7.5
9.0	2000	12.34	27.23	16.0	13.3	10.7	8.6	15.4	3.7	131	300	8.6	2.4	4.9
9.0	3000	12.34	28.69	13.7	11.8	9.9	8.4	13.3	2.6	91	314	7.0	1.9	3.8
12.0	100	12.34	16.23	55.4	27.6	15.2	8.9	39.0	20.2	842	93	26.7	10.1	20.2
12.0	200	12.34	19.11	37.4	22.2	14.1	9.1	29.5	12.8	524	118	19.0	7.0	13.9
12.0	500	12.34	23.22	23.1	16.6	12.1	8.9	20.0	6.6	259	148	11.9	3.9	7.8
12.0	1000	12.34	26.19	16.7	13.2	10.6	8.6	15.1	3.8	144	166	8.5	2.6	5.1
12.0	2000	12.34	29.06	12.7	10.9	9.4	8.2	11.9	2.2	78	179	6.1	1.6	3.3
12.0	3000	12.34	30.70	11.2	10.0	9.0	8.1	10.7	1.5	54	185	5.1	1.3	2.5
15.0	100	12.34	16.55	48.0	23.5	14.2	9.0	29.9	13.3	565	62	19.1	7.2	14.5
15.0	200	12.34	19.62	31.5	18.6	12.7	8.9	22.6	8.4	349	78	13.7	4.9	9.8
15.0	500	12.34	24.00	19.1	13.7	10.7	8.5	15.6	4.3	169	96	9.0	2.8	5.7
15.0	1000	12.34	27.26	14.0	11.2	9.5	8.2	12.3	2.4	93	107	6.5	1.9	3.7
15.0	2000	12.34	30.33	11.0	9.6	8.7	8.0	10.2	1.4	50	114	4.9	1.2	2.4
15.0	3000	12.34	31.62	10.0	9.0	8.4	7.9	9.4	1.0	34	117	4.3	0.9	1.8
18.0	100	12.34	16.62	43.1	20.6	13.1	8.9	23.9	9.2	393	43	14.5	5.3	10.7
18.0	200	12.34	19.89	27.6	16.0	11.6	8.7	18.2	5.8	241	54	10.7	3.6	7.2
18.0	500	12.34	24.54	16.7	11.9	9.8	8.2	13.0	2.9	115	65	7.2	2.2	4.3
18.0	1000	12.34	27.98	12.5	10.0	8.9	8.0	10.6	1.7	63	72	5.4	1.4	2.8
18.0	2000	12.34	31.07	10.1	8.9	8.3	7.8	9.2	1.0	33	76	4.4	0.9	1.8
18.0	3000	12.34	32.39	9.3	8.5	8.1	7.7	8.7	0.8	22	77	3.9	0.7	1.4

APPENDIX C

MEYERHOF ULTIMATE LOAD EQUATIONS

Notation

a = Radius of loaded area, inches

E = Modulus of elasticity of slab material, psi

f_b = Modulus of rupture for slab material, psi

h = Slab thickness, inches

k = Modulus of subgrade reation, psi/inch

ℓ = Radius of relative stiffness, inches = $\sqrt[4]{\frac{E\,h^3}{(1-\mu^2)\,k}}$

$M_o = \frac{f_b\,h^2}{6}$

m = Center to center spacing of tandem gear assembly (circular load area of radius a)

P = Collapse load, pounds

μ = Poisson's ratio

Single-Wheel Load

Interior Loading

$$P_i = \left(\frac{4\pi}{1 - \frac{a}{3\ell}}\right) M_o$$

Edge Loading

$$P_e = \left[\frac{4 + \pi}{(1 - \frac{2a}{3\ell})}\right] M_o$$

Corner Loading

$$P_c = \left[\frac{4}{(1 - \frac{a}{\ell})}\right] M_o$$

Tandem Gear

Interior Loading

$$P_i = \left[\frac{4\pi}{1 - \frac{a}{3\ell}} + \frac{1.8m}{\ell - \frac{a}{2}} \right] M_o$$

Edge Loading

$$P_e = 0.6\ P_i$$

Note: Equations valid for $a/\ell > 0.2$

Graphical solutions for the Meyerhof equations (single-wheel load conditions) are shown in Figure 14.